Florida A & M University - Florida State University
College of Engineering
Department of Civil and Environmental Engineering

INVESTIGATION OF FENDER SYSTEMS FOR VESSEL IMPACT

WPI No. 510846

A Final Report Submitted to
The Florida Department of Transportation

By
Nur Yazdani, Ph.D., P.E.
Jerry Wekezer, Ph.D., P.E.
Claudia Wilson
Rafal Wuttrich

Department of Civil and Environmental Engineering
Florida A&M University-Florida State University
College of Engineering
Tallahassee, FL 32310

July, 2000

Technical Report Documentation Page

1. Report No.	2. Government Accession No.	3. Recipient's Catalog No.
WPI No. 0510846		

4. Title and Subtitle	5. Report Due
Investigation Of Fender Systems For Vessel Impact	July 31, 2000
	6. Performing Organization Code: 1902-137-11
	8. Performing Organization Report No.: 1902-137-11
7. Author's: Nur Yazdani, Ph.D., P.E., Jerry Wekezer, Ph.D., P.E., Claudia Wilson, and Rafal Wuttrich	
9. Performing Organization Name and Address: FAMU-FSU College of Engineering, Civil and Environmental Engineering Department, 2525 Pottsdamer St., Tallahasse FL 32310	10. Work Unit No. (TRAIS)
	11. Contract or Grant No.: BB-348, 99700-3873-119
	13. Type of Report and Period Covered
12. Sponsoring Agency Name and Address: Florida Department of Transportation, 605 Suwannee Street, Tallahassee, FL 32399-0450	14. Sponsoring Agency Code

15. Supplementary Notes

Prepared in cooperation with the US department of Transportation and Federal Highway Administration

16. Abstract

Fender systems are currently placed between channel piers of bridges crossing navigable waterways, to guide vessels through the navigational channels. These systems are not designed to withstand any lateral load. This report presents evaluation of the existing bridge fender structures for an impact with a Jumbo Hopper barge and their possible retrofit analysis. The finite element method was selected for the modeling of the fender systems and the impact simulations. Two different analyses were performed: a static analysis with ANSYS using the equivalent force equation from AASHTO (1991), and a dynamic analysis with LS-DYNA where the model of the barge is included. It was found that the present FDOT fender configuration is very weak, and unable to support any significant barge impact force. Failure occurred at the cables connecting piles in the fender system. A retrofit scheme with steel plates connecting the piles showed limited success in barge impact resistance. Corrosion concerns may preclude the use of this retrofit. Another retrofit scheme using concrete wedges between piles was more effective in substantial energy absorption. However, the equivalent static force absorbed by the improved fender was relatively smaller. A cost-benefit analysis is needed to gauge the advantages of fender retrofit in relation to economic design of the actual bridge structure and rebuilding of fenders after an impact. Plastic lumber fenders and piles may be effectively used in fender systems, especially in consideration of long-term durability and economics.

17. Key Words	18. Distribution Statement
Bridge fender, ship impact, bridge design, pier protection, plastic lumber, fender retrofit	No restriction. This report is available to the public through the National Technical Information Service, Springfield VA 22161

19. Security Classif. (of this report)	20. Security Classif. (of this page)	21. No. of Pages	22. Price
Unclassified	Unclassified	128	

Form DOT F 1700.7 (8-72)

Prepared in cooperation with the State of Florida Department of transportation an the U.S. Department of Transportation.

TABLE OF CONTENTS

LIST OF TABLES

LIST OF FIGURES

CHAPTER 1

INTRODUCTION

1.1. Problem Statement

The consequences of an accident involving a ship or barge and a bridge can be catastrophic, as demonstrated by the collapse of a 396m (1300 ft) section of the main span of the Sunshine Skyway Bridge after it was hit by the bulk carrier "Summit Venture" in 1980. In addition to the huge economic losses caused by the bridge failure, 35 lives were lost in that accident.

In 1988, due to the increasing number of shipping accidents with bridges, a pool-funded research project sponsored by 11 states and the FHWA was initiated to establish design specifications for ship impact with bridges. The findings were adopted by AASHTO, and are presented in the Guide Specifications and Commentary for Vessel Collision Design of Highway Bridges (AASHTO 1991). These guidelines provide two alternatives for bridge design:

- to design bridge elements to withstand ship impact force.
- to design pier protection systems.

A variety of bridge pier protection systems have been used. The most common forms include large-diameter dolphins, and protective islands placed around the most vulnerable piers. Additional protective measures include the use of electronic navigational aids and motorist warning systems to interrupt traffic on the bridge in case of an accident.

Fender systems are currently placed between channel piers of bridges crossing navigable waterways, to guide vessels through the navigational channels. These structures are composed of prestressed concrete piles and treated timber wales, as shown on Figs. 1.1 and 1.2. These systems have not been designed to withstand any lateral load. Because they are part of the U.S. Coast

Guard requirements, it would be convenient and economically advantageous to adapt them to act as pier protective systems.

1.2. Objective

The objective of this research is to investigate the adaptability of the existing bridge fender systems as pier protection elements against vessel impact.

1.3. Methodology

The finite element method was selected for the modeling of the fender systems and the impact simulations, due to the complicated loading and geometry of the problem. Two different analyses were performed: a static analysis using the equivalent force equation from AASHTO (1991), and a dynamic analysis where the model of the barge is included. The static analysis was performed with the computer program ANSYS, version 5.5. It is described in detail in Wilson (2000), and summarized in Chapters 2 to 6. The dynamic analysis was performed with the computer code LS-DYNA, version 950, and is presented in Chapters 7 to 10. Appendices A through E from Wilson (2000) are also included at the end of this report.

Figure 1.1. Fender Systems Currently Used by FDOT

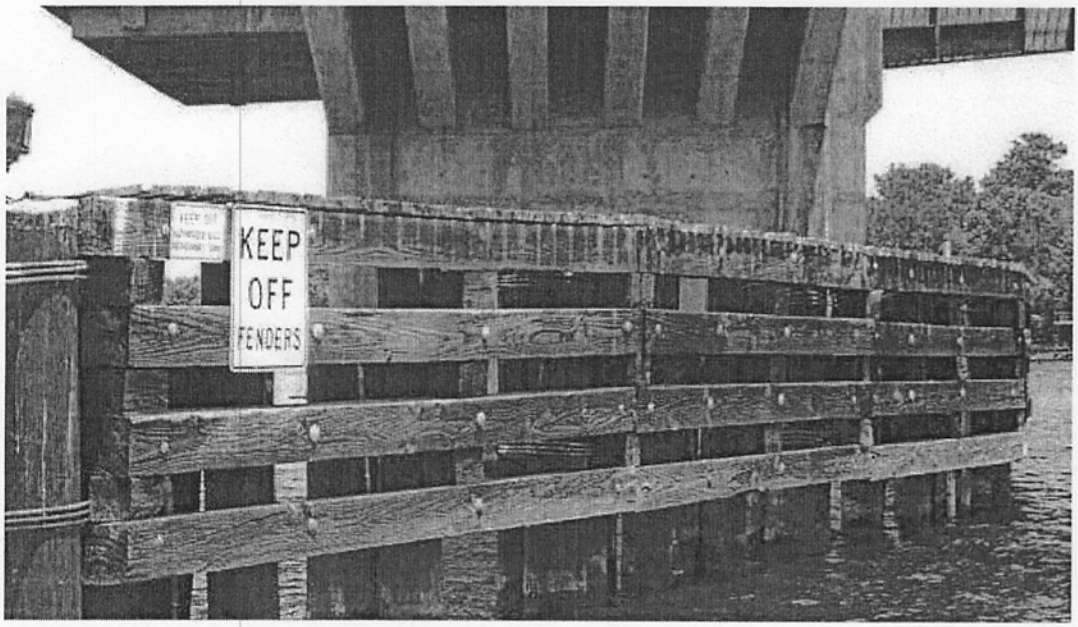

Figure 1.2. Fender Systems Detail

CHAPTER 2

LITERATURE REVIEW

2.1. AASHTO Specifications

The AASHTO Guide Specification and Commentary for Vessel Collision Design of Highway Bridges, Volume I: Final Report of February 1991 presents provisions for the vessel collision design of highway bridges. It presents guidelines for the selection of the type of design vessel, the design impact speed, and the determination and application of the equivalent impact force. These provisions represent minimum requirements. Specifications are also presented for the design of bridge protective systems intended to prevent, redirect, or reduce the impact loads on the bridges.

The choice of the design vessel is based on a probability based analysis procedure that considers the bridge characteristics and the vessel traffic. A simple semi-deterministic analysis procedure requiring less input information, and a cost-effectiveness analysis procedure can also be employed in special situations. The determination of the design speed is based on the typical vessel transit speed, and the dimensions of both the design vessel and the transit path.

Procedures for the determination of the static force equivalent to a vessel head-on impact are dependent on the vessel type. The following equations can be used to determine the equivalent static barge impact force on a bridge pier:

$$KE = \frac{C_H W(V)^2}{29.2} \tag{2.1}$$

where

KE = vessel collision energy (kip-ft)

W = vessel displacement tonnage, that is, weight of empty vessel plus weight of ballast and cargo (DWT) being carried by the vessel (tons)

V = vessel impact speed (fps)

C_H = hydrodynamic mass coefficient to account for the mass of water moving with the vessel. For vessels moving straight forward, the following values are to be used:

1) 1.05 for large underkeel clearances $(\geq 0.5 \times \text{draft})$

2) 1.25 for small underkeel clearances $(\leq 0.1 \times \text{draft})$

The underkeel clearance is the distance between the bottom (keel) of a vessel and the bottom of the waterway.

$$P_B = 4112(a_B)(R_B) \quad \text{for } a_B < 0.34 \tag{2.2}$$

$$P_B = [1349 + 110(a_B)]R_B \quad \text{for } a_B \geq 0.34 \tag{2.3}$$

where

$$a_B = \text{barge bow damage depth (ft)} = \left[\left(1 + \frac{KE}{5672}\right)^{\frac{1}{2}} - 1\right]\left(\frac{10.2}{R_B}\right) \tag{2.4}$$

P_B = equivalent static barge impact force (kips)

$$R_B = B_B/35 \tag{2.5}$$

B_B = barge width (ft)

The design of protective structures involves the development of a force versus deflection graph through analysis, testing, or modeling. The energy capacity of the structure to resist the design impact, determined as the area under this graph, is compared to the vessel impact force.

2.2. Bridge Pier Protective Structures

According to AASHTO (1991), the most commonly used protective structures are:

- Timber fenders, which may be attached to the bridge pier or stand independently.
- Concrete fenders, composed of thin-walled concrete boxes attached to the bridge pier.
- Steel fenders, consisting of thin-walled membranes and bracing elements placed in box-like arrays, and attached to the bridge pier.
- Rubber fenders.
- Pile supported systems, that is, groups of piles joined by rigid caps.
- Dolphins, which are structures formed by sheet piles driven in a circle, filled with rock or concrete, and topped by a concrete cap.

Man-made islands, composed of sand gravel, can be used as bridge protection systems where pier spacing, navigation channel width, and water depth are adequate. The use of such structures requires the assertion that the lateral capacity of the bridge pier and its foundations exceed the impact force transmitted through the material of the island (Tsinker 1995).

The movable protection system proposed by Tsinker *et al.* (1990) is presented in Fig. 2.1. It is composed of timber fenders mounted on multi-cell steel fenders, which are placed on a movable support capable of sliding on the foundation mattress, providing additional resistance when the crushing of the fenders is not sufficient to stop the colliding vessel.

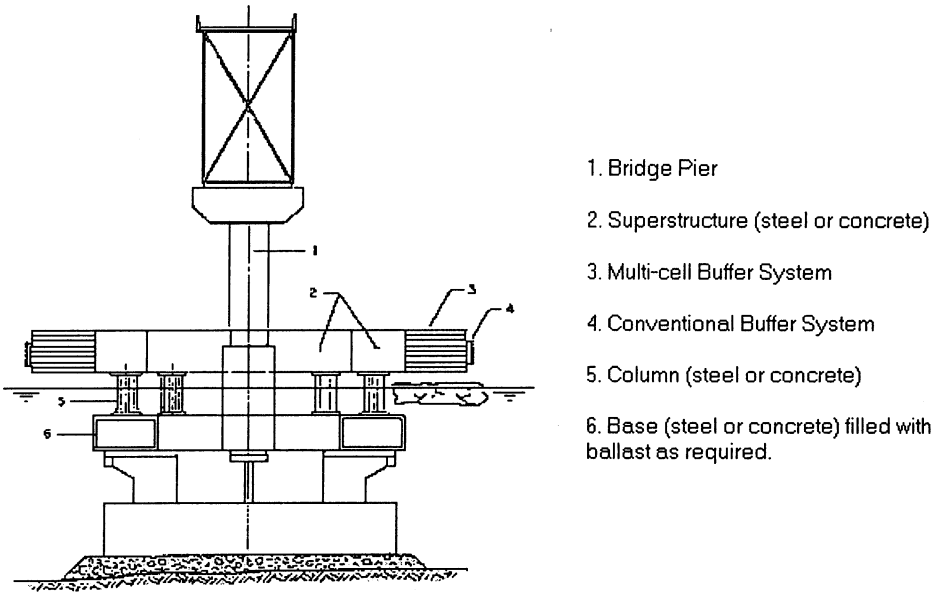

Figure 2.1. Movable Protection System (Tsinker *et al.* 1990)

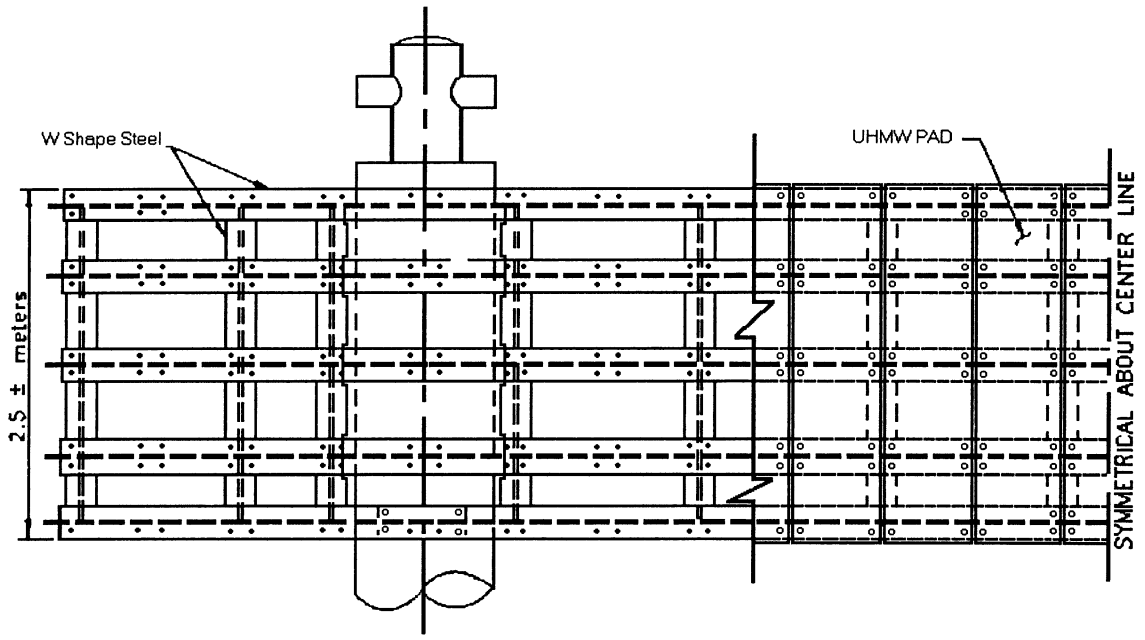

Figure 2.2. Fenderless Bridge Protection System (Hsu and Trepper 1995)

Hsu and Trepper (1995) proposed a fenderless fender system to protect the docks of the Port of Texas City, Texas. These systems consist of steel panels faced with ultra high molecular weight Polyethylene pads, and attached to high strength steel pipe piles (Fig. 2.2). According to the authors, a similar design could be developed to inexpensively protect bridge piers.

2.3. Alternative Materials

Hoy *et al.* (1996) believe that recycled plastic fenders may replace timber fenders and reduce construction and maintenance costs. The use of plastic fender systems would also avoid the environmental concerns related to the use of chemicals such as creosote and water-borne salts of copper, arsenic, and chromium in timber treatment. Recycled plastic piles proposed and tested presented two types of reinforcement: reinforcing rods (rebars) or steel pipes. The rebars can be made of steel or fiberglass. Composite piles, consisting of fiberglass tubes filled with concrete, and solid fiberglass piles are also being tested.

Lampo *et al.* (1996) specify what should be considered in the structural use of plastic lumber:

- Ultimate strength is similar to that of softwoods.
- Modulus of elasticity is lower than wood, but can be increased by the addition of fiberglass.
- Strain is larger than that of wood.
- Creep/time-temperature dependence is more pronounced than in wood because of plastic viscoelastic properties.
- Thermal expansion coefficients are higher than those of wood.

The main limitations to the use of plastic lumber are, therefore, low modulus of elasticity, and high creep and coefficient of thermal expansion. Larger cross sections or more closely spaced

supports may be necessary. The cost per board of plastic lumber is 25 to 50% higher than that of chemically treated wood. Installation is also more expensive, but lifetime cost evaluations show that it is more economical.

Other advantages of the use of plastic lumber are described in Lambert (1995) and include the fact that plastic lumber does not warp, splinter or rot. It retains its color and is often made of recycled plastic. When it does fade, it does so consistently across boards. It is low maintenance. Disadvantages include price, and the fact that some versions of plastic lumber weigh more than wood.

2.4. Computational Mechanics in Impact Analysis

A vessel collision with a fender structure is similar to a road vehicle collision with a roadside safety facility. Full-scale crash tests are required for certification of any roadside safety feature, thus there is a vast record of those tested with vehicles impacting at various speeds and impact angles. Computational analysis is another useful tool in crashworthiness studies. Several guardrails, guardrail terminals, light poles, etc., were analyzed using a non-linear finite element dynamic computer code, LS-DYNA (Plaxico *et al.* 1996, Ray 1995, Ray and Patzner 1997).

This technology has also been used for retrofit analysis of existing structures (Gilbert *et al.* 1998, Wekezer *et al.* 1998), as well as a design aid for development of new highway safety barriers (Reid and Sicking 1998). Since full-scale tests for barge impact would be expensive, computational analysis appears to be the most viable approach, and was used in this project.

CHAPTER 3

FDOT FENDER SYSTEM CONFIGURATION

The fender systems currently used by the FDOT consist of a series of bays, which are composed of a three-pile cluster, followed by two two-pile clusters, as shown on Figs. 3.1 and 3.2. Three-pile clusters consist of two plumb piles and one battered pile, while two-pile clusters consist of one plumb pile and one battered pile. Battered piles have a 3:1 grade and are placed 355-mm (14-in) below the top of the vertical ones (Fig. 3.3). All piles are 355-mm (14-in) square prestressed concrete and are attached by two wire ropes of 3-strands of 152 x 499 mm (6 x 19.6 in) outer diameter, black polypropylene impregnated space-lay galvanized, wrapped around the plumb piles and inserted through 51-mm (2 in) inner diameter PVC sleeves placed in the batter piles. Three standard clamps at 108 mm (4.25 in) minimum spacing are placed to secure cable ends, which are to be fused and covered according to the manufacturer's recommendations. A unique 610 mm (24 in) square prestressed concrete pile may be used where not enough space is provided for the use of battered piles.

Four horizontal 254 x 254 mm (10 x 10 in) structural timber wales are bolted to the plumb piles. These elements are as long as the bays, that is 4.875 m (16 ft) long on a typical straight section of the fender system. The bolts specified are 22 mm (0.87 in) diameter domehead bolts with cut washer and nut, and are inserted through 25 mm (1 in) inner diameter PVC sleeves placed through all vertical piles for this purpose.

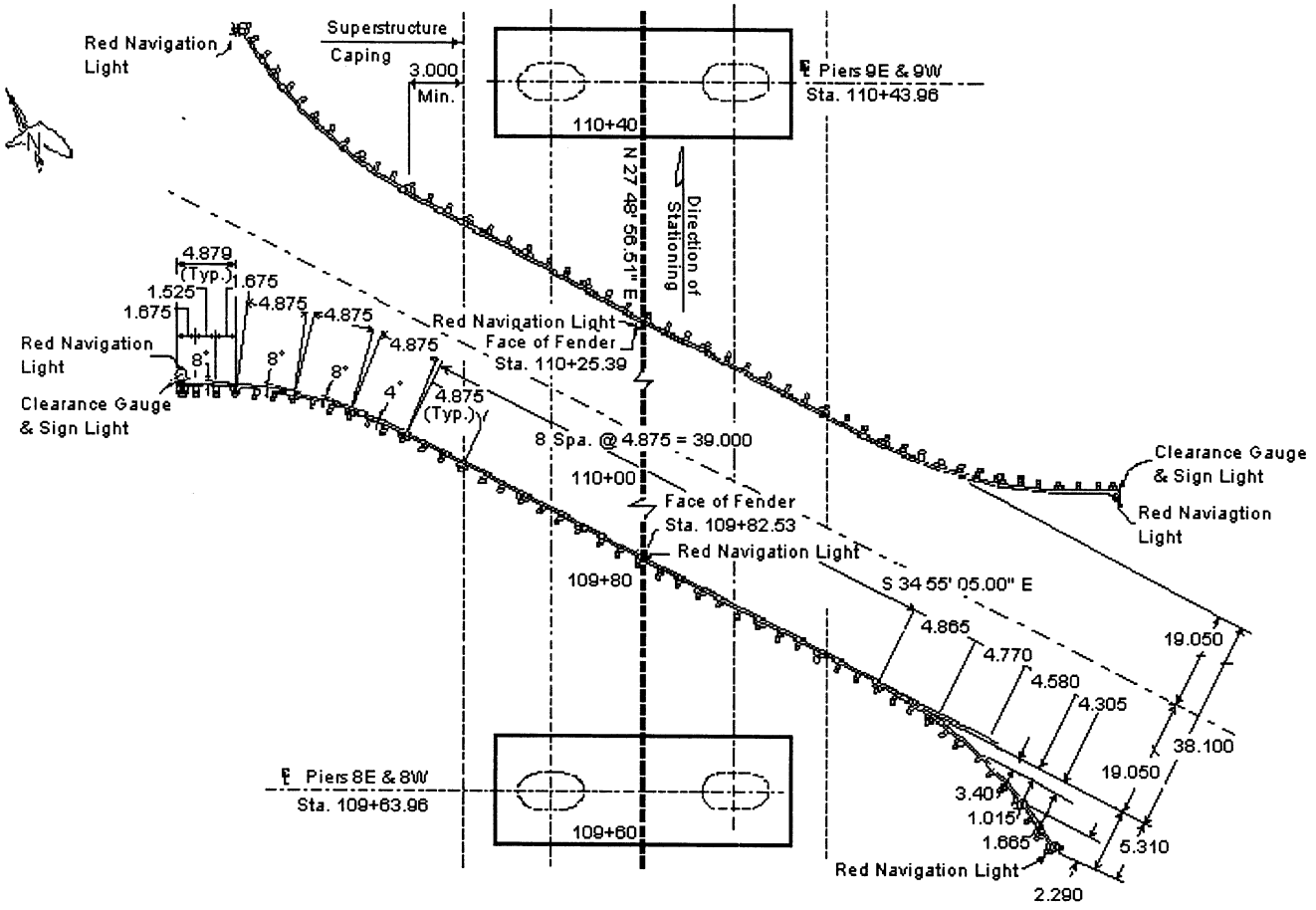

Figure 3.1. Fender System Plan from FDOT Project 79080-3544, SR-600 Bridge & Approaches Bridges Nos. 790187 and 790188 (FDOT 1997)

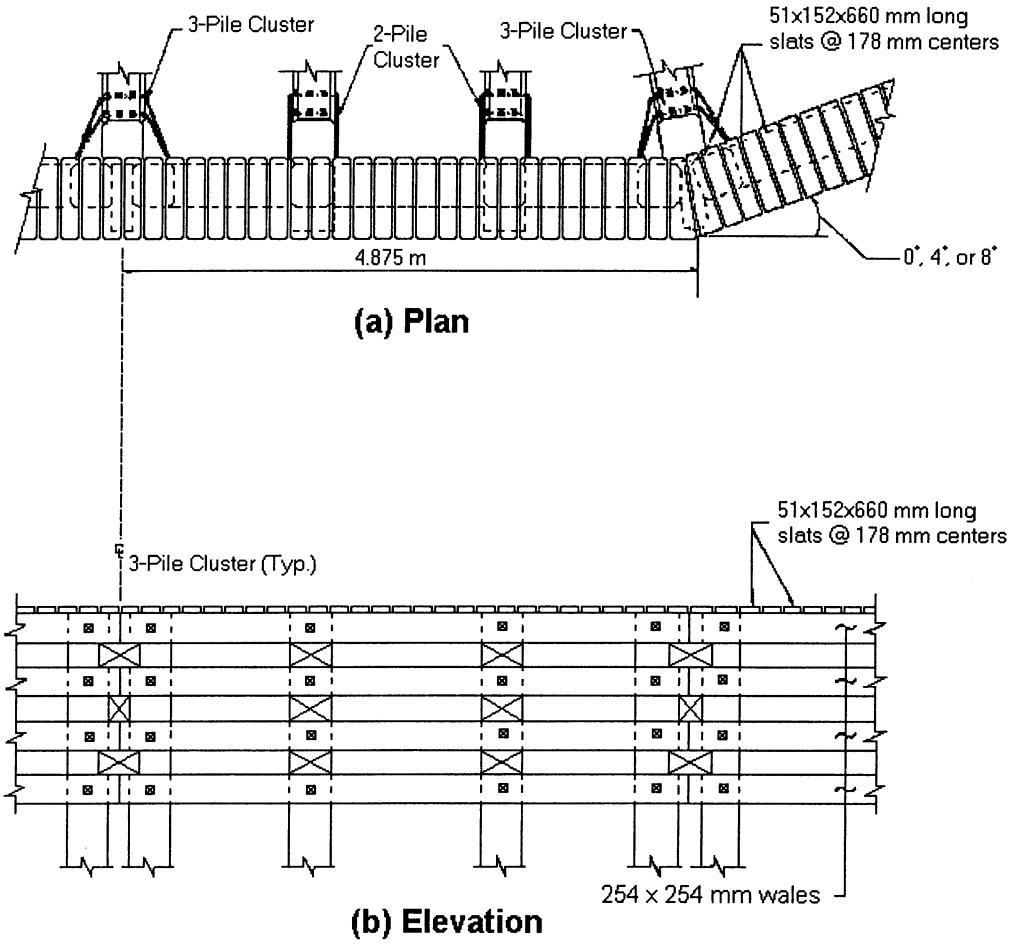

Figure 3.2. Partial Plan and Elevation of Fender System Project No. 79080-3544 (FDOT 1997)

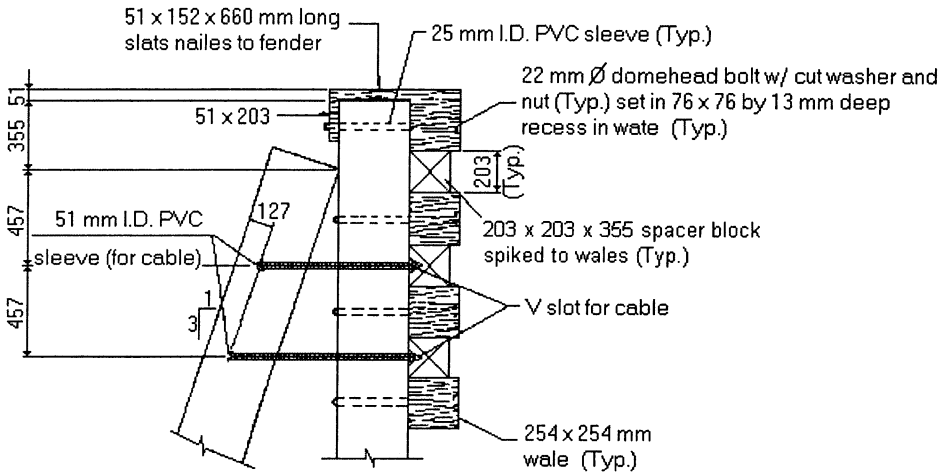

Figure 3.3. Typical Pile Cluster (FDOT 1996)

CHAPTER 4

VESSEL IMPACT FORCE

The vessel impact force was determined in accordance with Section 3 of the Guide Specifications and Commentary for Vessel Collision Design of Highway Bridges (AASHTO 1991). The method recommended in these guidelines is based on the kinetic energy method, which determines the amount of energy that needs to be absorbed by the fender systems. This method requires the selection of a design vessel, a design impact speed, and the depth of the waterway.

The vessel selected for this study is the Jumbo Hopper barge, whose dimensions are presented in Fig. 4.1. This barge is commonly found in Florida, and is the only one that can conveniently navigate through waterways, since bridge openings can be as narrow as 18.3 m (60 ft), rendering the passage of large barges difficult, if not impossible. Florida waterways are also rather shallow and further restrict the navigation of barges with larger loaded drafts.

The design velocity was taken equal to the maximum current prediction for reference stations in Florida, since accidents involving barges and bridges are more likely to occur when barges are detached from towboats. The maximum current prediction obtained was 3.8 knots, as shown in App. A.1 (U.S. Department of Commerce, NOAA, NOS 1992), and was selected as the design impact velocity.

The depth of the waterway was also a required parameter for the determination of the equivalent static force. It was selected as 4.6 m (15 ft), which, according to nautical charts readings presented in App. A (Balder 1986, 1988, and Better Boating Association 1979) is the most common waterway depth in Florida, allowing the passage of the design barge (Fig. 4.2).

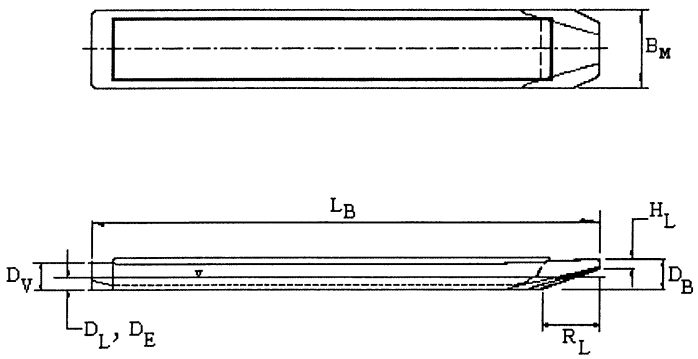

	AASHTO Designation	S.I. Units	U.S. Units
Length	L_B	59.4 m	195 ft
Width	B_M	10.7 m	35 ft
Depth of vessel	D_V	3.7 m	12 ft
Empty (light) draft	D_E	0.5 m	1.7 ft
Loaded draft	D_L	2.7 m	8.7 ft
Depth of bow	D_B	4.0 m	13 ft
Bow rake length	R_L	6.1 m	20 ft
Head log height	H_L	0.6 – 0.9 m	2 – 3 ft
Cargo capacity	C_C	1542.2 t	1700 tons
Empty displacement	W_E	181.4 t	200 tons
Loaded displacement	W_L	1723.7 t	1900 tons

Figure 4.1. Jumbo Hopper Barge Dimensions (AASHTO 1991)

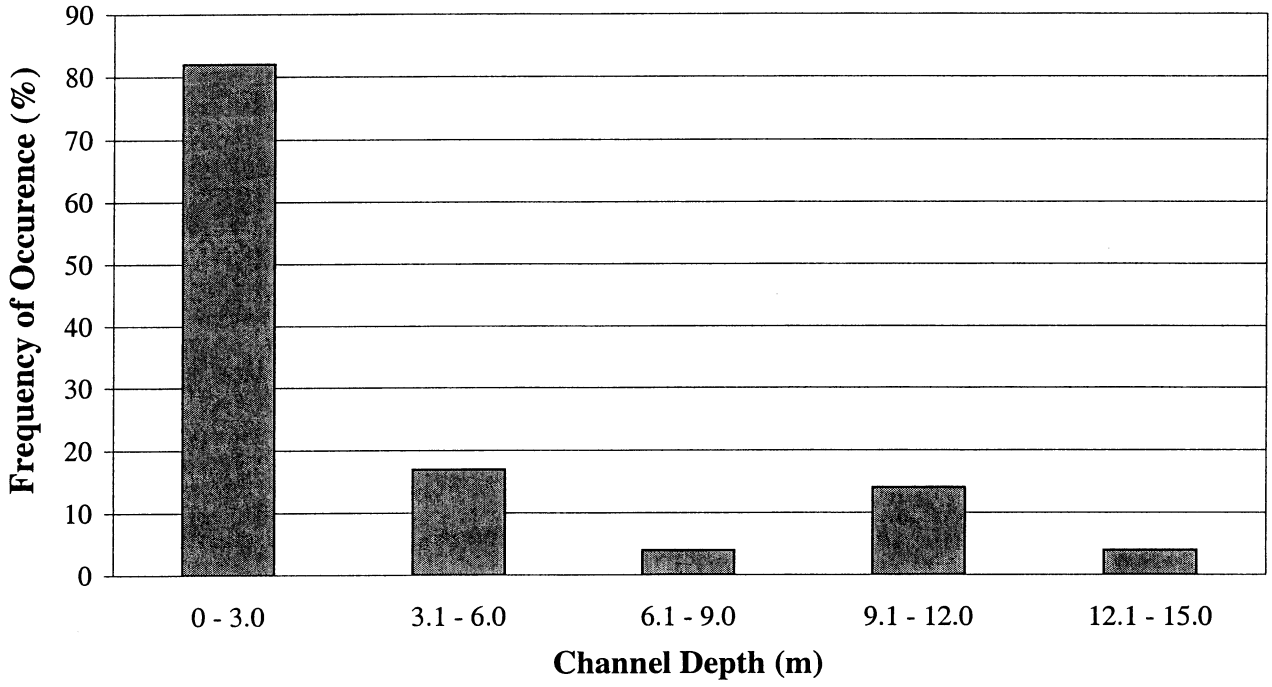

Figure 4.2. Florida's Most Common Channel Depths (Wilson 2000)

The impact force for a head-on collision involving the Jumbo Hopper barge was calculated as 7,112 kN (1,599 kips), according to Eqs. 2.1 to 2.5, presented in Ch.2. Calculations are presented in App. B.

CHAPTER 5

STATIC ANALYSIS OF EXISTING BRIDGE FENDERS

5.1. Introduction to ANSYS Software

ANSYS version 5.5 was the finite elements software used for the modeling and static analysis of the bridge fender systems. It was developed by Swanson Analysis Systems, Inc., now ANSYS, Inc. It can be used for structural, mechanical, thermal, electromagnetic, fluid, and couple-field analyses. The Structural Analysis part of ANSYS, which determines deformations, stresses, strains, and reaction forces, is most commonly used (ANSYS 1996).

5.2. Finite Element Model

5.2.1. Prestressed Concrete Piles Modeling

Details for the 355-mm (14 in) square prestressed concrete piles currently used by the FDOT in bridge fender systems were obtained from the FDOT Standard Drawings (1996) and are presented in Fig. 5.1. The length of both the batter and the plumb piles was determined as 12.4 m (40.7 ft), to include the 1.8 m (6 ft) extension above water level where timber wales are placed, the 4.6 m (15 ft) of waterway depth, and an embedded length of 6 m (19.7 ft), which is the minimum penetration into soft material required when no scour elevation has been specified in the plans (FDOT 1999). Concrete properties required for the modeling of the piles include modulus of elasticity of 24 GPa (3,481 ksi), Poisson's ratio of 0.2, and density of 2,400 kg/m^3 (4.7 slugs/ft^3) (Gere and Timoshenko 1997).

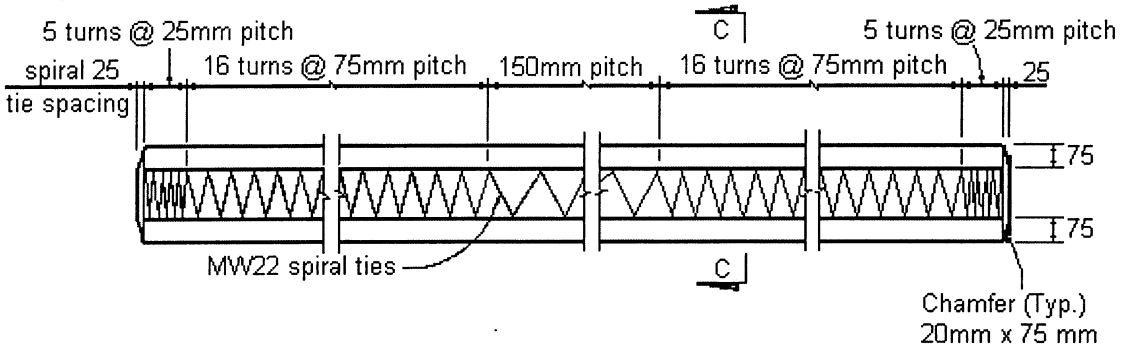

(a) Longitudinal Section

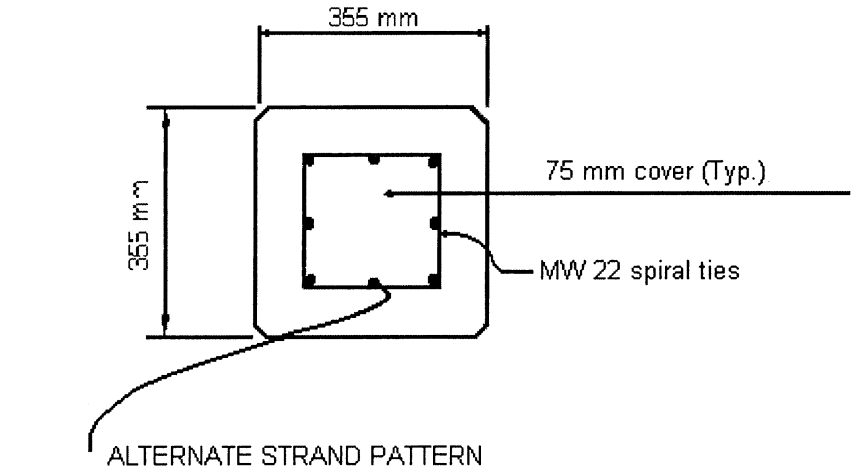

8 ~ No. 13, Grade 1860 (Spec.) LRS at 133.4 KN each
8 ~ No. 13, Grade 1860 (Spec.) SR at 140.4 KN each
8 ~ No. 13, Grade 1860 LRS at 131.2 KN each
12 ~ No. 11, Grade 1860 SR at 94.3 KN each
12 ~ No. 13, Grade 1725 SR at 100.5 KN each
16 ~ No. 9, Grade 1860 SR at 71.5 KN each

(b) Cross-Section C-C

Figure 5.1. Details for 355 mm Prestressed Concrete Pile (FDOT 1996)

The piles were modeled with SOLID65 – Reinforced Concrete Solid, which has eight nodes and three degrees of freedom at each node: translation in nodal x, y, and z directions. The mesh used consisted in 3 elements in each direction for the pile cross-section (Fig. 5.2), and 105 elements along the pile length. The elements obtained presented a 1:1:1 length to width to height aspect ratio, which reduces computational errors from individual stiffness matrices (Dietrich and Levy 1987).

5.2.2. Prestressing Strands Modeling

The alternate strand patterns that can be utilized in 355 mm (14 in) square prestressed concrete piles are presented in Fig. 5.1. The placement of the strands is specified as one strand at each pile corner, and the remaining, equally spaced between the corner strands (FDOT 1996). This report focused on the first pattern listed: 8 – No. 13, Grade 1860 (Spec.), low relaxation strands at 133.4 kN (30 kips). However, a comparison of other patterns is included. Prestress loss was taken as 310 MPa (45,000 psi) (AASHTO 1996), as shown in App. C.

The prestressing strands were modeled with LINK8 – 3-D Spar element, which is a uniaxial tension-compression element. It has two nodes with three degrees of freedom at each: translation in the nodal x, y, and z directions. The placement of the strands was restricted by the concrete mesh. In ANSYS the strands need to be placed on the concrete nodes to obtain the desired prestressing effect (Fig. 5.2). Since only four strands could be modeled, equivalent areas and strains had to be calculated to maintain the total amount of steel and prestress. These values were found to be 215.48 mm^2 (0.334 in^2) and 0.00464, respectively. Additional properties include modulus of elasticity of 200 GPa (29,000 ksi) and Poisson's ratio of 0.29 (Gere and Timoshenko 1997).

The piles were modeled with SOLID65 – Reinforced Concrete Solid, which has eight nodes and three degrees of freedom at each node: translation in nodal x, y, and z directions. The mesh used consisted in 3 elements in each direction for the pile cross-section (Fig. 5.2), and 105 elements along the pile length. The elements obtained presented a 1:1:1 length to width to height aspect ratio, which reduces computational errors from individual stiffness matrices (Dietrich and Levy 1987).

5.2.2. Prestressing Strands Modeling

The alternate strand patterns that can be utilized in 355 mm (14 in) square prestressed concrete piles are presented in Fig. 5.1. The placement of the strands is specified as one strand at each pile corner, and the remaining, equally spaced between the corner strands (FDOT 1996). This report focused on the first pattern listed: 8 – No. 13, Grade 1860 (Spec.), low relaxation strands at 133.4 kN (30 kips). However, a comparison of other patterns is included. Prestress loss was taken as 310 MPa (45,000 psi) (AASHTO 1996), as shown in App. C.

The prestressing strands were modeled with LINK8 – 3-D Spar element, which is a uniaxial tension-compression element. It has two nodes with three degrees of freedom at each: translation in the nodal x, y, and z directions. The placement of the strands was restricted by the concrete mesh. In ANSYS the strands need to be placed on the concrete nodes to obtain the desired prestressing effect (Fig. 5.2). Since only four strands could be modeled, equivalent areas and strains had to be calculated to maintain the total amount of steel and prestress. These values were found to be 215.48 mm^2 (0.334 in^2) and 0.00464, respectively. Additional properties include modulus of elasticity of 200 GPa (29,000 ksi) and Poisson's ratio of 0.29 (Gere and Timoshenko 1997).

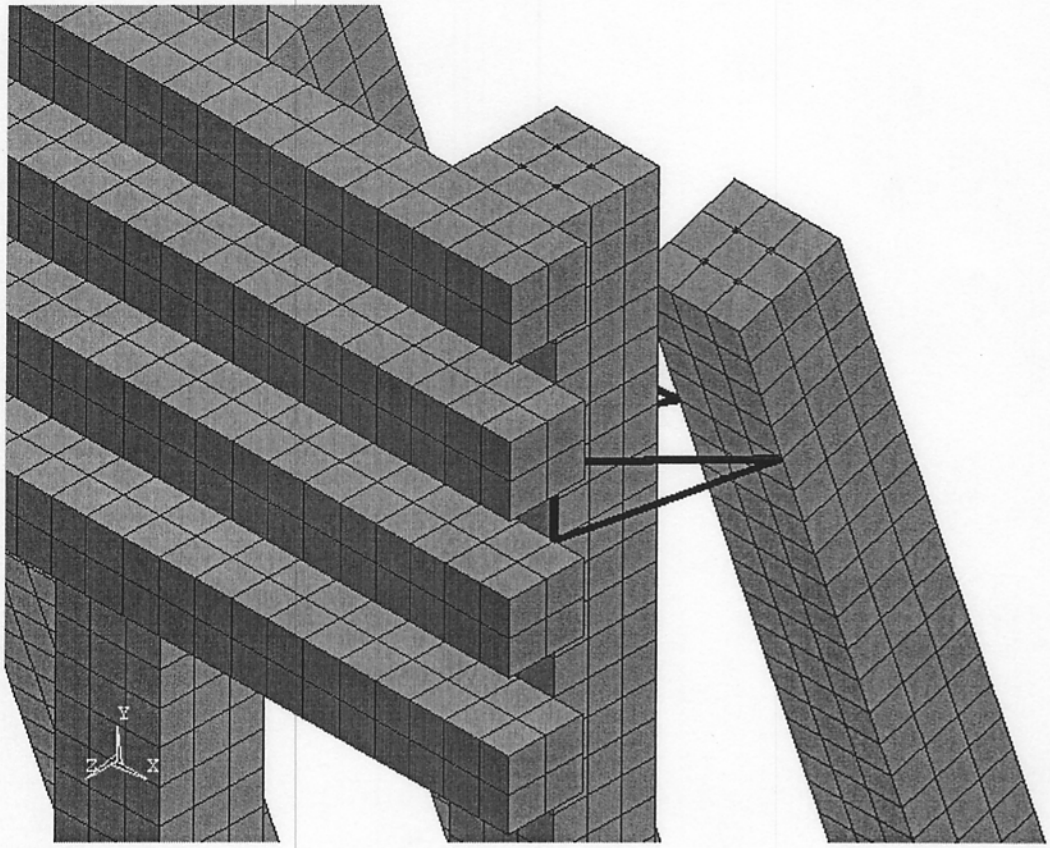

Figure 5.2. Detail of Finite Element Model Mesh (Wilson 2000)

5.2.3. Timber Wales Modeling

The timber wales are made of No. 3 Southern Pine (FDOT 1999) and are 4.875 m (16 ft) long covering the bay in a typical straight fender section. SOLID64 – Anisotropic Solid element was chosen for the modeling of timber. This element has eight nodes with three degrees of freedom at each, translation in the x, y, and z directions. The wales were meshed with 2 elements in each direction on the cross-section (Fig. 5.2), and 40 elements along the length. Orthotropic material properties used are presented in Table 5.1.

5.2.4. Cables Modeling

Cables used to connect the fender system piles are wrapped around the plumb piles and inserted through the batter ones. However, this configuration could not be used in ANSYS because it did not create sufficient contact area between the plumb and the batter piles for the program to consider the batter piles as part of the model. Therefore, a four member truss formed by LINK8 – 3-D Spar elements (Fig. 5.2) was used for the wire modeling. The two wire ropes consisted of 3 strands with 152 x 499 mm (6 x 19.6 in) outer diameter, black polypropylene impregnated space-lay galvanized. The properties required include modulus of elasticity of 200 GPa (29,000 psi) and Poisson's ratio of 0.29 (Gere and Timoshenko 1997).

5.2.5. Soil Modeling

The soil was modeled in the x and z directions with COMBIN14 – Spring-Damper element, which has two nodes with three degrees of freedom each: translation in the x, y, and z directions. These elements were placed on pile nodes at every 0.5 m (1.64 ft) along the embedded length of the piles (Fig. 5.3). Damping capabilities were removed, and the only

Table 5.1. Southern Longleaf Pine Properties (Bodig and Jayne 1993)

Property	SI Units	English Units
Density	500 kg/m^3	0.97 slugs/ft^3
Moduli of Elasticity:		
E_L	15.120 GPa	2,193 ksi
E_R	1.177 GPa	170.7 ksi
E_T	0.817 GPa	118.5 ksi
Shear Moduli:		
G_{LR}	0.925 GPa	134.1 ksi
G_{LT}	0.840 GPa	121.8 ksi
G_{RT}	0.112 GPa	16.25 ksi
Poisson's Ratios:		
ν_{LR}	0.37	0.37
ν_{LT}	0.42	0.42
ν_{TR}	0.35	0.35

where:

L = longitudinal axis

T = tangential axis

R = radial axis

required element properties were stiffness coefficients, which were determined according to tributary areas and soil reaction.

The soil type selected for this study was sand, since it represents most of the upper soil layers in Florida (Bice *et al.* 1989). The method selected for the soil reaction determination is described in Tomlinson (1987) and includes the use of equations developed by Matlock and Reese (1960) and p-y curves. These equations are presented below and are only valid for deflections in the elastic range of the soil:

$$y = \frac{A_y H T^3}{EI} + \frac{B_y M_t T^2}{EI} \tag{5.1}$$

$$T = \sqrt[5]{\frac{EI}{k}} \tag{5.2}$$

$$M_t = He \tag{5.3}$$

$$p = \frac{A_p H}{T} + \frac{B_p M_t}{T^2} \tag{5.4}$$

where:

y = deflection

A_y = soil reaction coefficient relative to depth x

H = lateral load applied to the pile

E = modulus of elasticity

I = moment of inertia

T = stiffness factor

B_y = soil reaction coefficient relative to depth x

M_t = moment at ground surface

k = subgrade reaction

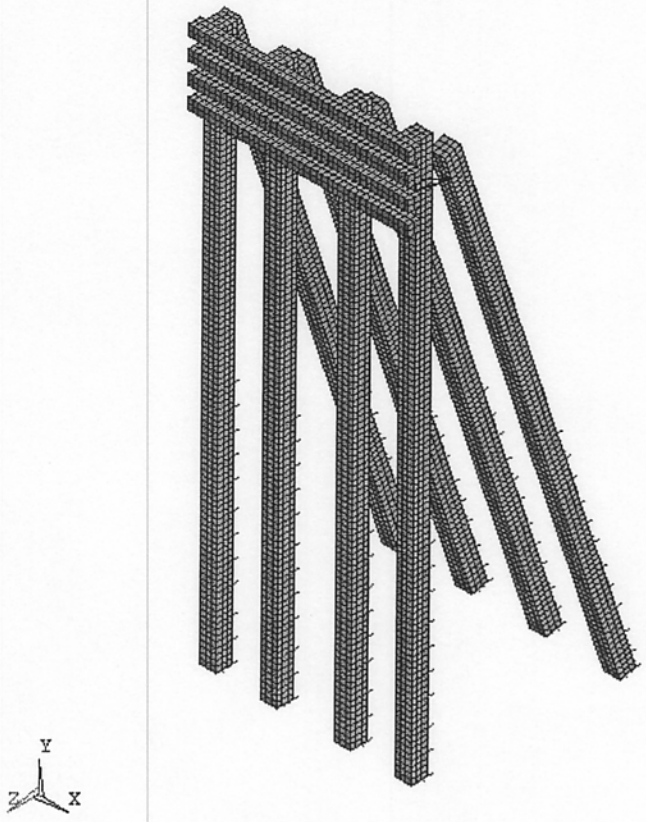

Figure 5.3. Springs Representing Soil Reaction (Wilson 2000)

e = distance from the ground surface to the lateral load

p = soil reaction

A_p = soil resistance coefficient

B_p = soil resistance coefficient

These equations can be calibrated by the use of p-y curves which consider the nonlinear relationship between the soil lateral resistance and the pile deflection. Since these methods only evaluate single piles, the magnitude of the load resisted by each pile and the soil behind it had to be determined prior to the analysis. Therefore, it was assumed that both the plumb and the batter piles would displace by the same amount. Equation 5.1 was then used to calculate the displacement of both the plumb and the batter pile caused by the application of different percentages of the load on each pile. After several trials, the deflections of the plumb and batter piles were found to be similar for 60 and 40 % of load application, respectively. Equation 5.4 was used to determine the soil reactions, which were then calibrated by p-y curves developed for every 0.5 m (1.64 ft) along the embedded length of the piles. Stiffness coefficients were calculated according to Eq. 5.5:

$$k = \frac{p}{y} \tag{5.5}$$

All calculations are presented in Apps. D and E.

Since only the downward movement needed to be restrained in the y direction, soil reaction was represented by the application of pressure, equivalent to the pile weight, to the bottom of the plumb piles and the lower side of the batter piles.

CHAPTER 6

SUMMARY RESULTS OF STATIC ANALYSIS

Linear analyses of the model were performed for both full impact load application, and 33% of such load, since it would be unreasonable to design fender systems capable of absorbing the total collision energy. The absorption of 33% of the force, without significant damage, would signify a possible reduction in the design impact load used in bridges.

The impact force was applied to the model as a pressure on the two middle timber wales, according to tributary areas and barge geometry. The modeling of only one fender bay assumes that the fender system does not behave as a continuous structure, that is, each bay absorbs the load applied to it with no collaboration from adjacent bays. This assumption is based on the weakness of the connections between the piles and the bays, which consist of only two cables.

The maximum displacements and stresses obtained are presented in Figs. 6.1 to 6.4. The maximum stresses, also presented in Tables 6.1 and 6.2, were compared to the material strengths, which are presented in Table 6.3. The compressive and tensile stresses on the piles, resulting from both 33 and 100% of load application, were greater than the compressive and tensile strength of concrete, respectively. Stresses on the timber wales include tensile stress parallel to grain, as well as compressive stresses parallel and perpendicular to grain. All stresses for both 33% and 100% of impact load were found to be greater than the respective timber strength. According to these results, failure of both the piles and the timber wales occurred even when only 33 % of the impact load was applied.

All cable elements had compressive axial force, indicating slack, confirming the assumption that connection between piles was weak and no collaboration existed between bays.

Figure 6.1. Nodal Displacements of Model with 33% of Impact Load (Wilson 2000)

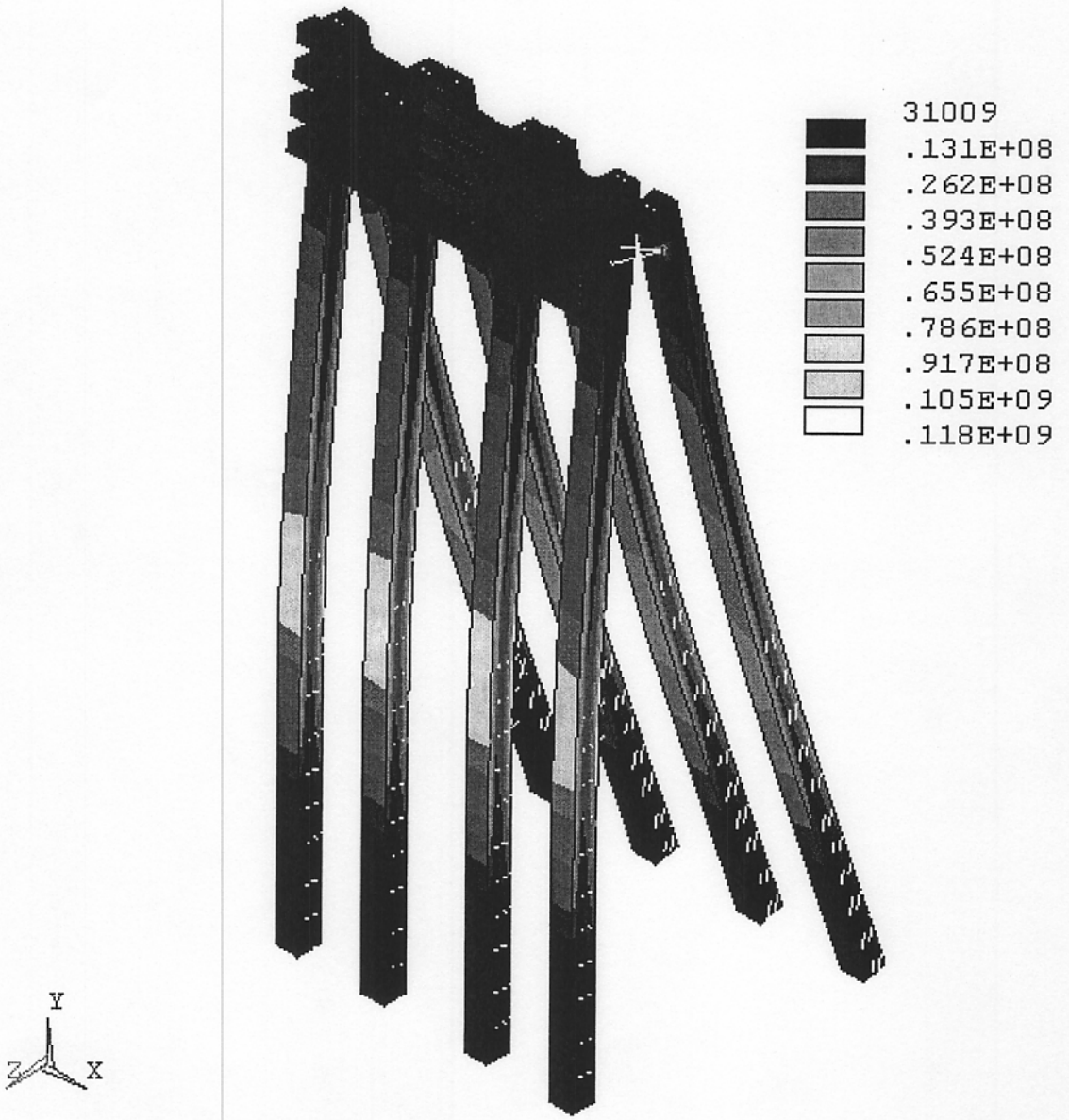

Figure 6.2. Nodal Stresses of Model with 33% of Impact Load (Wilson 2000)

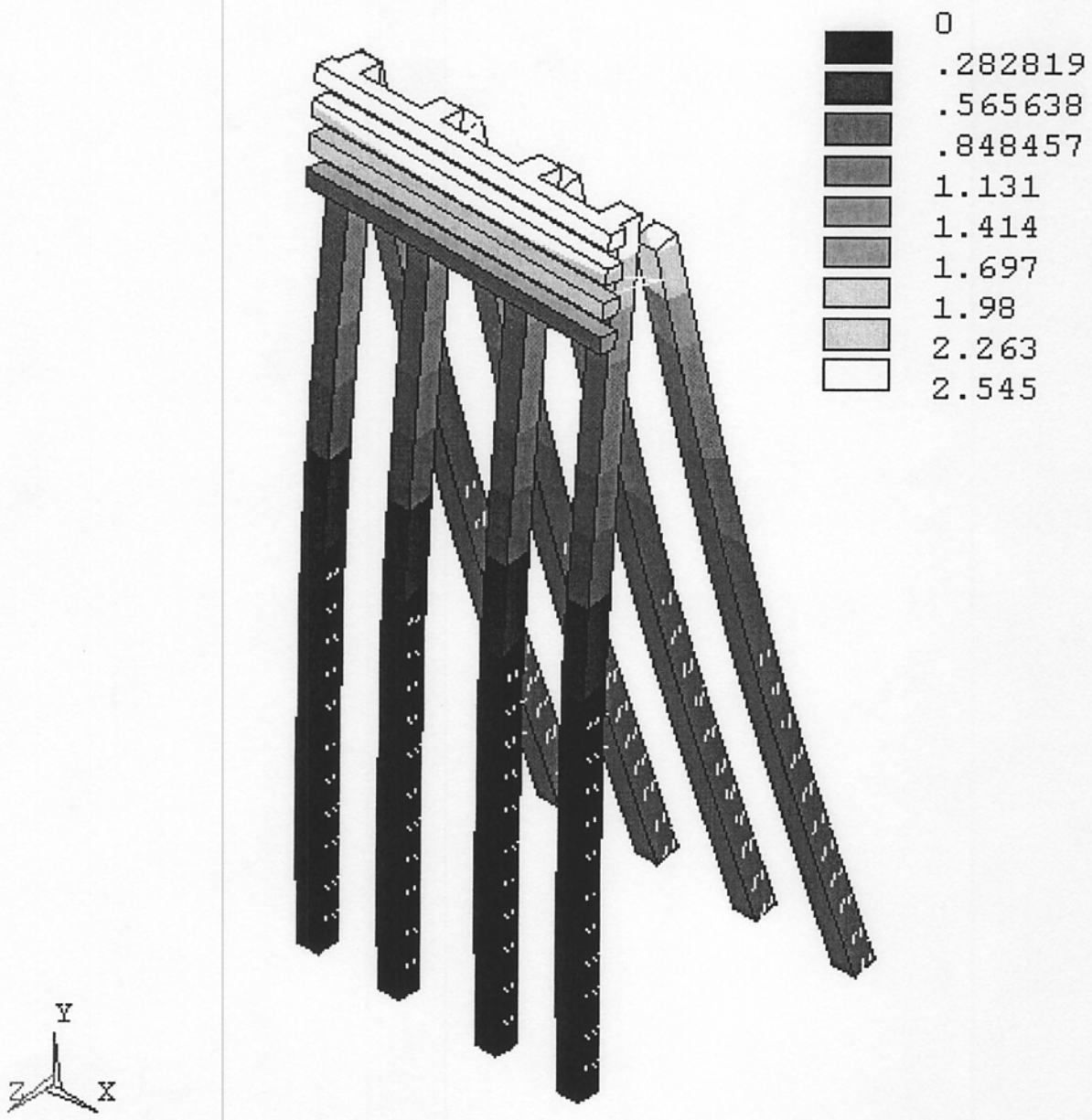

Figure 6.3. Nodal Displacements of Model with 100% of Impact Load (Wilson 2000)

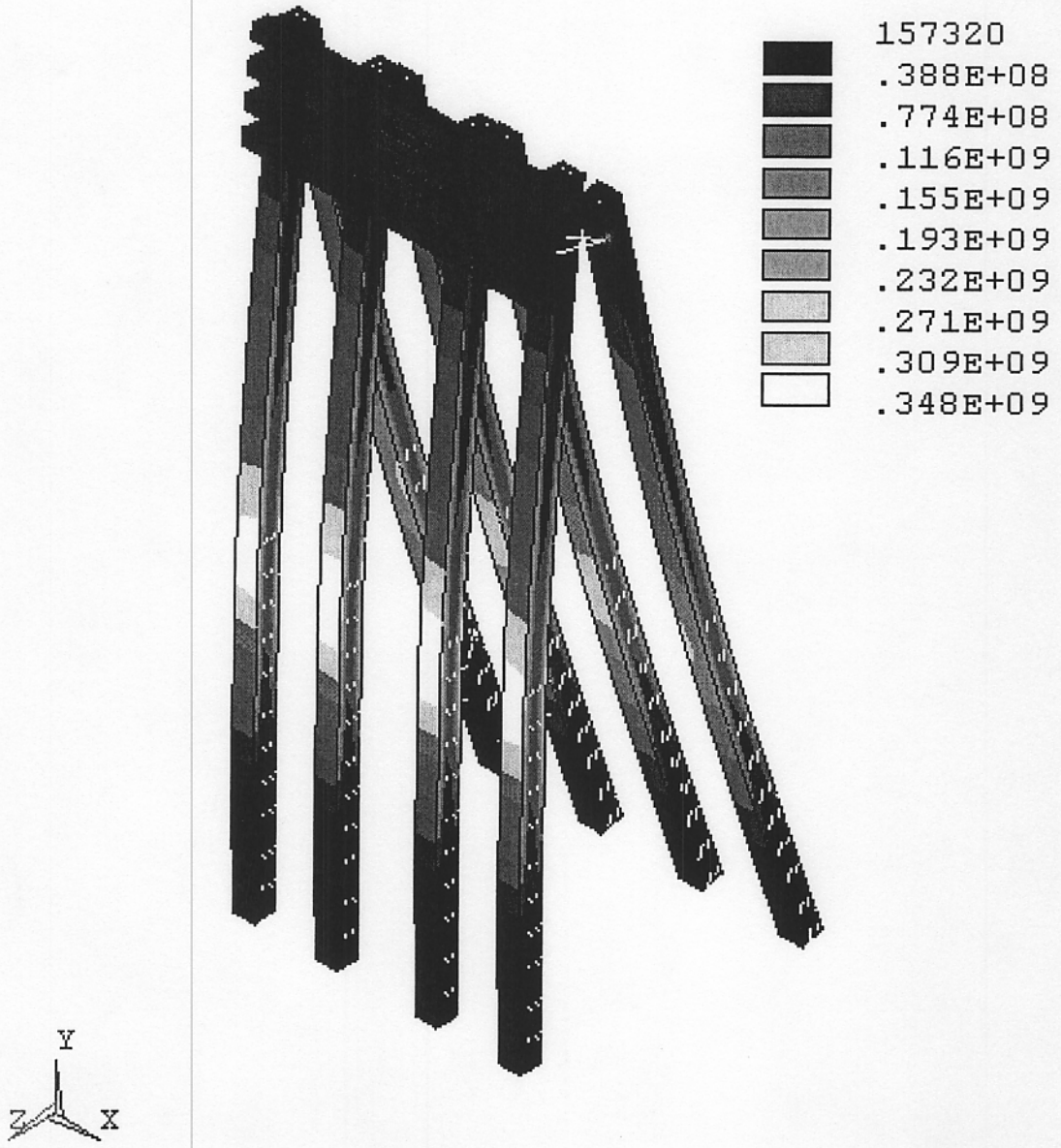

Figure 6.4. Nodal Stresses of Model with 100% of Impact Load (Wilson 2000)

Table 6.1. Maximum Stresses Resultant from 33% Impact Load (Wilson 2000)

	(MPa)	(ksi)
Plumb concrete piles		
Maximum tensile stress	105	15.23
Maximum compressive stress	118	17.06
Batter concrete piles		
Maximum tensile stress	88	12.83
Maximum compressive stress	101	14.72
Timber wales		
Maximum compressive stress parallel to grain (x direction)	18	2.59
Maximum tensile stress parallel to grain (x direction)	17	2.50
Maximum compressive stress perpendicular to grain (y direction)	6	0.91
Maximum compressive stress perpendicular to grain (z direction)	8	1.17

Table 6.2. Maximum Stresses Resultant from 100% Impact Load (Wilson 2000)

	(MPa)	(ksi)
Plumb concrete piles		
Maximum tensile stress	334	48.42
Maximum compressive stress	347	50.31
Batter concrete piles		
Maximum tensile stress	284	41.16
Maximum compressive stress	298	43.21
Timber wales		
Maximum compressive stress parallel to grain (x direction)	54	7.84
Maximum tensile stress parallel to grain (x direction)	52	7.58
Maximum compressive stress perpendicular to grain (y direction)	12	1.73
Maximum compressive stress perpendicular to grain (z direction)	23	3.36

Table 6.3. Strength of Materials (Wilson 2000)

	(MPa)	(ksi)
Concrete		
Compressive strength	41	5.95
Tensile strength (Nawy, 1996)	4	0.59
Timber (AFPA and AWC, 1997)		
Tensile strength parallel to grain	8	1.20
Compressive strength parallel to grain	8	1.10
Compressive strength perpendicular to grain	3	0.44

Models were also created with the alternate strand configurations presented in Subsection 5.2.2, and analyzed for 33% impact load. Stress intensity was found to be very similar for all configurations. Maximum stresses obtained are presented in Table 6.4, where the following notation is used for simplicity:

A : 8 No. 13, Grade 1860 (Spec.) SR at 140.4 kN each

B: 8 No. 13, Grade 1860 LRS at 131.2 kN each

C: 12 No. 11, Grade 1860 SR at 94.3 kN each

D: 12 No. 13, Grade 1725 SR at 100.5 kN each

E: 16 No. 9, Grade 1860 SR at 71.5 kN each

Table 6.4. Maximum Stresses on Piles Due to 33% Impact Load for Alternate Strand Configurations (Wilson 2000)

Strand Pattern	Maximum Compressive Stresses			Maximum Tensile Stresses		
	MPa	ksi	% difference	MPa	ksi	% difference
A	118.03	17.12	+ 0.36	104.59	15.17	- 0.41
B	117.48	17.04	- 0.11	105.14	15.25	+ 0.11
C	117.96	17.11	+ 0.30	104.54	15.16	- 0.46
D	116.54	16.90	- 0.91	104.15	15.11	- 0.83
E	118.11	17.13	+ 0.43	104.45	15.15	- 0.54

CHAPTER 7
DYNAMIC MODEL OF EXISTING BRIDGE FENDERS

7.1. Introduction

DYNA3D, a non-linear explicit three-dimensional finite element code was released by Lawrence Livermore National Laboratory (LLNL) in 1976. It became public domain in the late 1980s. The code was used for analysis of large displacement dynamic responses between two deformable bodies. Its unique feature of contact-impact algorithm was originally utilized in analysis for classified military applications. Since 1980, several new versions of the program have been released. The code deals with high nonlinearities, such as large deformations, material failure, and contact problems.

LS-DYNA was released by Livermore Software Technology Corporation (LSTC) as a derivative of the public domain DYNA3D. This version of the code supported the automotive and transportation applications particularly well. Several vehicle crash oriented features, such as models of airbag, seatbelts, and accelerometers, were introduced and made the software a very suitable tool for computational analysis of crash impacts.

7.2. Impacting Vessel Model

A special attention was paid throughout the project to model impact conditions as realistically as possible. Following the static analysis, a Jumbo Hopper barge was selected as the impacting vessel with the collision speed was set to 1.955 m/sec (3.8 knots).

The major goal of the project was an assessment of the lateral resistance of the fender system. Thus, the impacting vessel model should be only as accurate as it is necessary to provide sufficient and reliable information about general dynamic behavior of the vessel and its

influence on the fender. Two areas of the barge were identified for meshing. The rear of the barge (representing the cargo area) was modeled with coarse mesh, while the front of the barge was modeled with finer mesh. For the most reliable results, LS-DYNA contact algorithm requires similar size of meshes for both contacting bodies. Thus, the front of the vessel was modeled using shell elements of size matching those of the fender. As for modeling the cargo, the density of the rear of the barge was scaled to provide correct displacement of the barge. Eventually the barge model consisted of 7,685 shell elements and 128 solid elements (Fig. 7.1).

The model was assumed as moving on a frictionless horizontal rigid surface; thus, gravity was not applied. Table 7.1 presents dynamic properties of the finite element model obtained from the code. They demonstrate the need for the structure to absorb an amount of kinetic energy, which is unprecedented in civil engineering analysis. For comparison, a pickup truck impacting a barrier with a velocity of 100 km/h (62 mph) represents a kinetic energy value of 171.2 kJ, 5 % of that of the barge.

7.3. General Provisions of the Fender Model

The dynamic finite element model of the bridge fender consisted of square prestressed concrete piles embedded in soil. The section width taken as the distance from both ends of a wale is 4.875 m (16 ft). A fender system may consist of several sections, depending on the bridge width. For this study, a response of three sections, with overall width of 14.630 m (48 ft), was analyzed (Fig 7.2).

The model of the original fender consisted of 19,924 solid elements and 8,008 beam elements, from which 7,327 were subjected to initial stress. The model also included 1,320 non-linear springs attached to the piles to model soil response. Detailed description of the components is provided in the following.

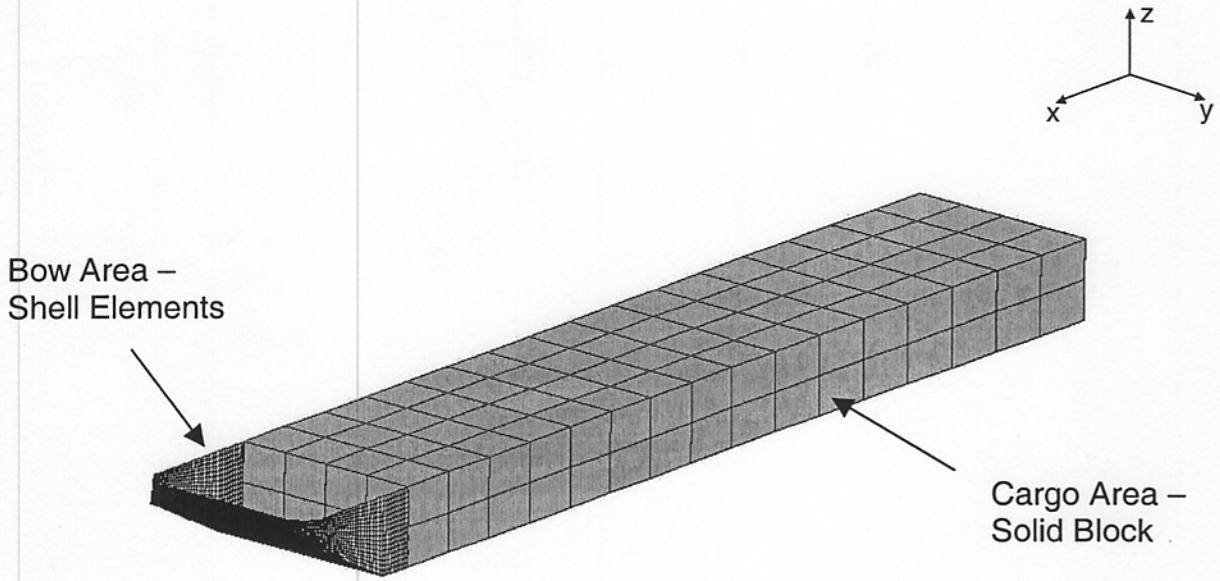

Figure 7.1. Finite Element Model of the Barge

Table 7.1. Kinetic Properties of Barge Model

	SI Units	US Units
Mass (loaded displacement)	1723.7 t	1900 ton
Kinetic energy	3,291 kN·m (kJ)	2,378 kip-ft
Center of gravity height	1.92 m	6.78 ft
Moment of inertia about centroid I_{xx}	22,218 $t \cdot m^2$	263,600 ton-ft^2
Moment of inertia about centroid I_{yy}	415,456 $t \cdot m^2$	492,900 ton-ft^2
Moment of inertia about centroid I_{zz}	430,721 $t \cdot m^2$	511,000 ton-ft^2

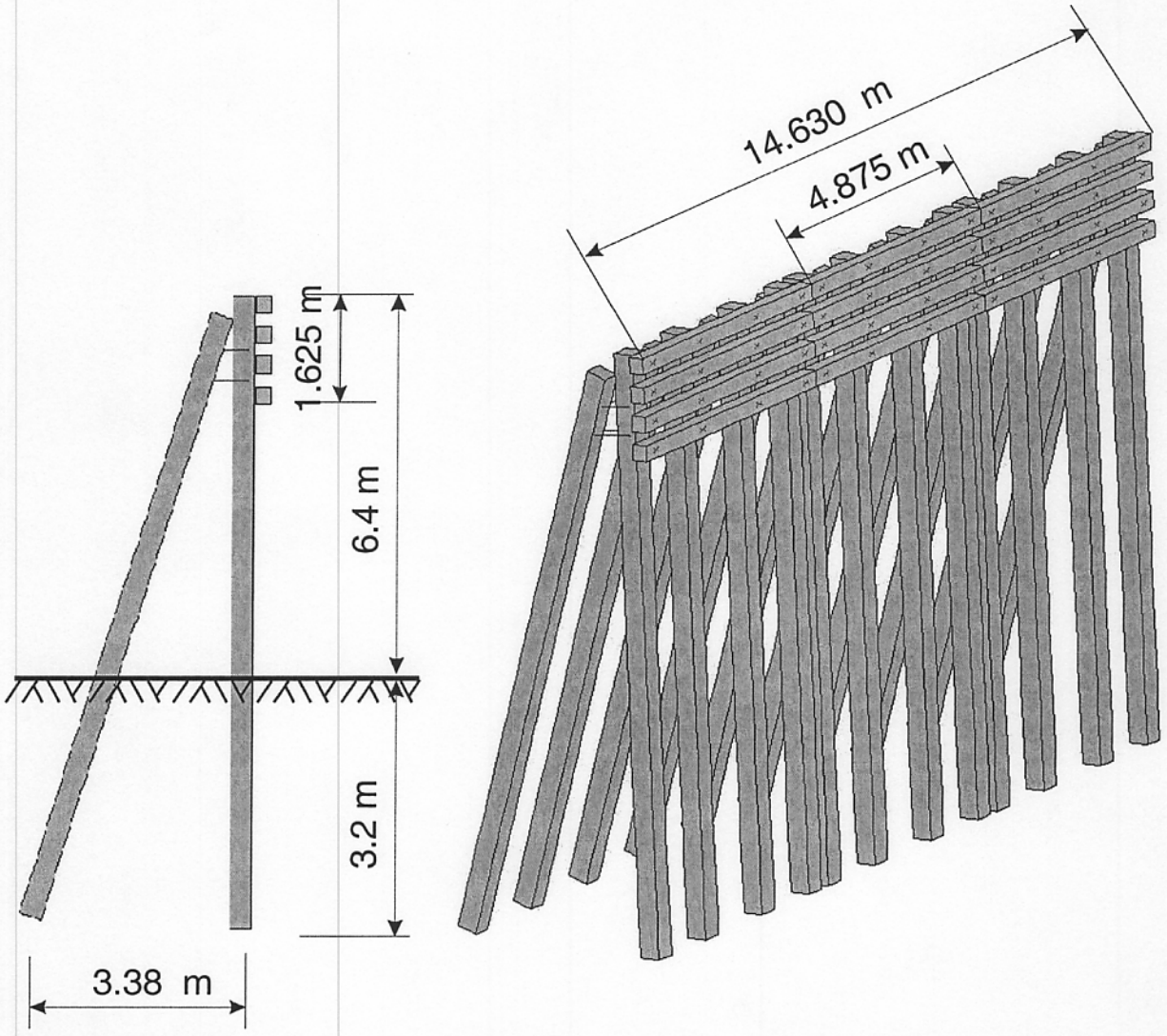

Figure 7.2. Three Sections of Bridge Fender

7.4. Prestressed Concrete Piles

7.4.1. Pile Properties

The original fender consisted of concrete prestressed square piles of 355 mm (14 in) and 9.6 m (31.5 ft) long. Figure 7.2 depicts configuration of battered and plumb piles. The assumed depth of pile embedment in soil was 3.2 m below the channel bed. The piles were modeled using solid elements with a 4 by 4 pattern, matching the strand pattern used (Fig. 7.6).

7.4.2. Concrete modeling in LS-DYNA

LS-DYNA material Pseudo-Tensor (Material 16) seems to be the most popular constitutive material model used in crashworthiness analysis (Wekezer *et al.* 1996). It has been recognized that the model doesn't account for bi- and tri-axial concrete failure, i.e. the overall behavior appears to be stiffer than actual. A new model of concrete for DYNA3D has been recently introduced and presented (Malvar *et al.* 1997). However, it is not available for LS-DYNA yet. The used model has complex non-linear behavior (LS-DYNA 1999). Plastic behavior is described by the following.

$$\sigma_{yield} = \sigma_{failed} + \eta(\sigma_{\max} - \sigma_{failed}) \tag{7.1}$$

where:

$$\sigma_{\max} = a_0 + \frac{p}{a_1 + a_2 p},$$

$$\sigma_{\text{failed}} = a_{0f} + \frac{p}{a_{1f} + a_2 p} \quad \text{(Fig. 7.3)},$$

p is pressure, η is a scale factor dependent on effective plastic strain and shown in Fig. 7.3. The coefficients $a_0, a_{0f}, a_1, a_{1f}, a_2$ and material properties used in analysis are presented in Table 7.2.

The model also uses an equation of state as relationship between volumetric strain and pressure p, as shown in Fig. 7.4.

7.4.3. Prestressing Strands Modeling

Eight (8) Grade 1860 low relaxation strands were assumed and modeled for each pile. The jacking force was 133.4 kN per strand. The strand cross-section area was determined as 98.71 mm^2. Thus, the prestress applied to each strands was 1,351.4 MPa.

Prestressing strand can be modeled as a nodal force at the pile end, or using explicit truss elements subjected to initial stress or deformation. The first method was chosen in initial project stage to save computational time. A follower force perpendicular to the surface was used (Fig. 7.6a). However, the study showed that it developed unrealistic excessive buckling in the late stages of impact. Impulse from the impact introduced large imperfections, causing pile buckling (Fig. 7.7). The truss option was chosen for further analysis. The strands were modeled using explicit truss elements having common nodes with piles (Fig. 7.6b). The stress, applied to all truss elements after prestress losses, was 1041.4 MPa. Specific calculations are presented in App. C.

7.5. Timber Wales

7.5.1. Properties

Each section of the fender consists of four 7.875 m (25.8 ft) long square timber wales 254 mm (10 in) wide. They were modeled using block elements, three on each side of the cross-section.

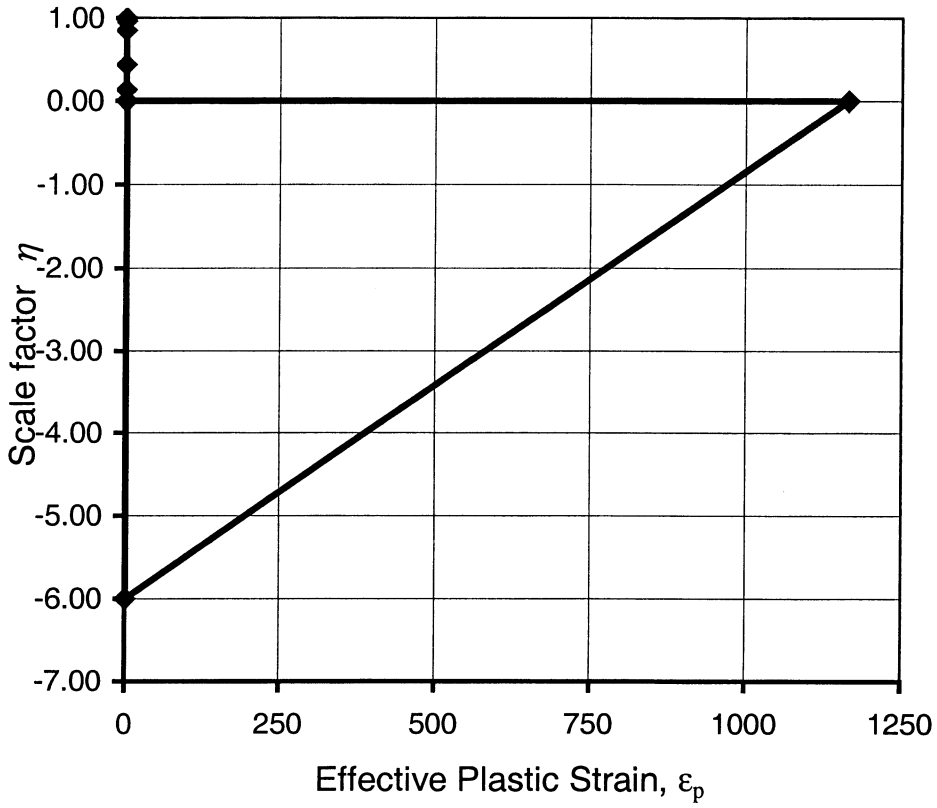

Figure 7.3. Curve for Scale Factor η

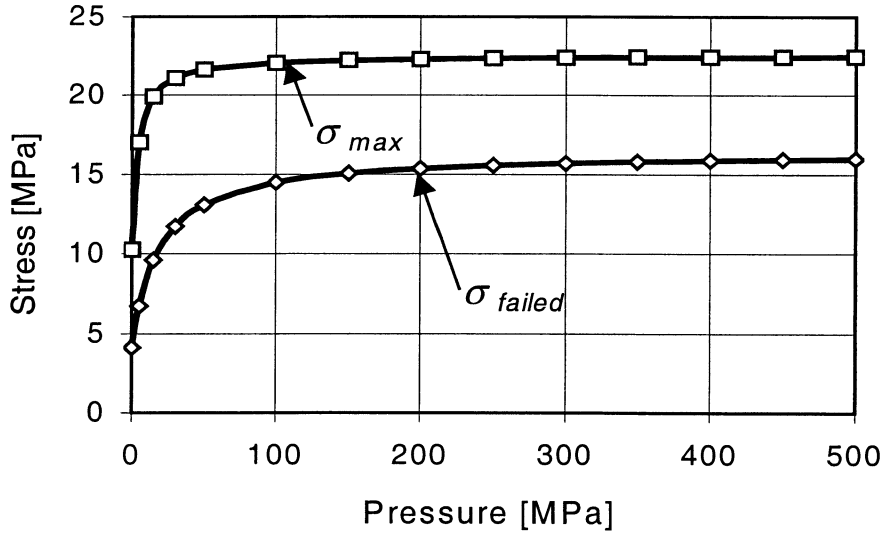

Figure 7.4. Assumed Curves for σ_{max}, and σ_{failed} (Eq. 7.1)

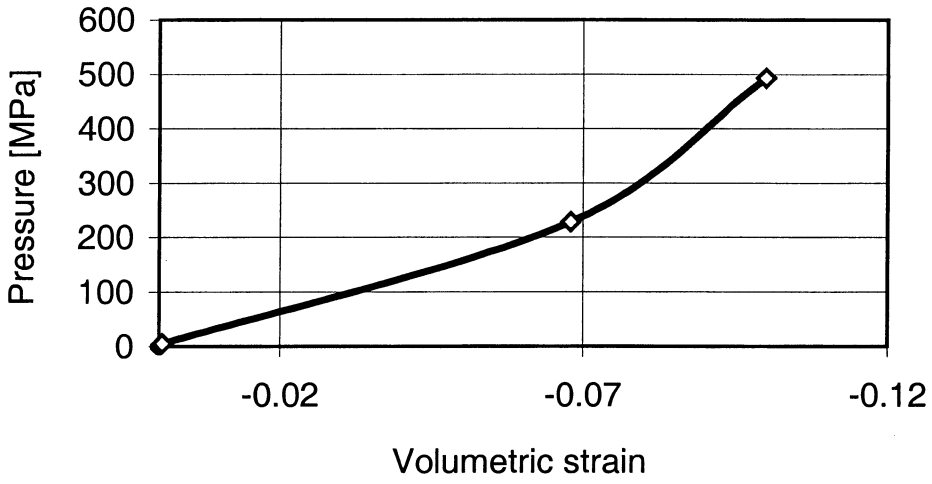

Figure 7.5. Graph of the Assumed Equation of State for Material no. 16 (Whirley and Engelmann, 1993)

Table 7.2. Concrete Properties of Material Model Used for Computations

	SI Units	US Units
Density ρ	2,400 kg/m^3	150 pcf (weight)
Shear modulus G	1000 MPa	145 ksi
Poisson ratio ν	0.2	
Tensile cutoff σ_f	4.10 MPa	595 psi
Cohesion (Eq. 7.1) a_0	10.25 MPa	1.487 ksi
Pressure hardening coefficient (Eq. 7.1) a_1	0.3333	
Pressure hardening coefficient (Eq. 7.1) a_2	$3.13 \cdot 10^{-3}$ mm^2/N	$2.2 \cdot 10^{-5}$ in^2/lb
Cohesion for failed material (Eq. 7.1) a_{1f}	4.10 MPa	595 psi
Pressure hard. coeff. for failed material (Eq. 7.1) a_{1f}	1.5	
Damage scaling factor b_1	0.0	
Damage curve	Defined in Fig 7.4 (SI units only)	
Equation of state	Defined in Fig. 7.5 (SI units only)	
Percent reinforcement	$p_r = 0.00$ %	

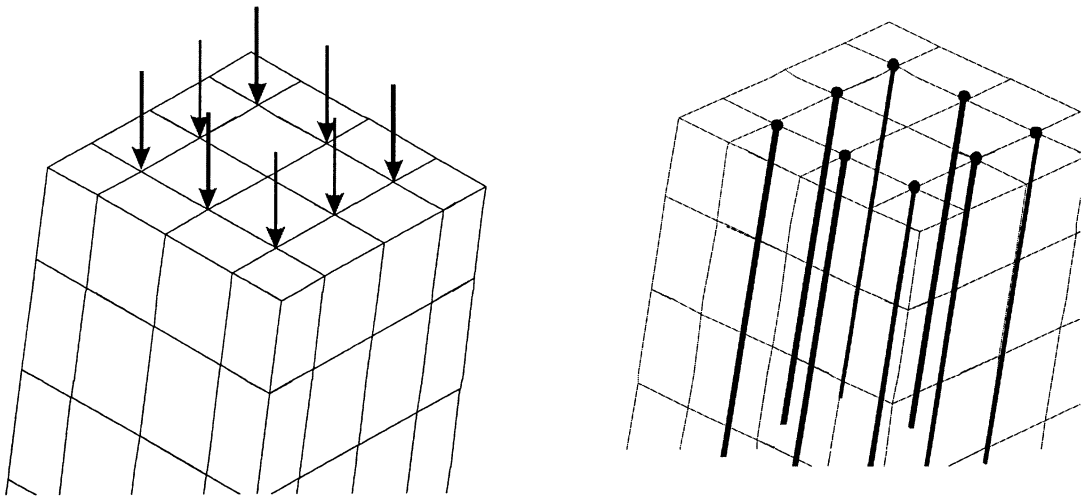

a) Forces Applied on the Pile End

b) Strands Modeled Explicitly

Figure 7.6. Modeling of Prestressing Strand Pattern

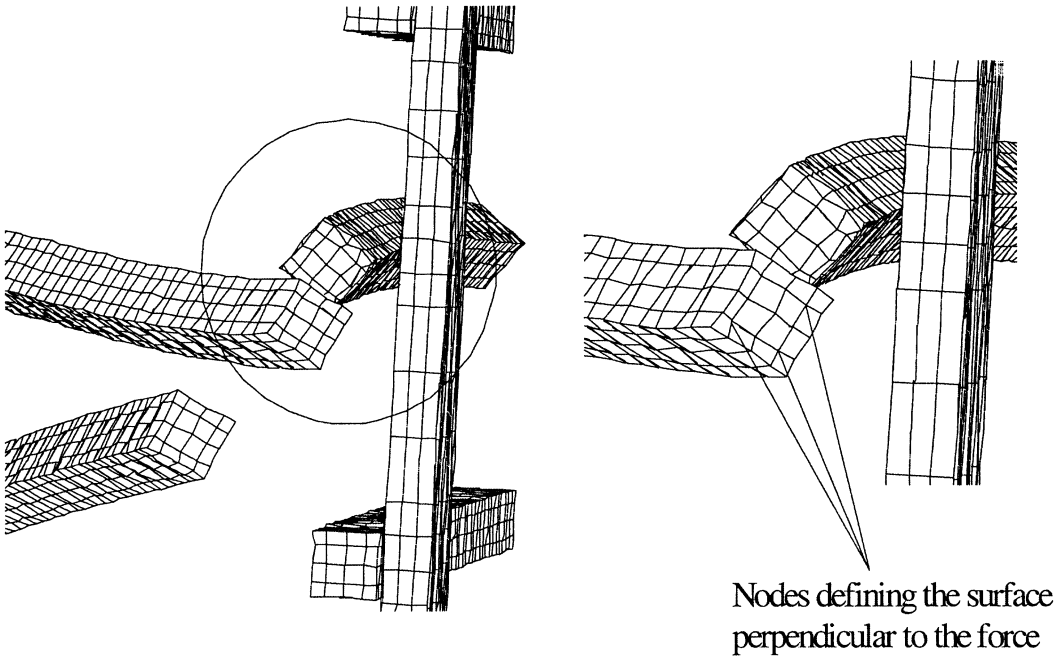

Figure 7.7. Excessive Buckling of Piles with Prestressing Force Applied to Pile Ends

7.5.2. Wood Model in LS-DYNA

Wood is an anisotropic material with complex behavior. Ray successfully used isotropic material with failure in modeling BCT timber post, when the main concern was acceleration and velocity histories of the impactor (Ray *et al.* 1997). In the current study, the wales were modeled using an isotropic material with piecewise plasticity curve (Material 24) and failure (LS-DYNA 1999).

7.6. Bolted Connections

Previous studies have used 20 percent tensile elongation or one-diameter displacement (shearing and bearing of the bolt) for bolts as failure criteria (Wekezer *et al.* 1996). A similar approach was used herein for models of bolt connections. The system of one truss element constrained to four beams was used, as shown in Fig. 7.8.

The spotwelded constraint allows using the following failure criterion:

$$\left(\frac{f_n}{S_n}\right)^2 + \left(\frac{f_s}{S_s}\right)^2 \geq 1 \tag{7.2}$$

where *f, S*, are the actual and maximum forces, and *n* and *s* indices indicate normal and shear forces, respectively (LS-DYNA 1999). AASHTO M164M - ASTM A 325M 22 mm diameter bolt was assumed with effective area of 303 mm^2. The tensile limit of the bolt is $S_n = 251kN$ and the shear limit is $S_s = \frac{S_n}{\sqrt{3}} = 144.9kN$. The linear elastic behavior of the system was assumed before its failure.

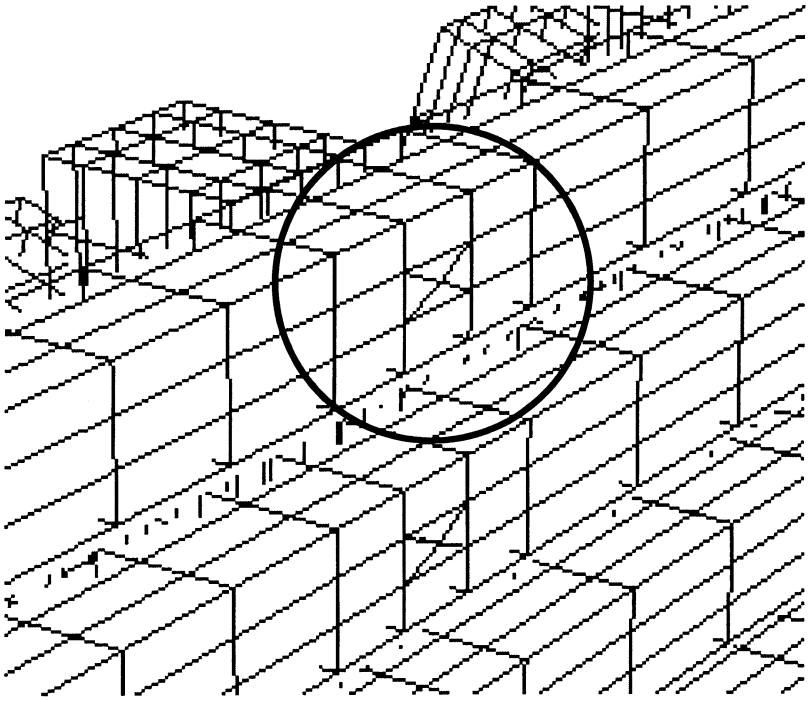

a) Beam-Grid System Merged with the Wale Mesh

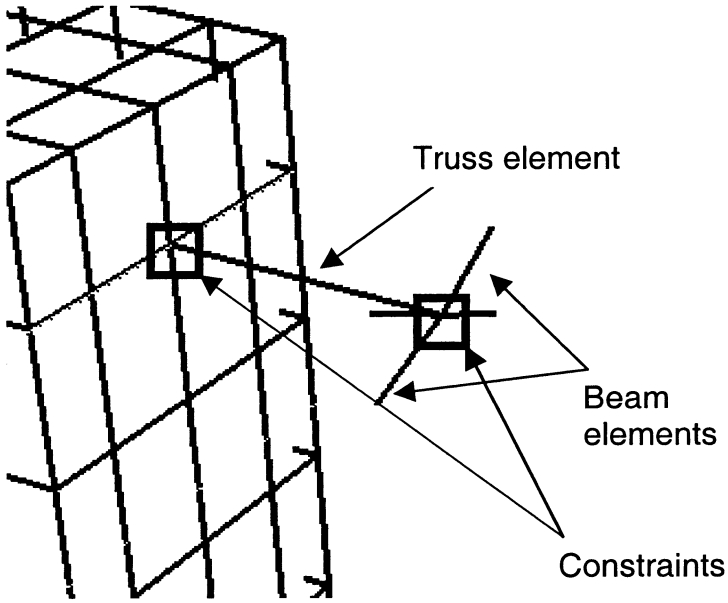

b) Truss Element Constrained on Both Sides (Wale Removed from the View)

Figure 7.8. Bolted Connection Model

7.7. Cables Connecting Piles

The head cables were also modeled using truss elements. Within the whole length of a modeled cable, several elements were introduced adjacent to each other. A chain of truss elements with no flexural strength was used to model each head connection. The cables were tied to piles also using spotwelded constraints with failure criteria. The maximum tensile force is the cable strength $S_n = 101.46\,kN$, provided by the manufacturer. Shear strength was assumed significantly larger than the tensile strength to ensure a small value of the second term in Eq. 7.2. Therefore, the tensile failure of the cable is predominant due to the small value of the shear component in the equation.

7.8. Soil-Pile Interaction

The piles were assumed to be driven to a depth of 3.2 m below the channel bed. Saturated sand was assumed as a typical soil. Table 7.3 presents the soil properties used. The soil was modeled using the subgrade modulus approach. The array of non-linear springs was attached to a pile. The horizontal subgrade modulus defines the stiffness of the non-linear springs, which represent the soil resistance. A variety of different methods of determining the modulus has been presented in literature. This study follows the method described by Habibagahi and Langer and applied for the modeling of the interaction between BCT post and granular non-cohesive soil by Plaxico (Habibagahi and Langer 1983, Plaxico *et al.* 1998).

The springs were attached to the pile at nodal points in both directions (Fig. 7.9). Subgrade modulus was lumped to a nodal force dependent on displacement of the node.
The force-displacement relationship of the spring is given by:

$$F = k_h y \tag{7.3}$$

Table 7.3. Soil Properties Used in Computations

Unit weight	1.81 N/mm^3 (6.665 kip/in^3)
Internal friction angle	30°
Saturation	85 %
Specific gravity	2.65

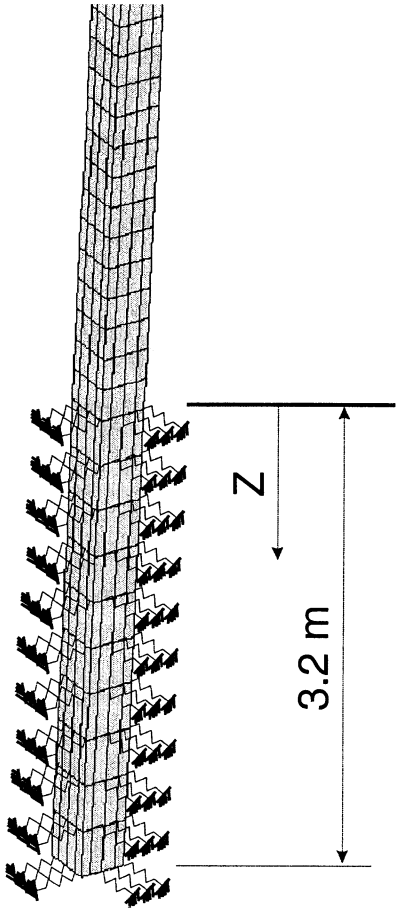

Figure 7.9. Array of Springs Attached to the Pile

where F is the horizontal reaction, k_h is the subgrade modulus, and y is the resulting displacement. For granular non-cohesive soil, the modulus value is given by:

$$k_h = N_q \frac{\sigma_e}{y} \tag{7.4}$$

where σ_e is the overburden stress depending on the type, void ratio, saturation and density of the soil. The saturation was assumed as 85% instead of 100% for two reasons. First, the formula for σ_e does not allow for 100% saturation (the obtained values are nonsense). Second, the study of Duncan *et al.* (1980) presented a variety of parameters for 80 different soils at several sites. The sands listed had initial saturation ratio bounded by 85%. N_q is a lateral bearing capacity factor given by:

$$N_q = MF\left(A + \sqrt{\frac{Z}{B}}\right) \tag{7.5}$$

MF is a modifying factor depending on internal friction angle, A is a semi-empirical non-dimensional function depending on the internal friction angle and depth Z below the ground level, and B is width of the pile. Thus, the subgrade modulus is a non-linear function dependent upon the soil properties, displacement, and the Z depth below the channel bed.

CHAPTER 8

DYNAMIC ANALYSIS OF EXISTING FENDER SYSTEMS

8.1. Collision Scenarios

Several initial conditions, including barge impacts at 90, 45, 30, and 15 degrees, were considered (Fig. 8.1). This matrix was intended to represent many possible scenarios of a severe collision. As shown in the following analyses, these different initial angles produced essentially different demands on the structure.

8.2. Impact at 90 Degrees

Although rare, impact at 90 degrees is possible when the bridge fender is wrapped around the pier and the barge is drifting towards the pier. It is seen from the results of analyses that the barge produced severe damage to the fender during this impact. The cables connecting the piles failed in the early stage of the collision (Fig. 8.2), which resulted in insufficient interaction between piles. As a result, the piles had to absorb the impact energy independently (Fig. 8.3).

Failure of the pile was assumed when effective plastic strain in concrete exceeded a value of 0.03. This level of failure strain was detected in several areas of the piles at approximately t=800 msec, as shown on Fig. 8.4.

During the first 800 msec, the resultant velocity of the center of mass of the barge decreased from 3.8 knots to 3.1 knots (0.7 knots drop). This represents 18% drop of speed. The collision dissipated approximately 30 percent of the kinetic energy of the barge. This decrease may vary with the different soil conditions for actual structures.

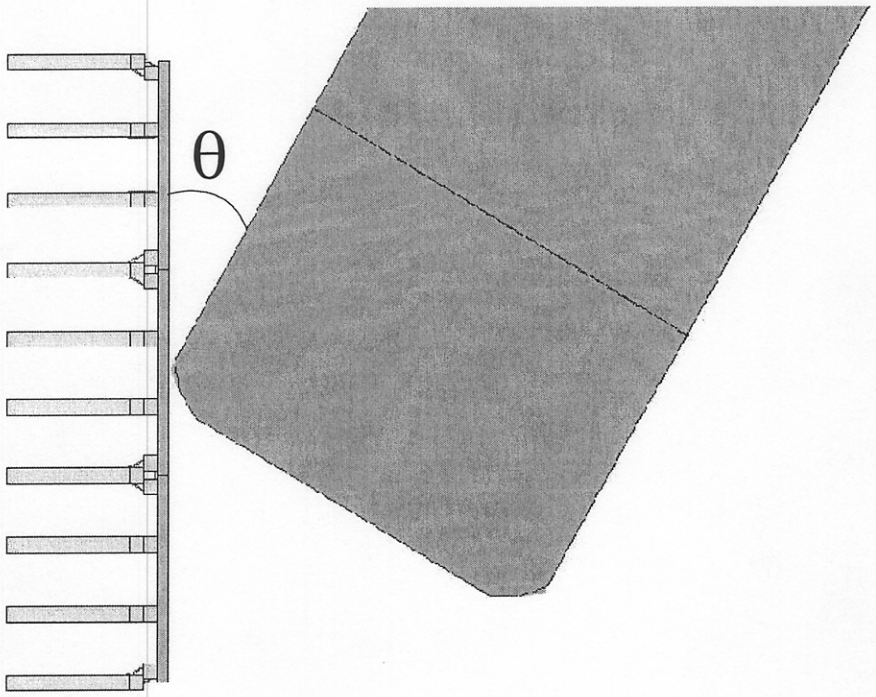

Figure 8.1. Definition of the Initial Impact Angle

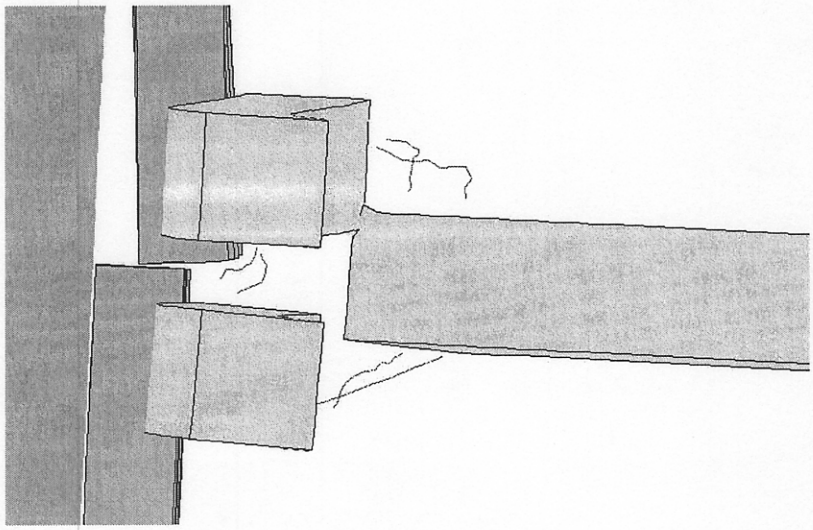

Figure 8.2. Failure of Cables Connecting Piles – Top View; 90° Impact

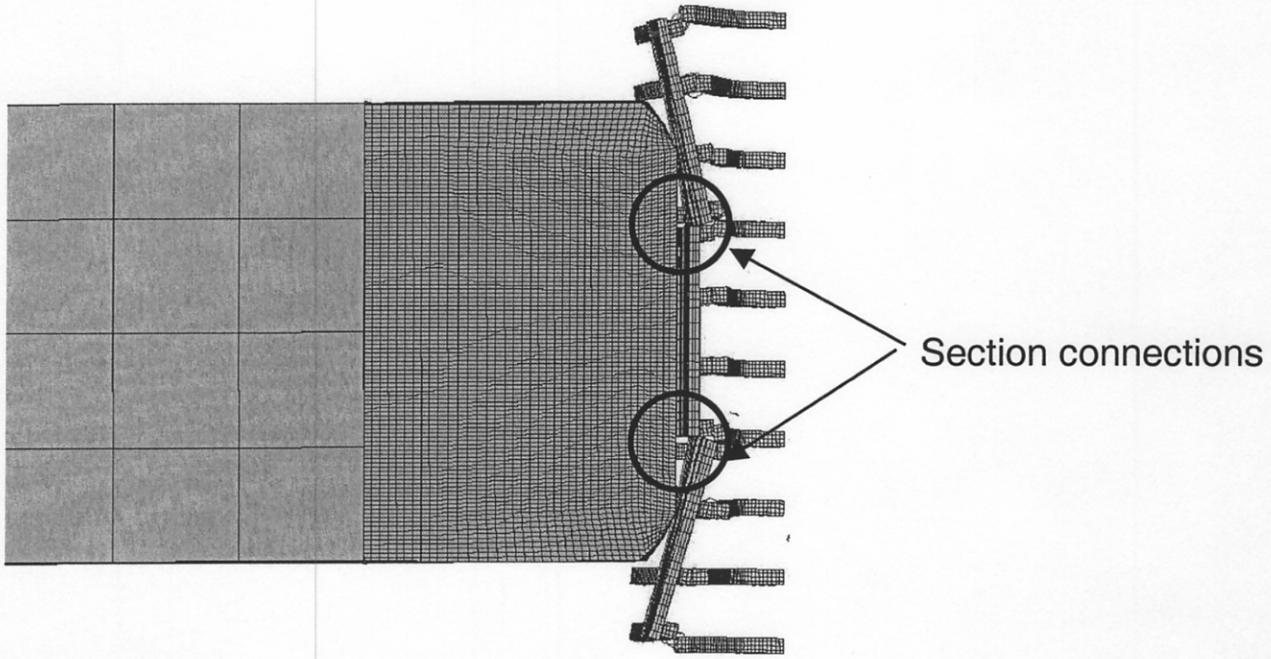

Figure 8.3. Piles Acting Independently; 90° Impact

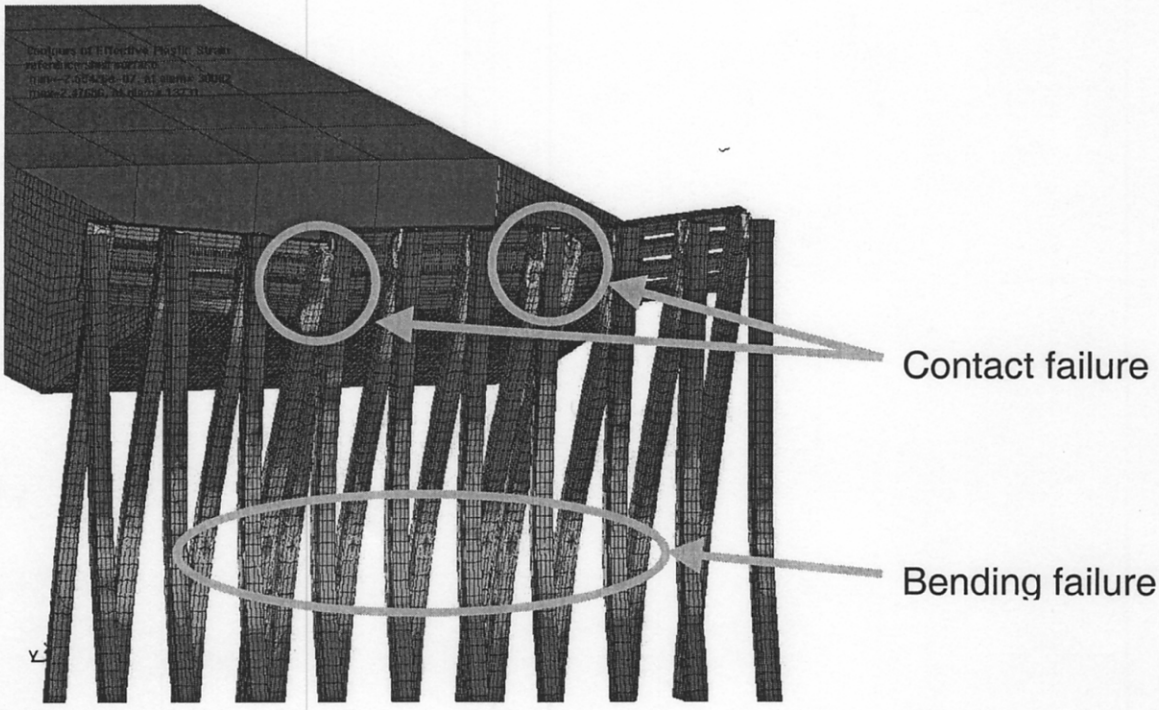

Figure 8.4. Fender Failure – Regions of High Effective Plastic Strain; 90° Impact

In accordance with previous research, the value of equivalent static force, which should be applied to the bridge pier for this collision, is 7112 kN (Chap. 4). The predicted force for barge impacting pier after fender failure is 6768 kN. This value is only 4.9% smaller than that determined for an unprotected bridge structure.

8.3. Impact at 30 Degrees

A barge drifting towards the fender at 30 degrees (Fig. 8.5) was also considered. The damage to the fender structure was still severe. In 90-degree impact, the pile connections were already identified as the weakest structural elements. They did not provide sufficient resistance. After approximately 2 seconds of the impact, the damaged fender no longer resisted the collision force, and the barge appeared to be drifting towards the bridge structure with a significant residual velocity of 3.3 knots (Fig. 8.6). The structure failed to dissipate sufficient amount of kinetic energy from the vessel.

8.4. Impact at 45 Degrees

This impact also produced very severe damage to the fenders. After 2 seconds, the structure could be considered as failed with the barge drifting toward the pier (Fig. 8.7). The residual velocity was 2.7 knots and the kinetic energy was reduced by 45%.

8.5. Impact at 15 Degrees

Computational mechanics confirmed, as one would expect, that 15-degree impact produced minimal damage to the bridge fender. The structure withstood collision very well; it redirected the barge and damage was minimal (Fig. 8.8). It may be concluded that this impact condition would not require any retrofit. However, fenders that can withstand impact from 30

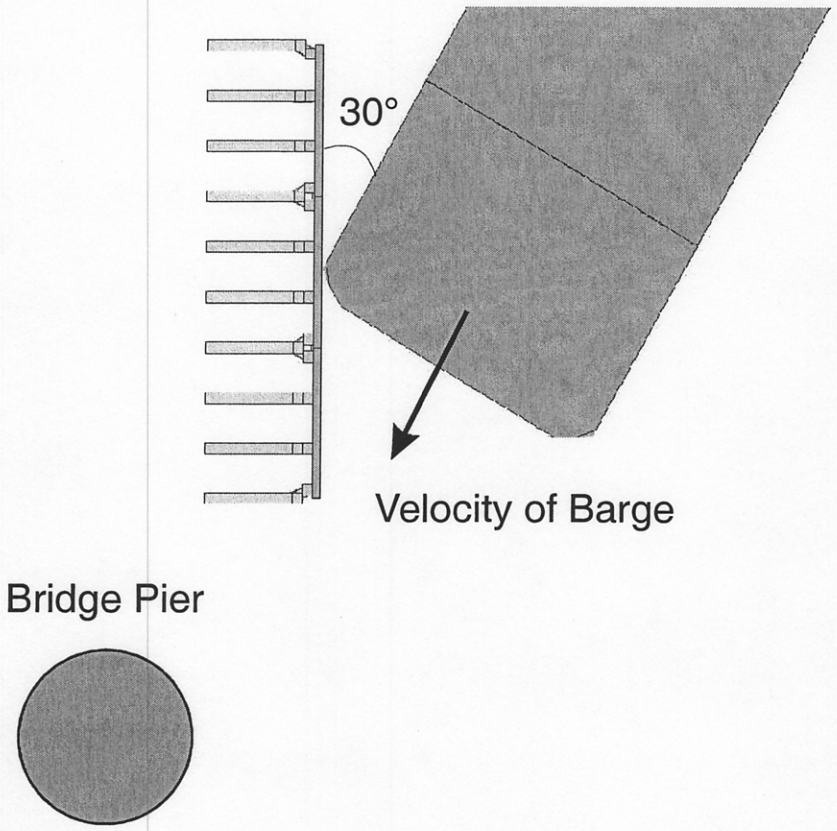

Figure 8.5. Configuration for 30° Impact

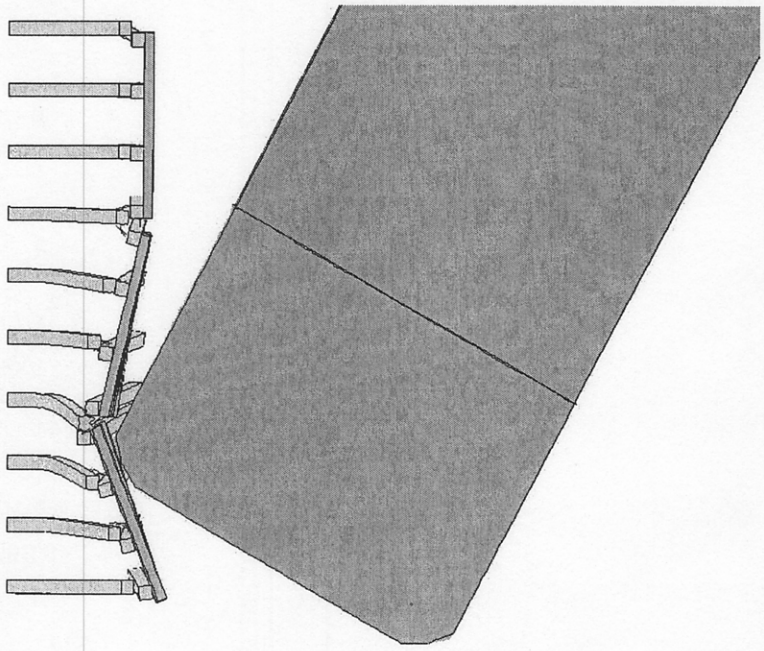

Figure 8.6. Excessive Damage to the Fender Structure after 2 sec; 30° Impact

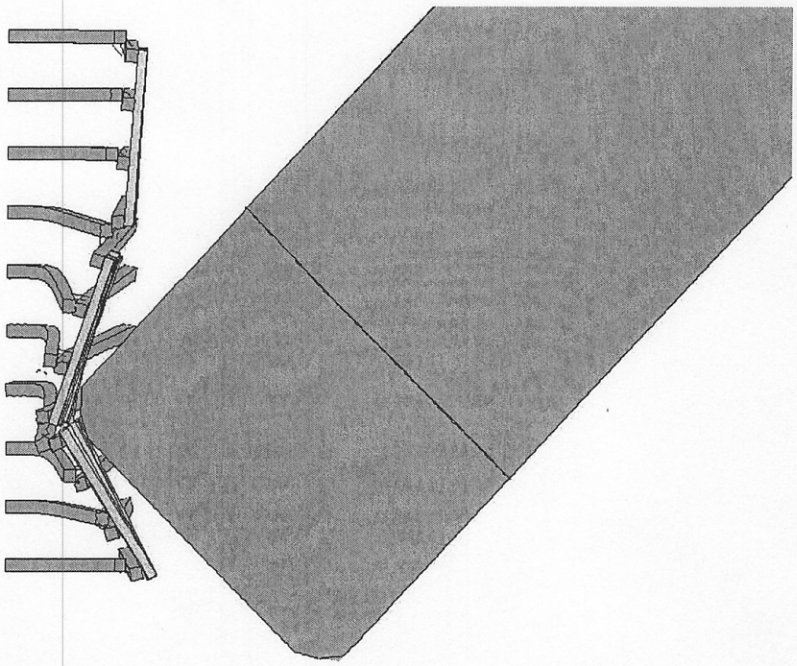

Figure 8.7. Fender Damage after 2 sec; 45° Impact

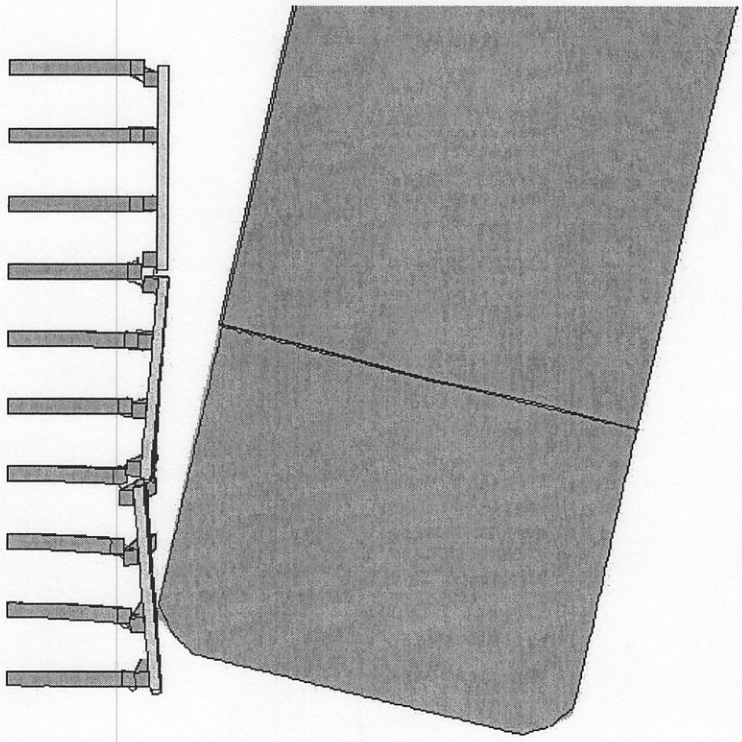

Figure 8.8. Barge Redirected by the Fender after 3 sec; 15° Impact

degrees will be able to sustain impact from 15 degrees as well. Thus, this impact angle was not considered for further analysis.

CHAPTER 9

DYNAMIC MODEL RETROFIT ANALYSIS

9.1. Description of Approach

The fender structure is flexible in nature and it was never expected to completely stop the movement of the impacting barge. Therefore, the goal of the additional investigation was to develop a viable retrofit recommendation, which would only partially resist the barge velocity. Almost all considered impacts (except for that at 15 degrees) produced severe damages to the structure and large residual velocities. Analyses of the structure behavior during impacts showed that the amount of the absorbed kinetic energy of the barge depended strongly on the pile connections. Stronger connections through steel plates or concrete wedges were identified as the two most viable modifications from all those considered in the study. The following sections contain a discussion of structural responses of modified fenders impacted at different initial angles.

9.2. Piles with Larger Cross-Sections

9.2.1. Model Description

Piles with larger cross-section were considered as one of the viable retrofit options. A 455-mm (18 in) square pile cross section with 16 prestressing strands was assumed herein. The differing strand pattern required more elements within the pile cross-section (Fig. 9.1) than the 355-mm (14 in) pile studied earlier. The three-section fender model with 455-mm (18 in) piles consisted of 35,244 solid elements, 15,336 beam elements, and 2,200 springs attached to the piles. Consequently, the computational time required for the analysis increased approximately

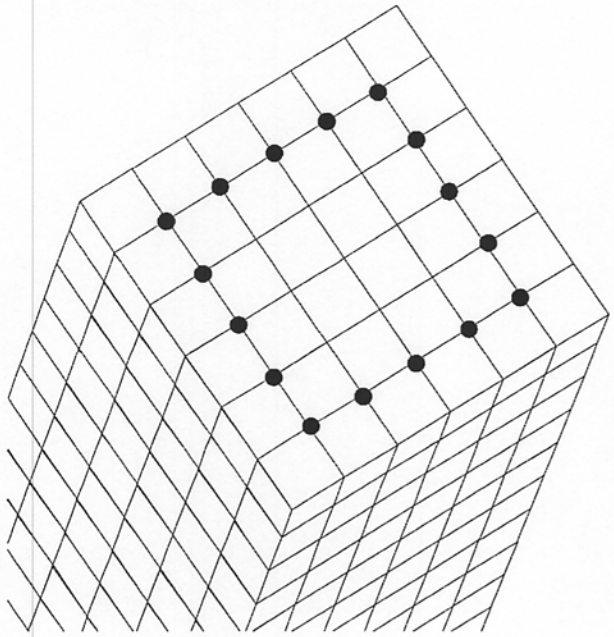

Figure 9.1. Strand Pattern for 455-mm Piles

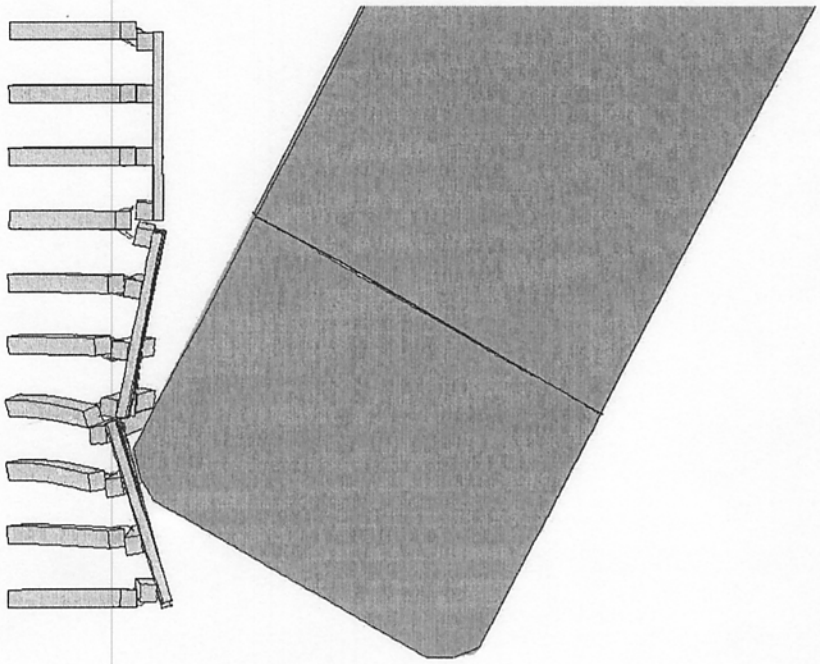

Figure 9.2. Damage to the 455-mm Pile Fender after 2 sec; 30° Impact

2.5 times as compared to the 355-mm (14 in) pile fender. All material properties were identical to the previous analysis (Table 7.3).

9.2.2. Analysis Results

As expected, output data revealed improved crashworthiness of the larger fender structure. It dissipated more kinetic energy. However, the gain was not as good as expected. Damage was still excessive and the amount of absorbed kinetic energy appeared to be unsatisfactory. After 800 msec of impact from 90 degrees, the residual velocity was 2.5 knots (1.3 knots drop), which corresponds to the kinetic energy reduction of 30 percent. After 2 seconds of the 30-degree impact, the velocity was 3.1 knots (0.8 knots drop) and kinetic energy was reduced by 27 percent. Figure 9.2 presents the damage to the fender with 455-mm piles impacted from 30 degrees. Analysis of 45-degree impact was truncated at 800 msec due to numerical difficulties. At this time, the velocity of the barge was 3.4 knots and kinetic energy reduction was 18%.

9.3. Plastic Lumber Wales

Reinforced plastic lumber is known for its durability, which is especially attractive in the tropical weather of Florida. Thus, they were considered in the analysis of the fender systems as a potential replacement for timber wales. Table 9.1 presents properties of the wales, as obtained from Seaward, Inc. Web page.

The finite element model of the plastic wales utilized a similar approach to the model of reinforced/prestressed concrete (Section 7.4). Linear elastic material with properties from Table 9.1 was used for plastic material, while the reinforcement was modeled using a chain of steel truss elements. The kinetic energy absorbed from the barge was similar to that of the timber

Table 9.1. Properties of Seward Plastic Lumber Wales

	SI Units	US Units
Width	255 mm	10 in
Diameter of reinforcement	25 mm	1 in
Number of bars in the wale	4	
Unit weight	1.91 kN/m^3	12.16 lb/ft^3
Modulus of elasticity	38.4 GPa	5567 ksi
Poison's ratio	0.2	

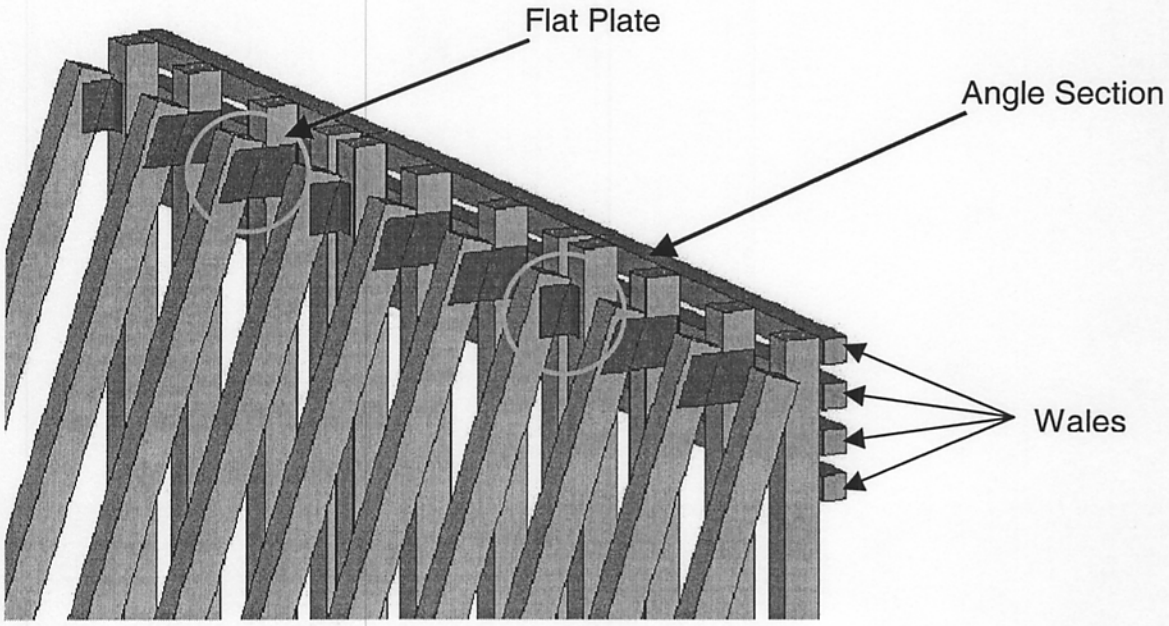

Figure 9.3. Model of Steel Plate Connections

models. Thus, from the point of view of crashworthiness of the fender, no gains were obtained. However, despite being excessive, deformation of plastic lumber is often elastic. After a release of the impacting force, the plastic lumber may recover to the original configuration. This may allow in later reuse of this component. Other reasons, e.g. better corrosion resistance, can also lead to a choice of the plastic lumber over timber.

9.4. Steel Plate Retrofit of Pile Connections

9.4.1. Model Description

In this retrofit scheme ½-inch-thick (12.5-mm) steel gusset plates were attached to piles (Figs. 9.3 and 9.4) replacing the weak cable links. The piles in the middle of each bay were connected by straight plates, while the piles at the ends of the sections were connected using angle plates. The plates were connected to the piles by bolts. For numerical analysis, bolts were modeled as the "spotwelded" constraints with brittle failure criteria (Section 7.6).

9.4.2. Results for 90-Degree Impact

Behavior of the modified fender was dramatically different from the original system. Strong connections provided very good pile-to-pile interaction and more piles were engaged in absorption of the kinetic energy of the barge. Stronger connections also resulted in earlier pile failure. After 375 milliseconds, the battered piles reached effective plastic strain of 0.03 (Fig. 9.5a). The structure could be considered as completely failed after approximately 600 milliseconds, when the effective plastic strain on all pile heads reached the value of 0.03 (Fig. 9.5b). After 600 milliseconds of the impact, the residual velocity of the barge was 2.8 knots. Kinetic energy of the barge was reduced by approximately 60 percent.

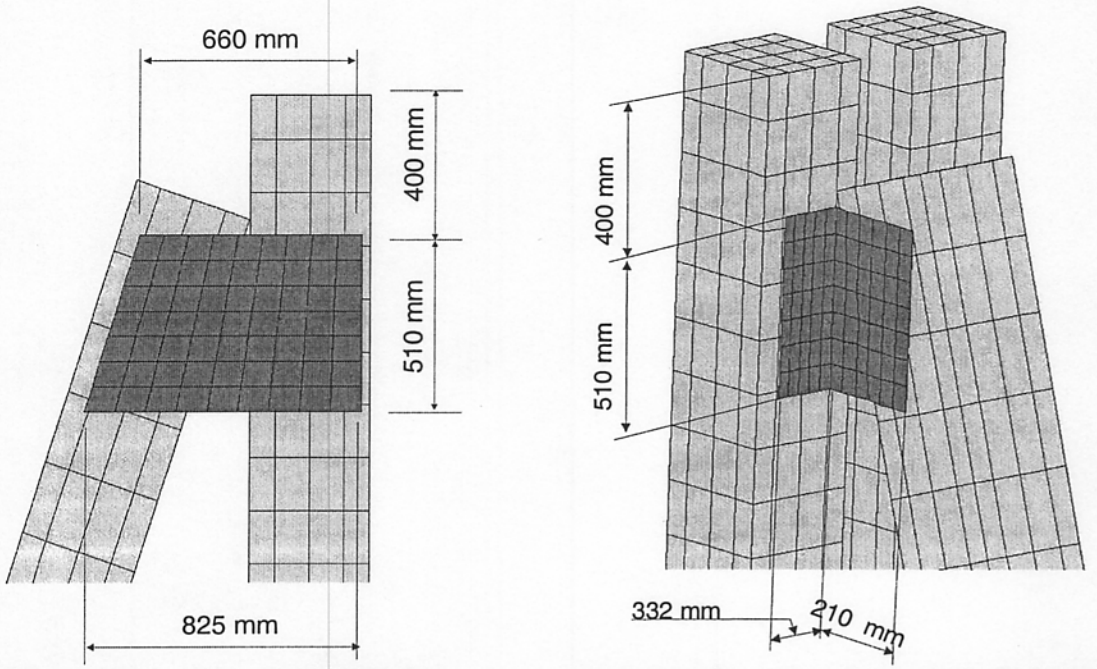

(a) Gusset Plate Connecting Mid-Piles

(b) Angle Plate Connecting End Section

Border Piles

Figure 9.4. Detailed View of Steel Plate Retrofit Connection

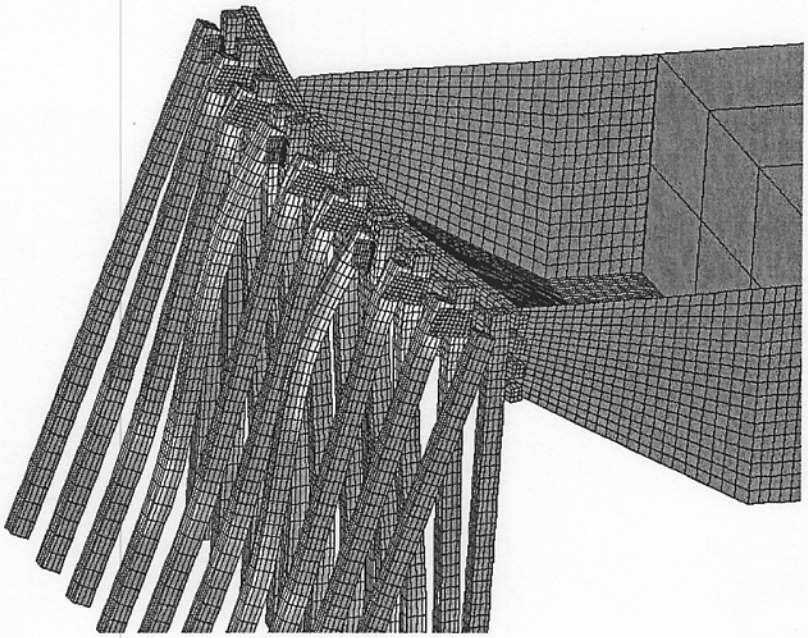

(a) Battered Piles Failed after t=375 msec

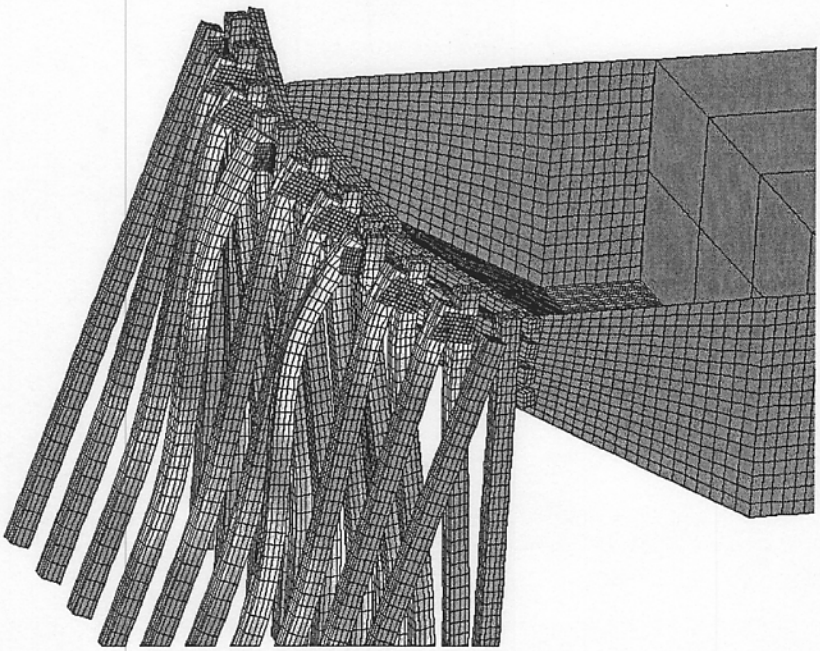

(b) Structure Failed after t=600 milliseconds

Figure 9.5. Effective Plastic Strain Areas in Concrete Piles; 90° Impact (Bright Areas Indicate Large Fringe Level)

9.4.3. Results for 45-degree impact

Similarly to the original design, the 45-degree impact produced more severe conditions for the fender than the 30-degree impact. The structure as a whole was essentially damaged – the wales were broken, the corner of the barge deeply penetrating the fender (Fig. 9.6). The modified fender neither completely stopped, nor redirected the barge. After 1.2 seconds, the barge was slowed down to 2.8 knots (1.0 knots drop) and kinetic energy was reduced by 45 percent. The analysis was terminated after 1.2 seconds due to numerical problems developed by the program in the later stage of the impact – "shooting nodes" indicating instabilities in the solution. In this case, the termination of the analysis did not indicate the maximum capacity of the fender system. However, it is clear that the structure was absorbing energy from the barge during the later stage of the impact.

9.4.4. Results for 30-degree Impact

At 30-degree impact, the steel plate retrofitted fenders performed very well. The barge was fully redirected by the fender after 3 seconds of the collision. As a result, the barge drifted away from the structure. The velocity of the barge was reduced to 2.9 knots (0.9 knots drop). In this case, the redirection is essentially more important to the analysis of crashworthiness of the fender, since the barge drifted away and did not pose any danger to the pier anymore. Figure 9.7 presents the results from this analysis.

9.5. Concrete Wedge Retrofit

9.5.1. Description of the Modification

A concrete wedge modification shown in Fig. 9.8 and Fig. 9.9 was used to provide a stiffer connection between the piles. The wedge was modeled using solid elements with nodes

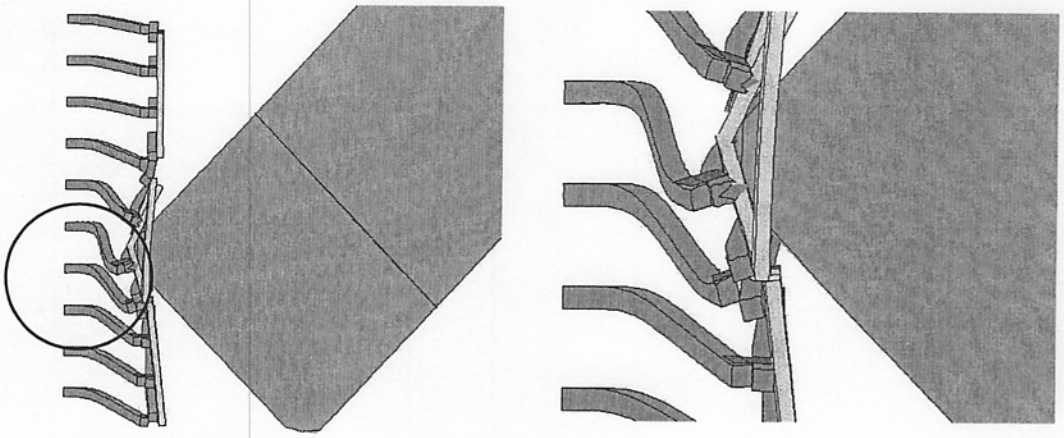

Figure 9.6. Damage to the Fender Modified by Steel Plates; 45° Impact

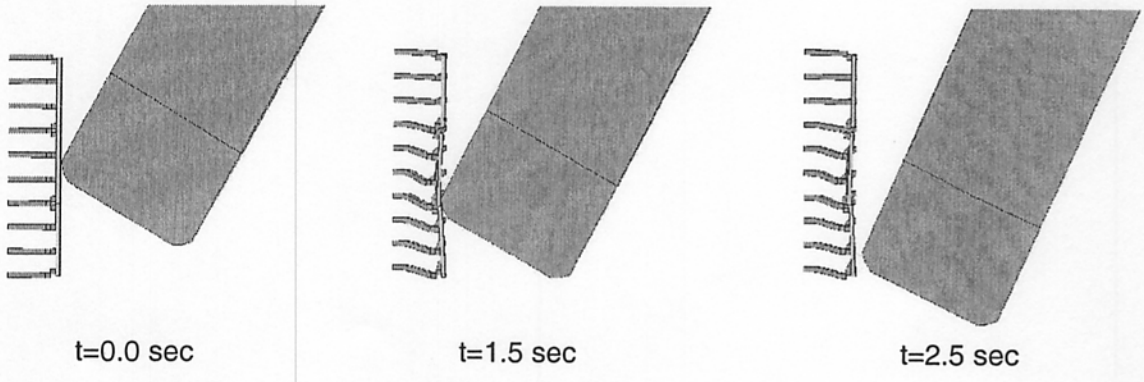

Figure 9.7. Redirection of the Barge; Steel Plate Retrofit; 30° Impact

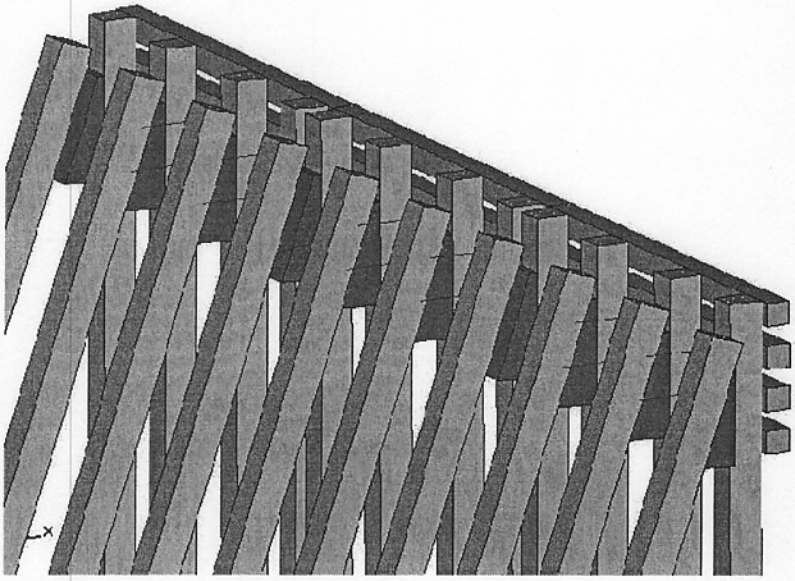

Figure 9.8. Concrete Wedge Connection Finite Element Model

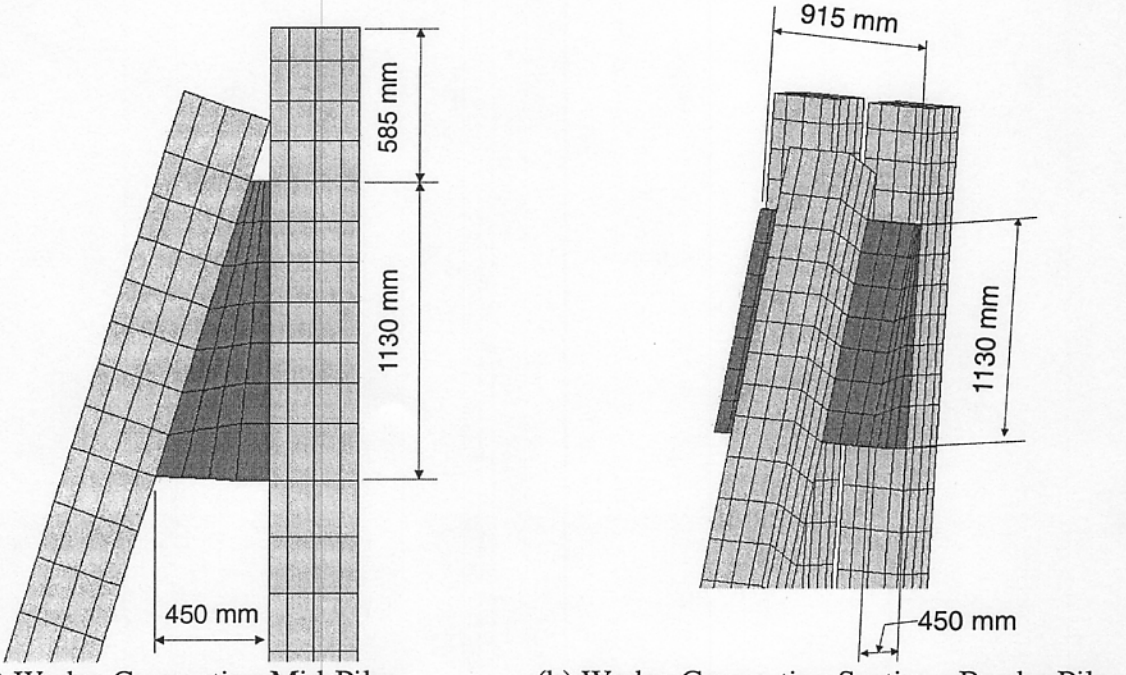

(a) Wedge Connecting Mid-Piles (b) Wedge Connecting Sections-Border Piles

Figure 9.9. Detailed View of Concrete Wedge Retrofit

common to both piles and heads, that is, the head and the pile were considered merged at their common nodes. This assumption can be satisfied only if the wedge-to-pile connection is constructed accurately. Connecting the concrete head to the pile, however, requires a customized solution, extensive labor, and strict technology with tight tolerance to avoid strand damage. It would be certainly more suitable for new installations, rather than for existing structures.

This wedge retrofit increased overall stiffness of the structure. Its energy dissipation capacity was found to be the largest of all options considered. The strong pile connections also provided good load transfer to the adjacent piles, an important aspect when considering angle impact. This solution can, therefore, be suitable for new fender systems where precast members can be used.

9.5.2. Results for 90-Degree Impact

The wedge-modified fender resulted in a behavior similar to that of the fender with steel plates; damage occurred earlier and the impact was more violent. After 500 milliseconds of the impact, the amount of effective plastic stain in the pile heads was larger that 0.03. Thus, the structure can be considered as failed (Fig. 9.10). Despite the shorter time of the impact, the energy absorbed by the modified system was essentially greater than the original structure. The velocity of the barge decreased to 2.1 knots (approx. 45 percent drop) and the kinetic energy was reduced by nearly 70 percent.

9.5.3. Results for 45-Degree Impact

Although improved, the performance of the retrofitted fender was still unsatisfactory for 45-degree impact. The damage to the fender was excessive. Moreover, due to the small area of

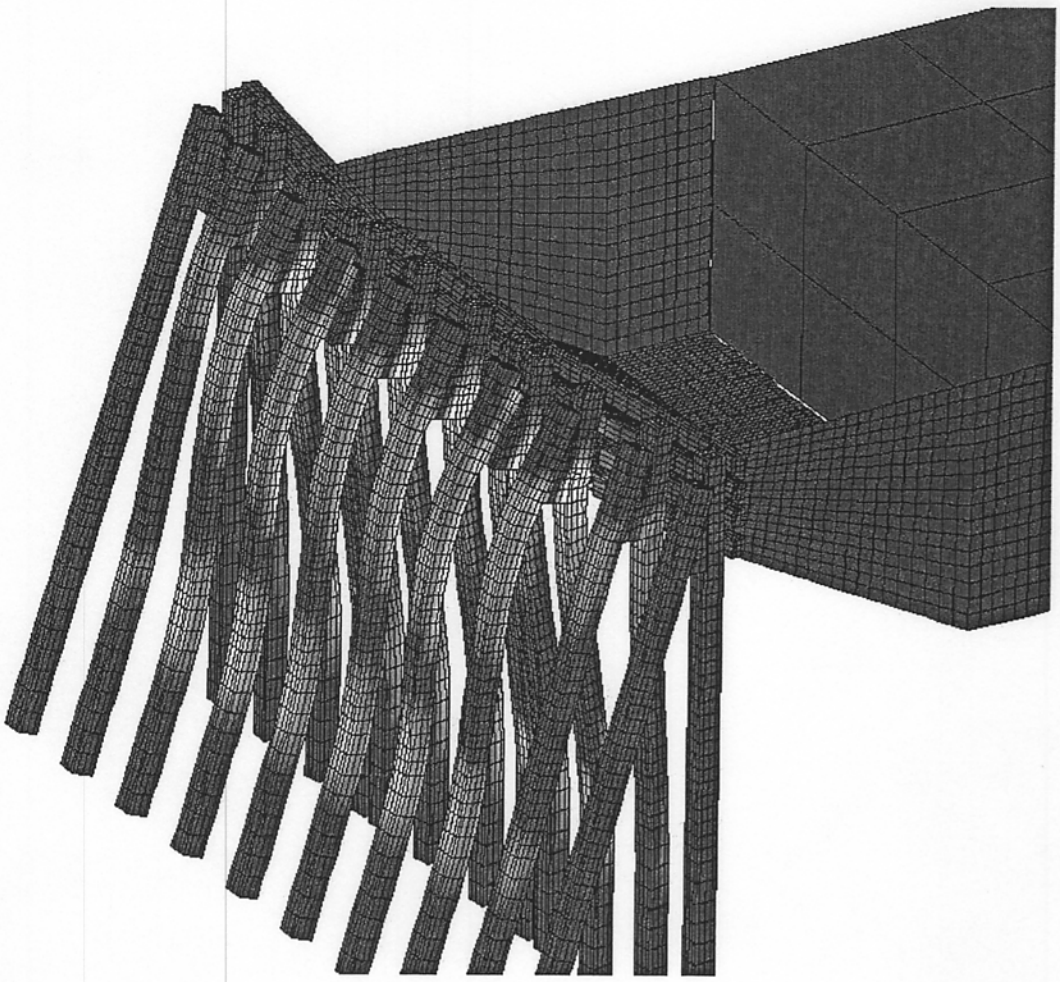

Figure 9.10. Effective Plastic Strain in the Concrete Wedge Retrofitted Fender after 500 msec of Impact; 90° Impact

contact between the impacting vessel and the fender the damage was not well distributed. The wedge connections provided pile-to-pile interaction within the pairs of the relevant vertical and battered piles. However, the failing wales were unable to transfer the force to the neighboring piles (Fig. 9.11). The fender was unable to redirect the vessel. After 1.2 seconds of the impact, the residual velocity of the barge was 2.55 knots (35 percent drop), while the kinetic energy was reduced by 50 percent. The analysis of the 45-degree impact was terminated earlier than that of the 30-degree impact (1.2 seconds versus 3 seconds) not only due to failure of the structure, but also due to the same numerical problems, as reported in Section 9.3.3 ("shooting nodes").

9.5.4. Results for 30-degree impact

The wedge-modified fender also performed very well when impacted from 30 degrees. The barge was fully redirected by the fender, as in the steel plate retrofit (Fig. 9.12). The velocity and kinetic energy reductions were 27 percent (2.75 knots residual velocity) and 40 percent, respectively.

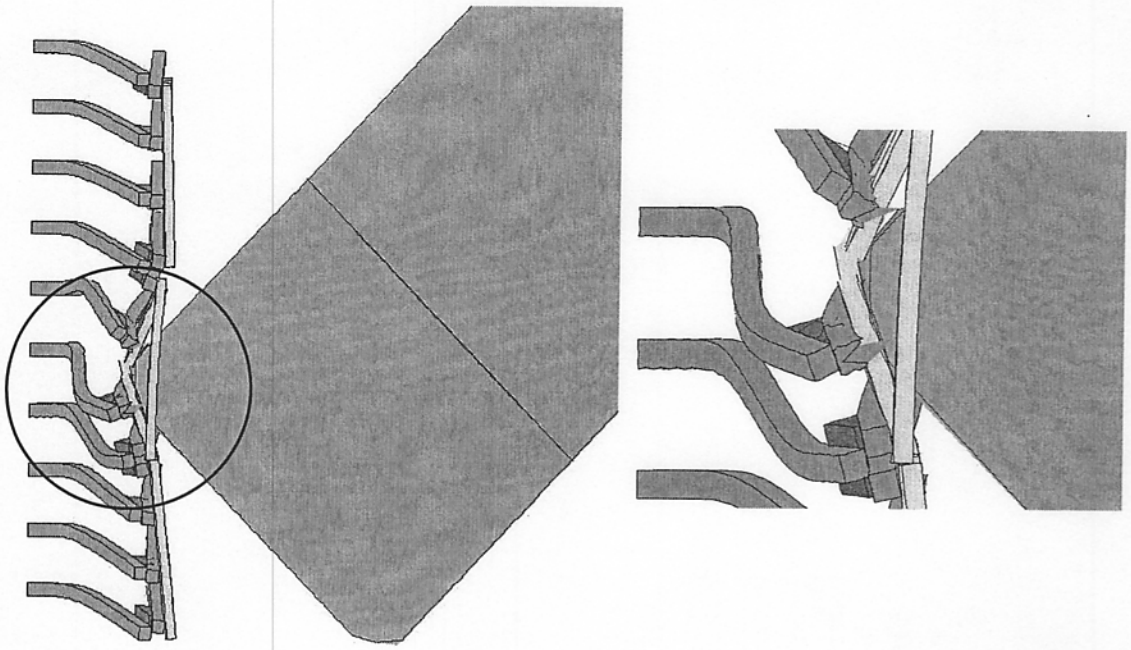

Figure 9.11. Damage to the Fender with Concrete Wedge Modification; 45° Impact

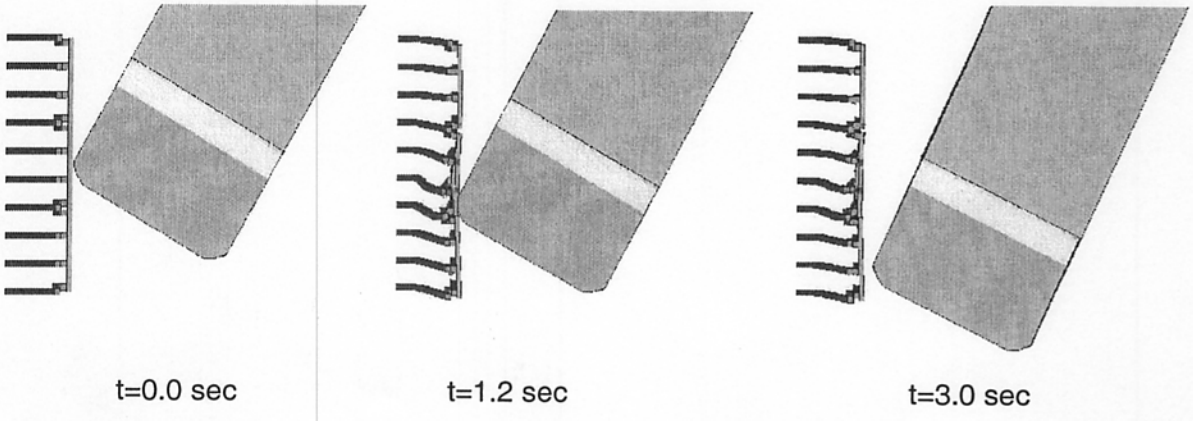

Figure 9.12. Redirection of the Barge – Concrete Wedge Modification; 30° Impact

CHAPTER 10

SUMMARY OF DYNAMIC ANALYSIS RESULTS

10.1. Kinetic Energy Absorption Approach

AASHTO ship impact procedure requires the computed static force to be applied to a bridge pier and design structures to withstand the impact force. Thus, it is governed by small displacement static theory, which can be used for bridge piers. Deflections of the impacted fender were large. The history of the force exerted on the structure consisted of several impulses; the barge hits the fender several times while the fender was being displaced. The force values were essentially smaller than the value of 7112 kN, computed by the AASHTO procedure (Chapter 4). Figure 10.1 depicts the time history of the dynamic forces during the 90° impacts. The values were obtained as resultant forces applied to the nodes on the wale surface for different fender solutions. They can be interpreted as the maximum force capacity of the fender system. However, they do not contribute to any effective reduction of the equivalent static force on the bridge pier due to protection by the fender. Hence, other tools are more appropriate in dynamic analysis of the crashworthiness of the structure, e.g. comparison of kinetic energy absorption. The residual impact energy of the vessel provides information about initial impact conditions for the bridge structure after the fender fails and the barge drifts towards the pier.

10.1.1. Impacts at 90 Degrees

Original and modified fender systems failed to completely stop the vessel during 90° impacts. However, the fender retrofit solutions with strong pile connections (steel plates, concrete wedges) absorbed far more kinetic energy than those with original weak cable

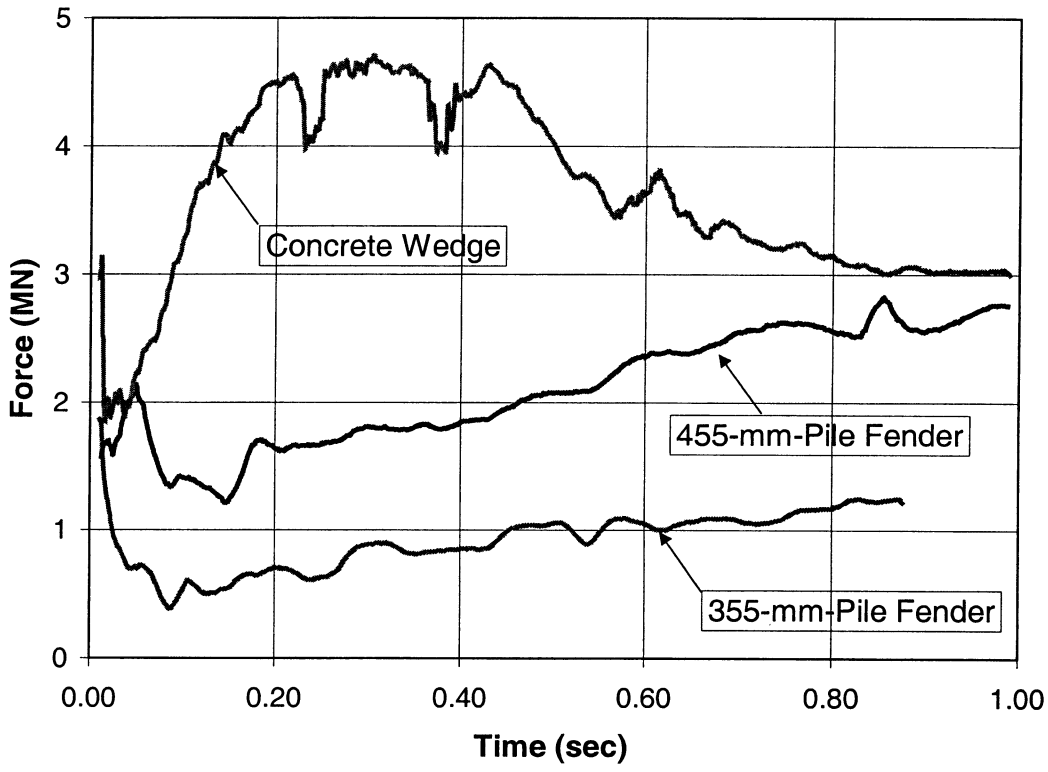

Figure 10.1. Resultant Nodal Forces on the Fender Wale for Various Models

connections. Figure 10.2 presents time histories of relative residual kinetic energy of the barge for various models. The initial energy is designated as 100%. The amount of energy absorbed by the concrete wedge fender was nearly three times larger than that for the original fender.

10.1.2. Impacts at 30 and 45 Degrees

Computer analysis of the impacts from 30 and 45 degrees revealed essentially different mechanics as compared with the 90° impact. Due to smaller contact area between the barge and the fender, local damage to the fender structure was greater, especially for the 45-degree impact. Final barge velocity, kinetic energy absorption, and barge redirection results are presented in Table 10.1 and 10.2.

The stronger retrofitted systems were able to redirect the vessel impacting at 30 degrees (Table 10.1). This is an important gain indicating that bridge structure can be saved from the damage due to the collision at smaller angles. For 45-degree impact scenario, the systems were neither able to completely stop the barge, nor to redirect it (Table 10.2). It seems that the limit angle of the ability of the retrofitted fender to redirect the barge lies between 30 and 45 degrees. It is also apparent that more energy is absorbed by the fender system at the 45-degree impact angle, especially for the retrofitted systems.

10.2. AASHTO Equivalent Design Static Force

In order to estimate an equivalent static force exerted to the bridge structure after the collision with the fender, AASHTO procedure was reapplied with the residual barge speed obtained from the LS-DYNA analysis (AASHTO 1991). Table 10.3 presents the results of the computations for the 30°, 45°, and 90° impacts. It may be noticed that the reduction of the

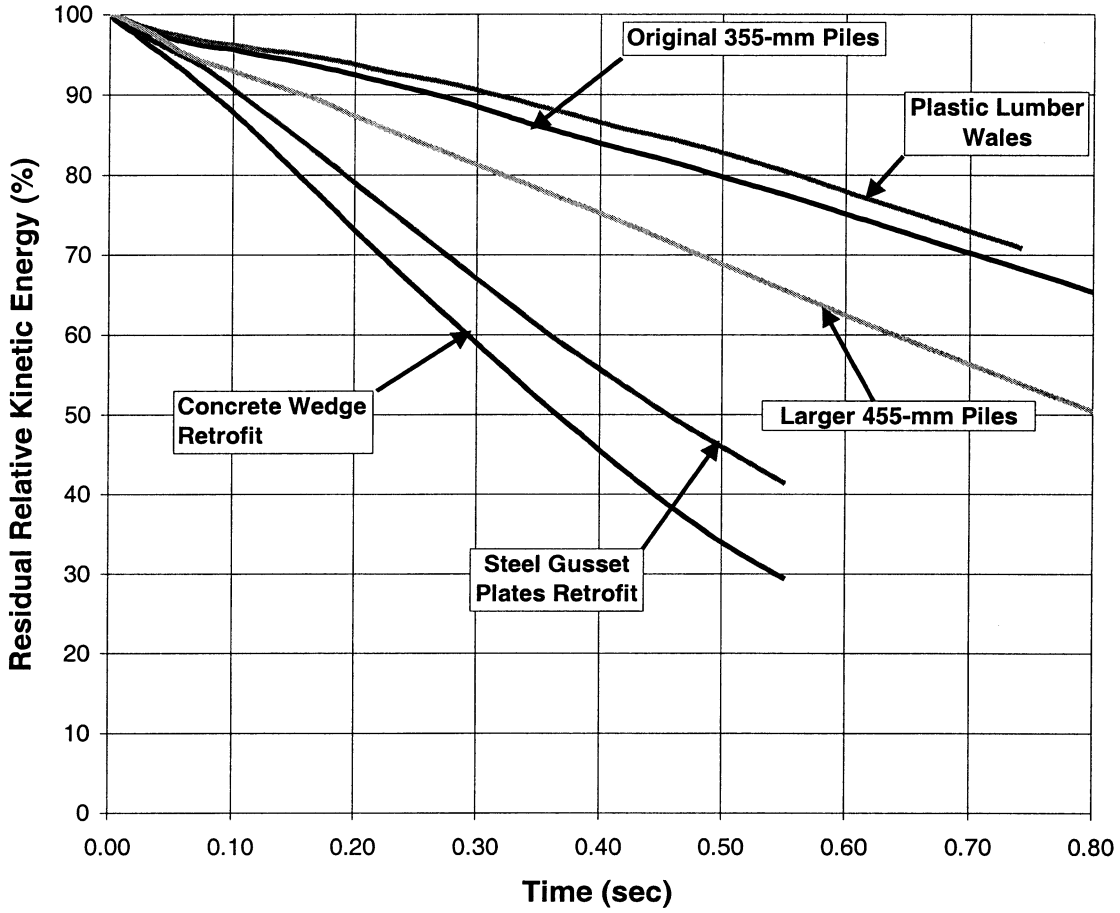

Figure 10.2. Residual Kinetic Energy of the Barge; 90° Impact

Table 10.1. Summary Results, 30-Degree Impact

Model	Final Velocity (knots)	Percentage of Absorbed Kinetic Energy	Barge Redirection
Original Design	3.3	22	NO
455-mm Pile	3.14	25	NO
Steel Plate Retrofit	2.9	31	YES
Concrete Wedge Retrofit	2.7	37	YES

Table 10.2. Summary Results, 45-Degree Impact

Solution	Final Velocity (after 1.2 sec) (knots)	Percentage of Absorbed Kinetic Energy	Barge Redirection
Original Design	3.1	27	NO
455-mm Pile*	3.4	18	NO
Steel Plate Retrofit	2.7	46	NO
Concrete Wedge Retrofit	2.4	57	NO

* Results after 0.8 sec of impact

Table 10.3. AASHTO Equivalent Static force on Pier after Impacts (AASHTO 1991)

Initial Impact Angle (deg)	Fender Type	Residual Velocity (knots)	Residual Energy (kip-ft)	Bow Damage Depth (ft)	Eq. Static Force (kips)	Eq. Static Force (kN)	Force Reduction (%)
30	No Fender	3.80	2811	2.27	1599	7116	0.0
	355-mm Piles	3.30	2120	1.75	1542	6862	3.6
	455-mm Piles	3.14	1919	1.60	1525	6786	4.6
	Steel Plates	2.90	1637	1.38	1501	6678	*
	Concrete Wedge	2.70	1419	1.20	1482	6593	*
45	No Fender	3.80	2811	2.27	1599	7116	0.0
	355-mm Piles	3.10	1871	1.56	1521	6768	4.9
	455-mm Piles **	3.40	2250	1.85	1553	6911	2.9
	Steel Plates	2.70	1419	1.20	1482	6593	7.4
	Concrete Wedge	2.40	1121	0.96	1455	6474	9.0
90	No Fender	3.80	2811	2.27	1599	7116	0.0
	355-mm Piles	3.10	1871	1.56	1521	6768	4.9
	455-mm Piles	2.50	1217	1.04	1463	6513	8.5
	Steel Plates	2.80	1526	1.29	1491	6635	6.8
	Concrete Wedge	2.10	858	0.74	1431	6368	10.5

* The barge was redirected; thus there is no real force exerted to the pier

** Results after 0.8 sec of impact

design force is relatively small. This is due to the fact that the AASHTO equivalent static force is related to the square root of the impact energy (Chapter 4). For large values of energy reduction, (e.g. more than 50 % in case of concrete wedge retrofit) produce small reduction in the computed equivalent static force. The estimation of the AASHTO equivalent static force appears to be very conservative compared to the dynamic analysis using energy comparison.

CHAPTER 11

CONCLUSIONS

1. Bridge fenders have a potential for being used an energy absorbing system for errant barges. Their crashworthiness can be improved by the suggested retrofit solutions, which provide better protection for the main bridge structure.

2. Behavior of the fender system during ship impact largely depends on the pile connections. Stiffer connections provide better energy transfer between adjacent piles resulting in improved crash energy distribution throughout the system. Additional studies may be needed to determine barge crashworthiness and any possible tugboat crew's threat in the collision with the improved bridge fender structure.

3. The concrete head seems to be more suitable for new fender systems than for existing structures. Some elements can be precast, tightening of the concrete head to the pile can use a customized solution.

4. Plastic lumbers can be used as replacement for timber wales. Their durability, corrosion resistance, and reusability after an impact, make them very attractive for the corrosive environment in Florida.

5. The retrofitted fender is capable of absorbing up to 70% of the kinetic energy of the barge impacting with the assumed collision velocity. For initial impact angle 30 degrees or less, it is capable of redirecting the barge and saving the bridge pier.

6. Both modified and original structures will not contribute to essential reduction of the design equivalent static force applied to the bridge pier (up to 10%). On the other hand, the analysis showed that the modified fender is capable of resisting less severe collisions. There is also a

great possibility that a barge impacting with a smaller impact velocity would be essentially slowed down by the modified fender, which would reduce potential damage to the protected pier.

7. These benefits are worth considering since most collisions that would take place are not as extreme as those considered in the study.

8. The use of alternate strand patterns proposed by the FDOT did not significantly influence stress intensity resultant from impact load.

9. The actual behavior of the barge and fender may vary depending on various conditions in the collision site, depth of the waterway, soil conditions, deterioration of the structure, etc.

APPENDICES

APPENDIX A

FLORIDA WATERWAYS

A.1. Depth of Florida Waterways

Table A.1. Depth of Florida Waterways

Channel Name	Location or Channel Section	Depth		Year
		(m)	(ft)	
	Near Gulf Harbor (Chart11409)	1.2	4	1986*
	Near Gulf Harbor (Chart11409)	1.2	4	1986*
	Off Intracoastal – near Ozona	0.8	2.5	1985*
	Off Intracoastal– south of Ozona	1.5	5	1972*
North Channel		2.9	9.5	1984*
	Into Port Manatee	10.4	34	1983*
Intracoastal Waterway	(Chart 11425)	2.7	9	*
Boca Grande Channel	Left quarter	8.3	27.3	1983-1985*
	Middle quarter	9.5	31.1	1983-1985*
	Right quarter	9.4	30.9	1983-1985*
	Widener	9.8	32.0	1983-1985*
Inland Waterway		1.5	5	1981*
Gordon Pass	Entrance Channel	3.1	10	1983*
Indian Key & Everglades Harbor		2.1	7	1981*
Clearwater Pass	Gulf to highway bascule bridge	2.7	9	1986*
	Highway bascule bridge to Intracoastal junction	1.8	6	1986*
Clearwater Beach	To Clearwater Beach basin	1.2	4	1979-1986*
	In Clearwater Beach turning basin	2.1	7	1979-1986*

Table A.1. continued

Channel Name	Location or Channel Section	Depth		Year
		(m)	(ft)	
Johns Pass	From channel entrance to Light6	1.5	5	1984*
	From Light 6 to Intracoastal junction	1.8	6	1984*
Cats Point		1.8	6	1984*
North Channel		3.1	10	1986*
Sunshine Skyway Channel		2.4	8	1984*
Bunces Pass	Near Madelaine Key	4.9	16	*
Mullet Key Channel	Under Sunshine Skyway Bridge	13.1	43	*
Manatee River	From entrance to Mc Neil Point	2.7	9	1969-1982*
	From Mc Neil Point to Rocky Bluff	0.9	3	1969-1982*
	From Rocky Bluff to Rye	0.3	1	1969-1982*
Longboat Pass Channel	From channel entrance to bascule bridge	2.4	8	1984*
	From bascule bridge to Intracoastal junction	2.4	8	1984*
Intracoastal Waterway	Under bascule bride south of Perico Island	2.4	8	*
	Under bascule bridge south of Palma Sola Bay	3.7	12	*
New Pass Channel	From channel entrance through Natural Channel to Light 7	3.1	10	1975-1983*
	Within the basin	2.4	8	1975-1983*
Intracoastal Waterway	From Caloosahatchee River to Anclote River	2.7	9	*
	SW of Golden Gate Point	2.4	8	*
Mantanzas Pass	From entrance to beacon 14	3.1	10	1984*
	From beacon 14 to turning basin	2.7	9	1984*
	In turning basin	2.7	9	1984*
Gordon Pass		2.3	7.5	1984*
Inland Waterway	From Big Marco to daybeacon73	1.5	5	1981*
Indian Key and Everglades Harbor	Through Indian Pass to Barron River	1.5	5	1984*
Rodgers River	After crossing the bar	0.9	3	1961*
The Cut Off		2.0	6.5	1930*
Wilderness		0.9	3	1977*
Key West	Main Ship Channel	9-10.4	30-34	*

Table A.1. continued

Channel Name	Location or Channel Section	Depth		Year
		(m)	(ft)	
West Pass	Through West Pass to West Pass Bay	1.5	5	1979*
	From West Pass Bay eastward to Chekoloskee Bay and southeastward to Barron River and Everglades City	0.6	2	1979*
Boca Chica		2.4	8	1978*
Key West Harbor Channel	Main Channel Range	10.4	34	1982*
	From buoy 23 to turning basin	9.1	30	1982*
	Key West Bight Channel	3.7	12	1982*
	Turning Basin	3.7	12	1982*
Cow Key		0.9	3	1983*
Garrison Bight		2.1	7	1981*
Okeechobee Waterway	Saint Lucie to Fort Myers via Route 1	2.4	8	*
	Saint Lucie to Fort Myers via Route 2	1.8	6	*
	Fort Myers to Punta Rassa	3.1	10	*
	Punta Rassa to Gulf of Mexico	3.7	12	*
Intracoastal Waterway	Norfolk, VA to Fort Pierce, FL	3.7	12	*
	Fort Pierce, FL to Miami, FL	3.1	10	*
	Miami, FL to Cross Bank, Florida Bay	2.1	7	*
Fly Creek	From channel entrance to basin	1.2	4	1986*
	In basin	1.8	6	1986*
Pass Aux Herons		2.1	7	*
Escambia Bay and River		2.3	7.5	1987*
Perdido Pass	In west channel	1.8	6	1987*
	In east channel	2.1	7	1987*
Bon Secour		1.4	4.5	1987*
Caucus Channel		10.7	35	1985*
Pensacola Harbor Channel		10.1	33	1986*
Bayou Chico Channel	Entrance channel	4.6	15	1986*
	Inner channel and turning basin	4.3	14	1986*
Blackwater Bay and River		2.1	7	1987*
Grand Lagoon		2.4	8	1987*

Table A.1. continued

Channel Name	Location or Channel Section	Depth		Year
		(m)	(ft)	
La Grange Bayou	From Choctawhatchee Bay to Freeport	2.6	8.5	1987*
	In turning basin	3.4	11	1987*
Port Saint Joe Harbor Channel	Entrance channel	11.3	37	1987*
	North channel	10.7	35	1987*
	Turning basin	9.8	32	1987*
	Harbor channel	10.7	35	1987*
	South channel	8.2	27	1987*
Apalachicola River	From Jackson River to Chattahoochee River	2.3	7.5	1981*
	Into Fort Pierce Inlet	8.1	26.5	1983**
Lake Worth Inlet Channel		8.4	27.5	1984♦
	Into Port Everglades	12.2	40	1978♦
New River and Dania Cut-Off Canal	In New River from Intracoastal Waterway to William H. Marshall Memorial Bridge	2.0	6.5	1976-1978♦
	From William H. Marshall Memorial Bridge to point 26°05'54"N, 80°09'56"W	1.8	6	1976-1978♦
	From point 26°05'54"N, 80°09'56"W to Dania Cut-Off Canal	1.1	3.5	1976-1978♦
	From Dania Cut-Off Canal to US1 Highway Bridge	0.6	2	1976-1978♦
	From US 1 Highway Bridge to Intracoastal Waterway in Dania Sound	1.5	5	1976-1978♦
Port Everglades Channels	Outer bar cut (from sea buoy 2 to east end of south jetty)	13.2	43.2	1978♦
	Bar Cut (east end south jetty to turning basin, LT9)	12.4	40.7	1978♦
Main Channel	Into Port of Miami	11	36	1983♦
Intracoastal Waterway	Norfolk, VA to Fort Pierce, FL	3.7	12	♦
	Fort Pierce, FL to Miami, FL	3.1	10	♦
	Miami, Fl to Cross Bank, Florida Bay	2.1	7	♦
Angelfish Creek	From daybeacon 3 to 12	1.5	5	1977♦
Dinner Key		2.4	8	1983♦

Table A.1. continued

Channel Name	Location or Channel Section	Depth		Year
		(m)	(ft)	
Four Way		1.5	5	1983♦
Crystal River	Entrance	0.5	1.5	1977✧
Homosassa River		0.6	2	1975✧
Suwanee River		0.3	1	1967-1973✧
Steinhatchee River	From entrance to the turning basin	1.5	5	1975✧
	In the turning basin	0.6	2	1975✧
Peninsula Point		1.8	6	1974✧
Crooked River	From New River to Oclockonee River	0.9	3	1953✧
Northwest Channel		2.1	7	1977✧
	Channel South of Suwanee Reef	0.9	3	1978✧
Flamingo Canal		1.2	4	1958✧
West Pass	Through West Pass to West Pass Bay	1.5	5	1973✧
	From West Pass Bay to Chokoloskee Bay and southeastward to Barron River and Everglades City	0.6	2	1973✧
Gordon Pass	Southern half	2.9	9.5	1977✧
	Eastern half	1.8	6	1977✧
	To Naples	2	6.5	1977✧
Hillsborough River	From Garcia Avenue to 2200 ft northwest of Columbus Drive Bridge	2.6	8.5	1960✧
Seddon Channel		2.7	9	1960✧
Anclote River		2.6	8.5	1977✧
Apalachicola River	From Jackson River to Chattahoochee River	2.3	7.5	1973✧
Grand Lagoon Channel		2.4	8	1977✧

* Balder, A.P. 1988
♦ Balder, A.P. 1986
✧ Better Boating Association 1979

A.2. Maximum Current Predictions in Florida

A.2.1. Reference Stations (U.S. Department of Commerce, NOAA, NOS, 1992)

Table A.2. St. Johns River Entrance Monthly Current

Month	Current (knots)
January	3.0
February	3.0
March	2.9
April	2.8
May	2.7
June	2.8
July	3.0
August	3.0
September	3.0
October	2.9
November	2.7
December	2.7

Table A.3. Miami Harbor Entrance Monthly Current

Month	Current (knots)
January	2.5
February	2.5
March	2.5
April	2.4
May	2.3
June	2.3
July	2.4
August	2.5
September	2.6
October	2.5
November	2.3
December	2.2

Table A.4. Key West Monthly Current

Month	Current (knots)
January	2.6
February	2.5
March	2.4
April	2.4
May	2.4
June	2.4
July	2.6
August	2.5
September	2.5
October	2.5
November	2.4
December	2.4

Table A.5. Tampa Bay Entrance (Egmont Channel) Monthly Current

Month	Current (knots)
January	3.8
February	3.4
March	2.7
April	3.1
May	3.5
June	3.8
July	3.7
August	3.2
September	2.9
October	3.3
November	3.5
December	3.7

A.2.2. Subordinate Stations (U.S. Department of Commerce, NOAA, NOS 1992)

- St. Johns River

Pablo Creek bascule bridge 5.2 knots

- Florida Coast

Lake Worth Inlet (between jetties)	3.6 knots

- Port Everglades

17th Street Bridge	1.9 knots

- Miami Harbor

Government Cut East Entrance, off north jetty	0.4 knots

- Florida Reefs to Midnight Pass

Boca Grande Pass, Charlotte Harbor	2.2 knots

- Sarasota Bay

Longboat Pass	1.8 knots

- Tampa Bay

Tampa Bay Entrance (Egmont Channel)	1.4 knots

- Boca Ciega and St. Joseph Sound

Pass-a Grille Channel	1.4 knots
Bridge, 0.8 mi. south of Maximo Pt.	

- Apalachee Bay

St. Marks River approach	0.6 knots

- Pensacola Bay

Pensacola Bay Entrance midchannel	1.8 knots

APPENDIX B

EQUIVALENT STATIC BARGE IMPACT FORCE

B_B = Barge width (ft) = 35 ft

R_B = Ratio of $B_B/35$ = 35 / 35 = 1

Channel depth = 15 ft

D_L = loaded draft = 8.7 ft

C_H = Hydrodynamic mass coefficient

For large underkeel clearances ($\geq$ 0.5 x draft), C_H = 1.05

For small underkeel clearances ($\leq$ 0.1 x draft), C_H = 1.25

Underkeel clearance = channel depth – loaded draft = 15 ft – 8.7 ft = 6.3 ft

Underkeel clearance = 6.3 ft > 0.5 (D_L) = 0.5 (8.7 ft) = 4.35 ft

$\Rightarrow$ Large underkeel clearance

C_H = 1.05

V = impact speed = 3.8 knots = 6.41 ft/s

W = vessel displacement tonnage = 1,900 tonnes

$$\text{KE} = \text{Barge collision energy} = \frac{C_H W(V)^2}{29.2} = \frac{(1.05)(1900)(6.41)^2}{29.2} \text{ kips-ft}$$

$$a_B = \text{Barge bow damage depth} = \left[\left(1+\frac{KE}{5672}\right)^{1/2} - 1\right]\left[\frac{10.2}{R_B}\right] = \left[\left(1+\frac{2{,}807.22}{5672}\right)^{1/2} - 1\right]\left[\frac{10.2}{1}\right]$$

KE = 2,807.22 kips-ft

a_B = 2.27 ft

For $a_B \geq 0.34$:

$$P_B = [1349 + 110(a_B)]\, R_B$$

P_B = Equivalent static barge impact force = [1349 + 110(2.27)] (1)

P_B = 1,599 kips = 7,112 kN

33% P_B = 528 kips = 2,347 kN

APPENDIX C

EFFECTIVE PRESTRESSING FORCE

AND INITIAL STRAIN FOR PRESTRESSING STRANDS

The chosen alternate strand pattern consists of 8 No. 13 grade 1860 (Spec.) low-relaxation strands prestressed at 133.4 kN (30 kips) each. According to ASTM A 416, the area of the No. 13, grade 1860 (Spec.) prestressing strands is 107.74 mm^2 (0.167 in^2). Prestress loss was assumed to be 310 MPa (45,000 psi) according to AASHTO Standard Specifications (1996), and the effective prestressing force after losses is calculated according to the following equations (Nawy, 1996):

$$f_{pi} = \frac{P_i}{A_{ps}} = \frac{133.4 \times 10^3 N}{107.74 mm^2} = 1{,}238.17 MPa \qquad (C.1)$$

$$f_{pe} = f_{pi} - \Delta f = 1{,}238.17 MPa - 310.00 MPa = 928.17 MPa \qquad (C.2)$$

$$P_e = f_{pe} A_{ps} = 928.17 MPa \times 107.74 mm^2 = 100.00 \times 10^3 N \qquad (C.3)$$

where:

f_{pi} = initial strand stress

P_i = initial prestress force

A_{ps} = area of prestressing strand

f_{pe} = effective strand stress after losses

Δf = prestress loss

P_e = effective prestressing force after losses

Since only four equivalent strands could be used due to node locations (Fig. C.1), their areas (A_{es}) and prestressing forces (P_{es}) were determined as twice that of the original strands to maintain the same total steel area and prestressing force. The equivalent prestressing strain (ε_{es}) was then calculated by Eq. C.4 (Nawy, 1996) for each strand of the finite element model.

$$\varepsilon_{es} = \frac{P_{es}}{A_{es}E_{ps}} = \frac{200\times10^{3}\,\mathrm{N}}{(2.155\times10^{-4}\,\mathrm{m}^{2})(200\times10^{9}\,\mathrm{N/m}^{2})} = 0.00464 \qquad \text{(C.4)}$$

where:

E_{ps} = modulus of elasticity of prestressing strands = 200 x 10^9 N/m^2 (Gere and Timoshenko 1997)

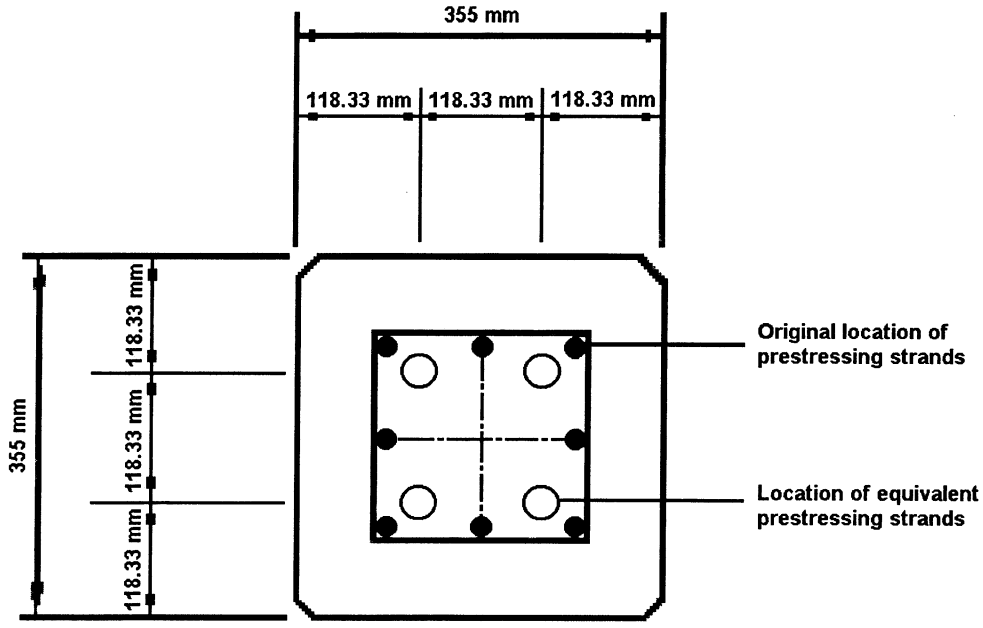

Figure C.1. Equivalent Prestressing Strands Location on Concrete Pile and on Finite Element Model

APPENDIX D

P-Y CURVES

D.1. P-Y Curves for Plumb Piles

P-y curves for the soil were determined every 0.5m (1.64 ft) along the embedded length of the piles, according to the procedure described in Reese, Cox, and Koop (1974). The curves consist of four distinct regions, three straight lines and a parabola, as shown in Fig. D.1. Calculations are presented below and contain the determination of the three points that define each p-y curve, as well as the equations for each of the four portions of the curves.

1. Determination of preliminary factors:

b = pile diameter = 0.355 m

k = empirical factor = 16.29 x 10^6 N/m^3 (60 lb/in^3) (Reese, Cox and Koop 1974)

γ = saturated unit weight = 20.02 x 10^3 N/m^3 (127.46 lb/ft^3) (Bas 1998)

ϕ = angle of internal friction = 30° (Tomlinson 1987)

K_0 = coefficient of earth at rest = 0.4 (Meyer and Reese 1979)

$$K_a = \left(\tan\left(\frac{\pi}{4} - \frac{\phi}{2}\right)\right)^2 = 0.333 \text{ (Reese, Cox, Koop 1974)} \qquad \text{(D.1)}$$

where:

K_a = active earth pressure coefficient

$$\alpha = \frac{\phi}{2} = 0.262 \qquad \text{(D.2)}$$

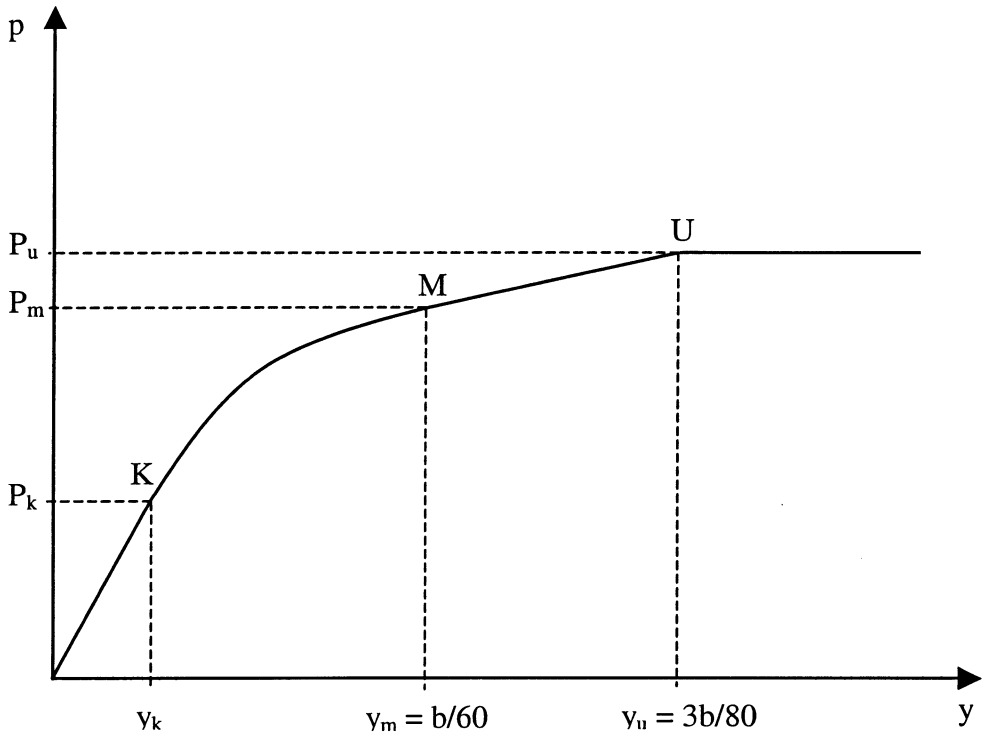

Figure D.1. Typical Shape of P-Y Curve in Sand (Reese, Cox, Koop 1974)

$$\beta = \frac{\pi}{4} + \frac{\phi}{2} = 1.047 \qquad \text{(D.3)}$$

where:

α and β = angles from Mohr-Coulomb soil failure wedge (Reese, Cox and Koop 1974)

2. Calculation of the abscissa of point U:

$$y_u = \frac{3b}{80} = \frac{3 \cdot (0.355\text{m})}{80} = 0.013 \text{ m} \qquad \text{(D.4)}$$

3. Calculation of the abscissa of point M:

$$y_m = \frac{b}{60} = \frac{0.355\text{m}}{60} = 0.00592 \text{ m} \qquad \text{(D.5)}$$

4. The abscissa of point K, as well as the ordinates of points K, M, and U are dependent on the theoretical ultimate soil resistance (P_c), which is calculated in the following for every 0.5 m (1.64 ft) along the embedded length of the pile. Two equations are required for the calculation of P_c. Equation D.6 is applicable to depths near the ground surface, while Eq. D.7 is applicable below the critical depth (H_{cr}), that is, where there is horizontal flow around the pile.

$$P_{ct} = \gamma H\left[\frac{K_o H \tan\phi \sin\beta}{\tan(\beta-\phi)\cos\alpha} + \frac{\tan\beta(b + H\tan\beta\tan\alpha)}{\tan(\beta-\phi)} + K_o H \tan\beta(\tan\phi\sin\beta - \tan\alpha) - K_a b\right] \qquad \text{(D.6)}$$

$$P_{cd} = K_a b\gamma H\left[\tan^8(\beta) - 1\right] + K_o b\gamma H \tan(\phi)\tan^4(\beta) \qquad \text{(D.7)}$$

where:

P_{ct} = theoretical ultimate soil resistance near the ground surface (N/m)

P_{cd} = theoretical ultimate soil resistance well below ground surface (N/m)

H = depth at which the curve is to be computed (m)

The critical depth (H_{cr}) is determined from Fig. D.2 as 4.9 m (1.61 ft), the intersection of Eqs. D.6 and D.7. Values for P_c are presented in Table D.1.

5. Calculation of the ordinate of point U, or ultimate soil resistance:

$$P_u = AP_c \qquad \text{(D.8)}$$

where:

A = adjustment factor with depth x, presented in Fig. D.3

Values for the adjustment factor A and ultimate soil resistance P_u along the embedded length of the pile are presented in Table D.1.

6. Calculation of the ordinate of point M:

$$P_m = BP_c \qquad \text{(D.9)}$$

where:

B = adjustment factor with depth x, presented in Fig. D.4

Values for P_m and adjustment factor B along the embedded length of the pile are presented in Table D.1.

7. Calculation of slope of line between points M and U:

$$m = \frac{P_u - P_m}{y_u - y_m} \qquad \text{(D.10)}$$

Values for m along the plumb pile are presented in Table D.2

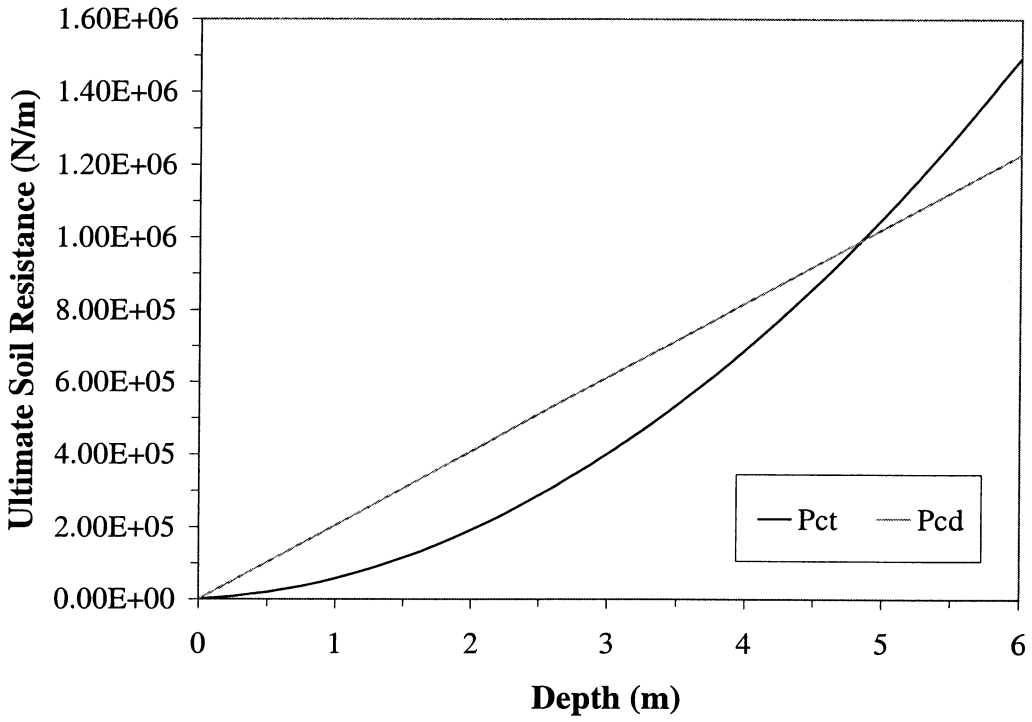

Figure D.2. Plot of Theoretical Ultimate Soil Resistance Equations for Determination of the Critical Depth

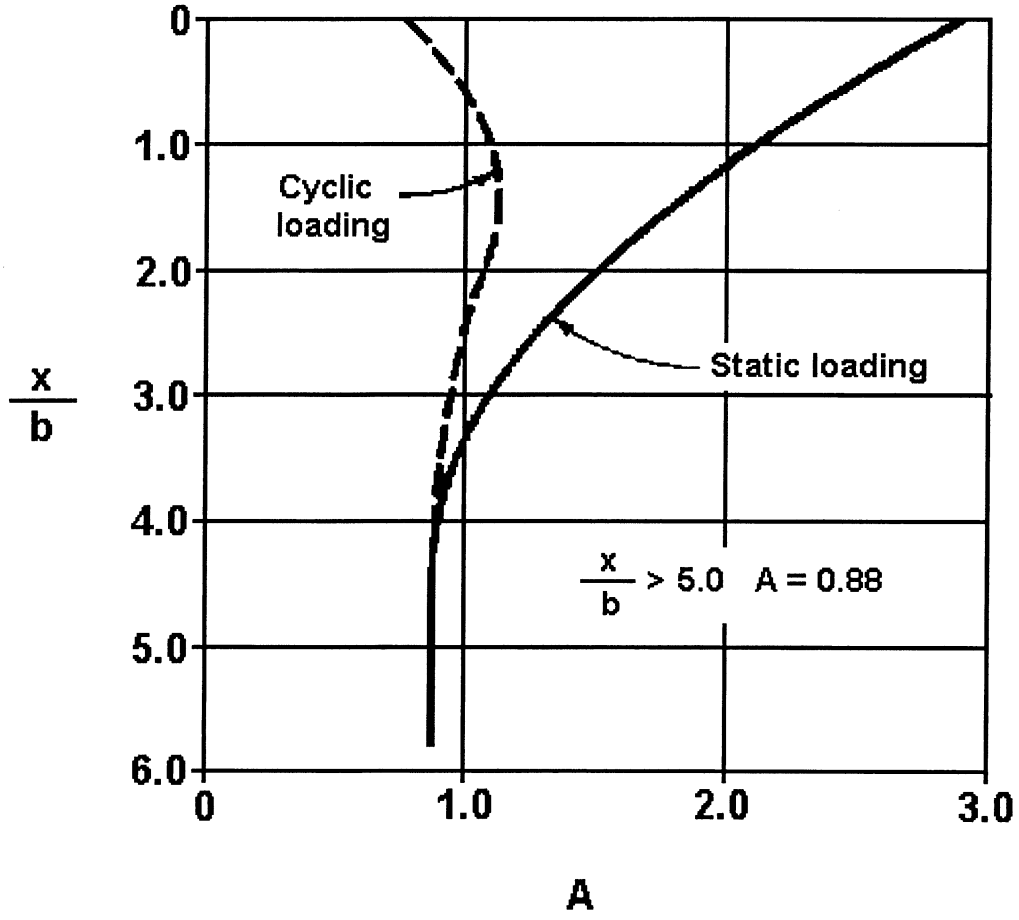

Figure D.3. Non-Dimensional Coefficient A for Ultimate Soil Resistance vs. Depth (Reese, Cox and Koop 1974)

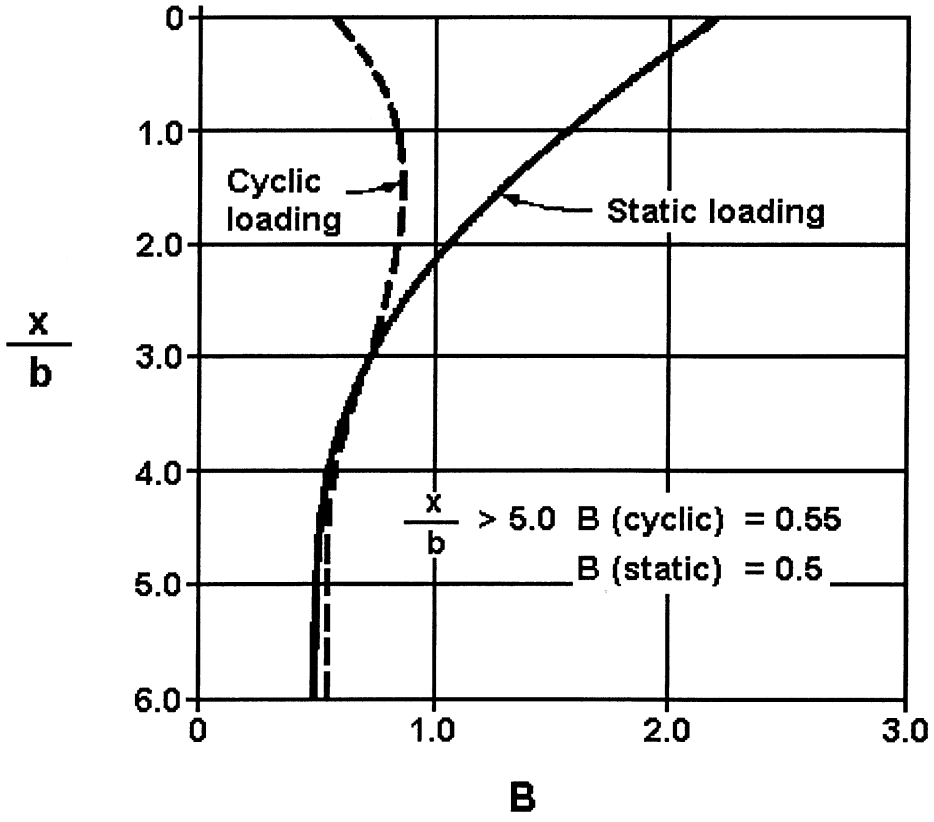

Figure D.4. Non-Dimensional Coefficient B for Soil Resistance vs. Depth (Reese, Cox and Koop 1974)

Table D.1. Theoretical Ultimate Soil Resistance (P_c), Adjustment Factors A and B, and Ordinates of Points U and M on P-Y Curves

Depth (m)	P_c (N/m)	A	P_u (N/m)	B	P_m (N/m)
0.0	0	2.875	0	2.15	0
0.5	1.905×10^4	1.900	3.619×10^4	1.35	2.571×10^4
1.0	5.723×10^4	1.175	6.725×10^4	0.80	4.579×10^4
1.5	1.146×10^4	0.900	1.031×10^5	0.50	5.728×10^4
2.0	1.910×10^5	0.880	1.681×10^5	0.50	9.551×10^4
2.5	2.866×10^5	0.880	2.522×10^5	0.50	1.433×10^5
3.0	4.014×10^5	0.880	3.532×10^5	0.50	2.007×10^5
3.5	5.352×10^5	0.880	4.710×10^5	0.50	2.676×10^5
4.0	6.883×10^5	0.880	6.057×10^5	0.50	3.441×10^5
4.5	8.604×10^5	0.880	7.572×10^5	0.50	4.302×10^5
5.0	1.022×10^6	0.880	8.990×10^5	0.50	5.108×10^5
5.5	1.124×10^6	0.880	9.889×10^5	0.50	5.619×10^5
6.0	1.226×10^6	0.880	1.079×10^6	0.50	6.130×10^5

Table D.2. Coordinates for Point K, Factors n and C, and Slope of Straight Line Between Points K and M, Along the Embedded Length of the Plumb Piles.

Depth (m)	m	n	C	y_k (m)	P_k (N/m)
0.0	0	0	0	1	0
0.5	1.416×10^{6}	3.068	1.369×10^{5}	2.393×10^{-3}	1.914×10^{4}
1.0	2.902×10^{6}	2.667	3.135×10^{5}	1.851×10^{-3}	2.961×10^{4}
1.5	6.196×10^{6}	1.562	1.527×10^{6}	4.751×10^{-4}	1.140×10^{4}
2.0	9.815×10^{6}	1.645	2.161×10^{6}	1.033×10^{-3}	3.305×10^{4}
2.5	1.473×10^{7}	1.645	3.242×10^{6}	1.646×10^{-3}	6.583×10^{4}
3.0	2.062×10^{7}	1.645	4.540×10^{6}	2.440×10^{-3}	1.171×10^{5}
3.5	2.750×10^{7}	1.645	6.055×10^{6}	3.432×10^{-3}	1.922×10^{5}
4.0	3.536×10^{7}	1.645	7.786×10^{6}	4.636×10^{-3}	2.967×10^{5}
4.5	4.421×10^{7}	1.645	9.733×10^{6}	6.067×10^{-3}	4.368×10^{5}
5.0	5.249×10^{7}	1.645	1.156×10^{7}	7.186×10^{-3}	5.749×10^{5}
5.5	5.774×10^{7}	1.645	1.271×10^{7}	7.186×10^{-3}	6.324×10^{5}
6.0	6.299×10^{7}	1.645	1.387×10^{7}	7.186×10^{-3}	6.899×10^{5}

8. Determination of abscissa of point K:

$$y_k = \left(\frac{C}{k \cdot H} \right)^{\frac{n}{n-1}} \tag{D.11}$$

where:

$$C = \frac{P_m}{(y_m)^{\frac{1}{n}}} \tag{D.12}$$

$$n = \frac{P_m}{m \cdot y_m} \tag{D.13}$$

Values for y_k, and parameters n and C along the embedded length of the pile are presented in Table D.2.

9. Equation for parabola to be fitted between points K and M:

$$P = Cy^{\frac{1}{n}} \tag{D.14}$$

10. Calculation of the ordinate of point K:

$$P_k = Cy_k^{\frac{1}{n}} \tag{D.15}$$

Values for P_k along the embedded length of the pile are presented in Table D.2.

Additional points were calculated between points K and M for the fitting of the parabola, and one of the p-y curves for the plumb piles is presented in Fig. D.5.

D.2. P-Y Curves for Batter Piles

Factors to account for the batter of the piles were developed by Kubo (1967) and presented in Meyer and Reese (1979). For the batter piles in this study, the modification factor

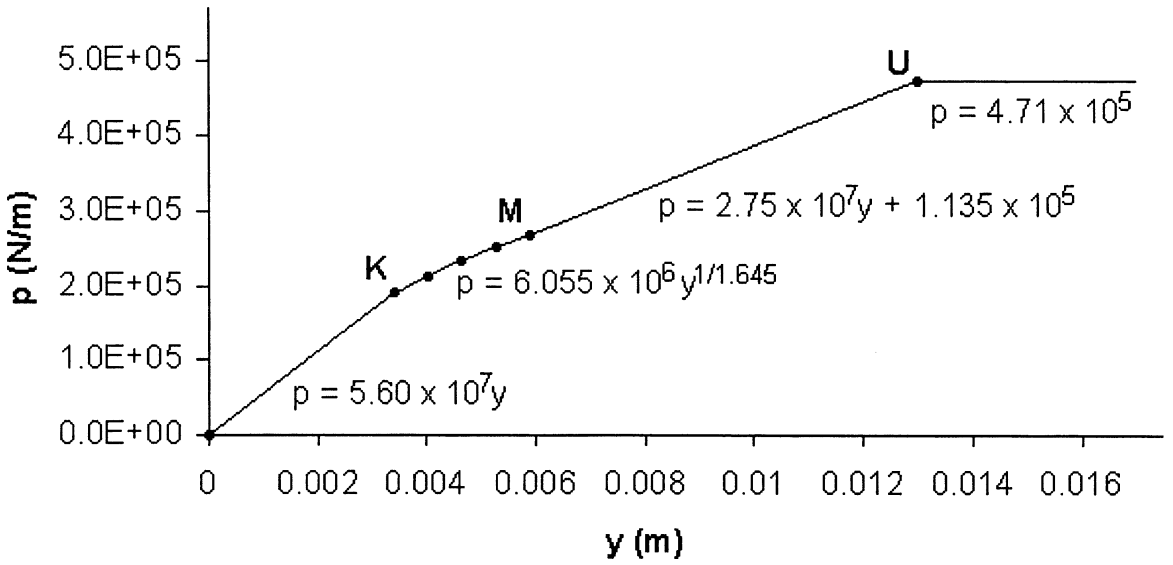

Figure D.5. P-Y Curve for Plumb Pile at Depth of 3.5 m

was determined as 0.55 and multiplied by the theoretical ultimate soil resistance (P_c) calculated in the previous section. Results for the theoretical ultimate soil resistance, as well as coordinates for point K, and ordinates of points M and U of p-y curves along the embedded length of the batter piles are presented in Table D.3. The abscissas of points M and U remained unchanged: y_m = 0.00592 and y_u = 0.013. Graphical representation of one of the p-y curves is presented in Figs. D.6.

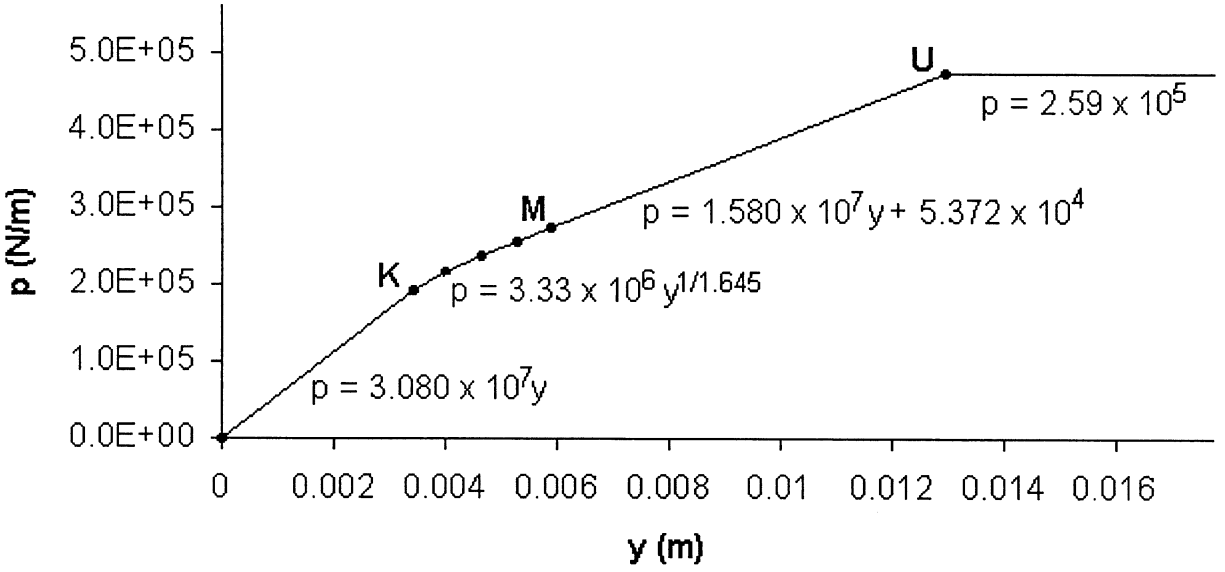

Figure D.6. P-Y Curve for Batter Pile at Depth of 3.5 m

Table D.3. Theoretical Ultimate Soil Resistance (P_c), and Coordinates for Points K, and Ordinates of Points M, and U Along the Embedded Length of the Batter Piles

Depth (m)	P_c (N/m)	y_k (m)	P_k (N/m)	P_m (N/m)	P_u (N/m)
0.0	0	1	0	0	0
0.5	1.048×10^{4}	2.393×10^{-3}	1.053×10^{4}	1.414×10^{4}	1.990×10^{4}
1.0	3.148×10^{4}	1.851×10^{-3}	1.629×10^{4}	2.518×10^{4}	3.699×10^{4}
1.5	6.301×10^{4}	4.751×10^{-4}	6.272×10^{3}	3.150×10^{4}	5.671×10^{4}
2.0	1.051×10^{5}	1.033×10^{-3}	1.818×10^{4}	5.253×10^{4}	9.245×10^{4}
2.5	1.576×10^{5}	1.646×10^{-3}	3.620×10^{4}	7.882×10^{4}	1.387×10^{5}
3.0	2.208×10^{5}	2.440×10^{-3}	6.441×10^{4}	1.104×10^{5}	1.943×10^{5}
3.5	2.944×10^{5}	3.432×10^{-3}	1.057×10^{5}	1.472×10^{5}	2.591×10^{5}
4.0	3.785×10^{5}	4.636×10^{-3}	1.632×10^{5}	1.893×10^{5}	3.331×10^{5}
4.5	4.732×10^{5}	6.067×10^{-3}	2.403×10^{5}	2.366×10^{5}	4.164×10^{5}
5.0	5.619×10^{5}	7.186×10^{-3}	3.162×10^{5}	2.809×10^{5}	4.945×10^{5}
5.5	6.181×10^{5}	7.186×10^{-3}	3.478×10^{5}	3.090×10^{5}	5.439×10^{5}
6.0	6.743×10^{5}	7.186×10^{-3}	3.794×10^{5}	3.371×10^{5}	5.934×10^{5}

APPENDIX E

SOIL REACTION AND SPRING COEFFICIENTS

E.1. Soil Reaction Calculation Procedure

As mentioned on Chap. 3, it was necessary to determine the percentage of load resisted by the soil behind each individual pile. The initial assumption that each pile would resist 50% of the load was found to be incorrect. Calculations for the second trial, where it was assumed that the plumb pile would resist 60% of the load, while the batter one would resist only 40%, were performed according to the procedure described in Tomlinson (1987) and are presented below.

Pile deflections are initially calculated by elastic analysis, according to Eq. E.1, developed by Matlock and Reese (1960).

$$y = \frac{A_y H T^3}{EI} + \frac{B_y M_t T^2}{EI} \qquad \text{(E.1)}$$

$$T = \sqrt[5]{\frac{EI}{k}} \qquad \text{(E.2)}$$

$$M_t = He \qquad \text{(E.3)}$$

where:

y = deflection

A_y = soil reaction coefficient relative to depth x (Fig. E.1)

H = lateral load applied to the pile

E = modulus of elasticity

I = moment of inertia

T = stiffness factor

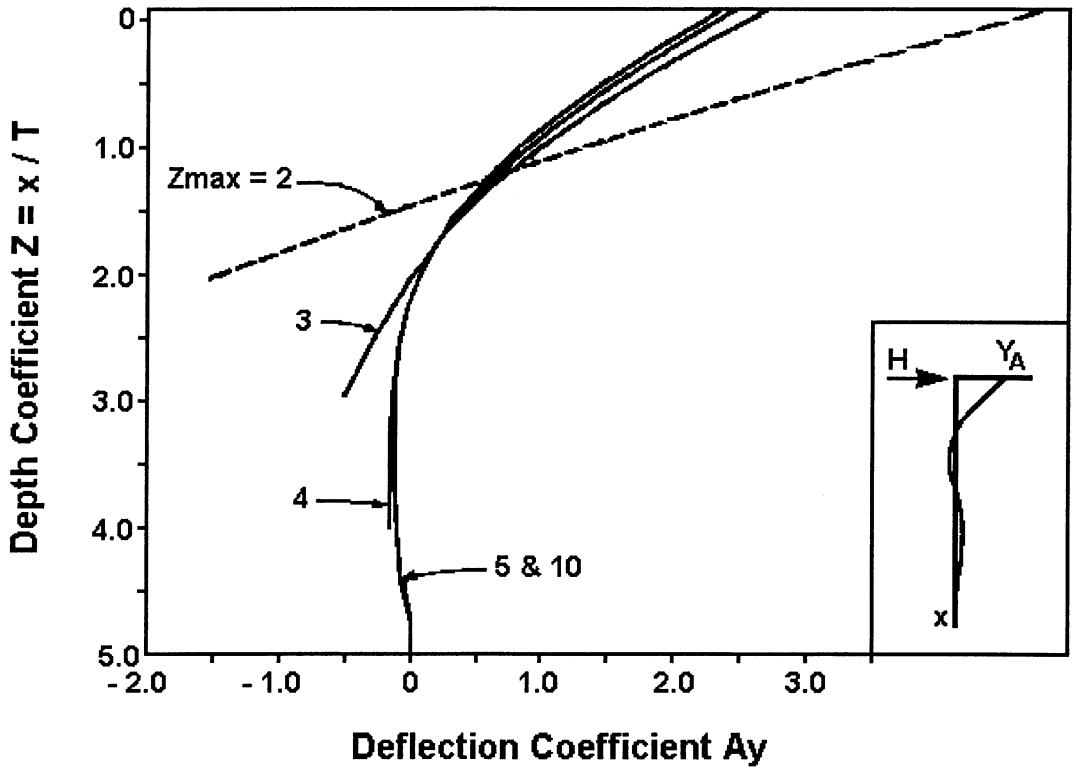

Figure E.1. Soil Reaction Coefficient for Deflection, A_y (Meyer and Reese 1979)

B_y = soil reaction coefficient relative to depth x (Fig. E.2)

M_t = moment at ground surface

k = subgrade reaction

e = distance from the ground surface to the lateral load

The reactions obtained by Eq. E.1 and the corresponding lateral soil response p, from the p-y curves are used to calculate the soil modulus:

$$E_s = -\frac{p}{y} \tag{E.4}$$

The values obtained for the soil modulus are then plotted against depth. A straight line passing through the origin is drawn through the points, giving weight to those nearer the ground surface, that is, those at depths of less than 0.5T where the deflections are more significant. The slope of such line is the subgrade modulus k and is used to compute the stiffness factor T according to Eq. E.2. This value of T is then compared to the value assumed for the iteration. If they are equal, no additional iterations are necessary since the pile deflection values obtained by Eq. E.1 are compatible with the p-y curves. If they differ, a new iteration is required. The T values obtained are plotted against those from the previous trial, and a line is traced through these two points. The final T value is determined as the intersection of this line and the equality line. Final deflections and soil reactions can then be calculated with the final T value according to Eqs. E.1 and E.5:

$$p = \frac{A_p H}{T} + \frac{B_p M_t}{T^2} \tag{E.5}$$

where:

p = soil reaction

A_p = soil resistance coefficient from Fig. E.3

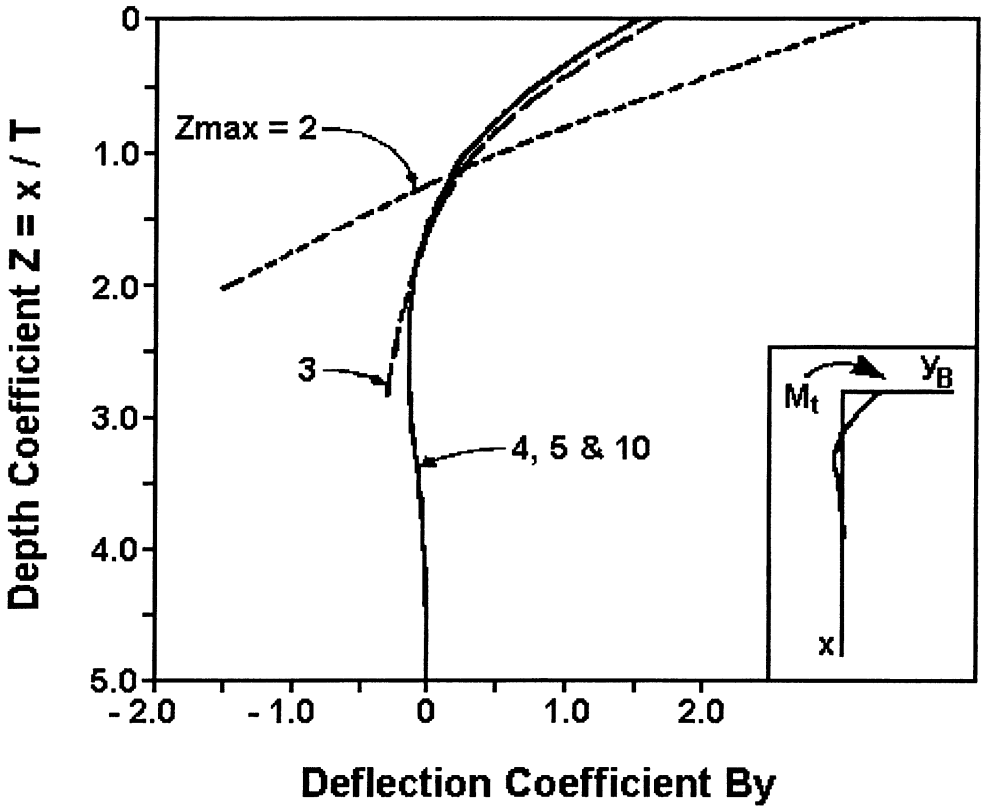

Figure E.2. Soil Reaction Coefficient for Deflection, B_y (Meyer and Reese 1979)

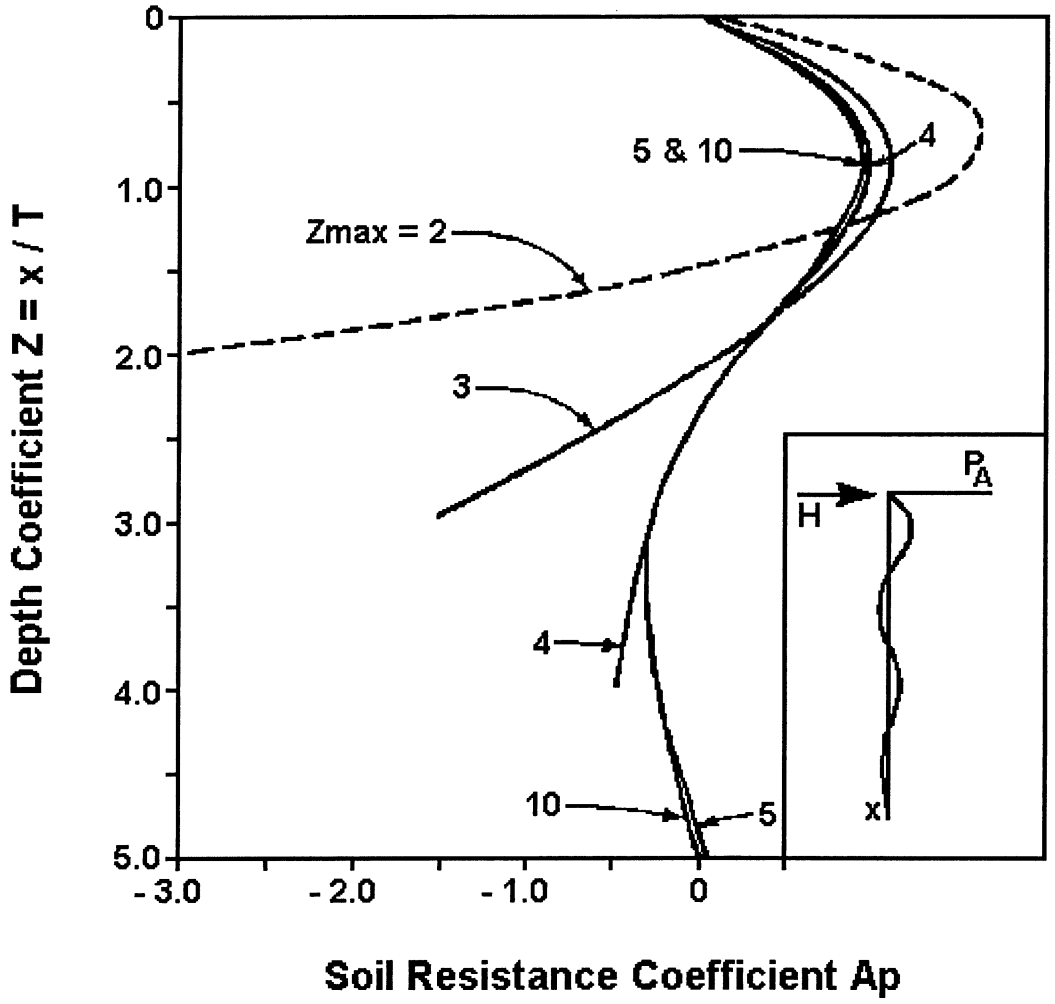

Figure E.3. Soil Resistance Coefficient, A_p (Matlock and Reese 1956)

B_p = soil resistance coefficient from Fig. E.4

E.2. Soil Reaction and Spring Coefficients for 33% of Total Load

E.2.1. Soil Reaction Behind Plumb Pile

H = 60 % of the total load considered = 2.140 x 10^5 N

e = 6.4 m

E = 24 x 10^9 N/m^2

I = 0.00132 m^4

k = 16 x 10^6 N/m^3 (Reese, Cox and Koop 1974)

$$M_t = He = (2.140 * 10^5 \text{ N})(6.4 \text{ m}) = 1.37 \times 10^6 \text{ Nm}$$

$$T = \sqrt[5]{\frac{EI}{k}} = \sqrt[5]{\frac{(24 \times 10^9 \text{ N/m}^2)(0.00132 \text{ m}^4)}{16 \times 10^6 \text{ N/m}^3}} = 1.146 \text{ m}$$

$$0.5T = (0.5)(1.146 \text{ m}) = 0.573 \text{ m}$$

Values for factors Z, A_y, B_y, deflection y from Eq. E.1, and corresponding lateral soil response p from the p-y curves are presented in Table E.1. The plot for the determination of the soil modulus is presented in Fig. E.5a. The straight line through the origin is drawn with weight given to points above 0.573 m, and the soil modulus is determined as 7 x 10^6 N/m^3. Since this value is different from the assumed k value, a second trial is necessary:

$$T = \sqrt[5]{\frac{EI}{k}} = \sqrt[5]{\frac{(24 \times 10^9 \text{ N/m}^2)(0.00132 \text{ m}^4)}{7 \times 10^6 \text{ N/m}^3}} = 1.353 \text{ m}$$

$$0.5T = (0.5)(1.353 \text{ m}) = 0.676 \text{ m}$$

Values for factors Z, A_y, and B_y, deflection y from Eq. E.1, and corresponding lateral soil response p from the p-y curves are presented in Table E.2. The plot for the determination of the

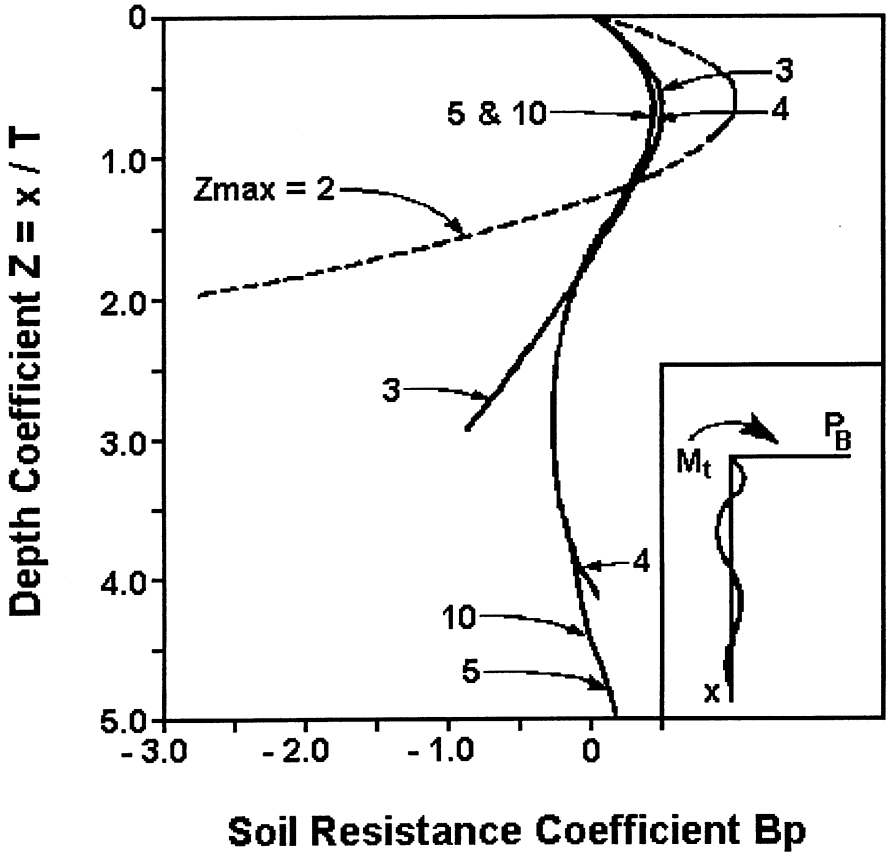

Figure E.4. Soil Resistance Coefficient, B_p (Matlock and Reese 1956)

Table E.1. Plumb Pile Deflection Obtained by Elastic Analysis and Lateral Soil Response Obtained from p-y Curves for the First Iteration

Depth (m)	Z	A_y	B_y	y (m)	p (N/m)
0	0	2.30	1.60	0.114	0.000
0.5	0.436	1.80	1.00	0.075	3.620×10^{4}
1.0	0.872	1.00	0.50	0.039	6.730×10^{4}
1.5	1.308	1.70	0.20	0.029	1.029×10^{5}
2.0	1.745	0.25	-0.05	-2.966×10^{-4}	1.550×10^{4}
2.5	2.181	0.10	-0.10	-4.664×10^{-3}	1.240×10^{5}
3.0	2.617	-0.10	-0.10	-6.700×10^{-3}	2.230×10^{5}
3.5	3.053	-0.10	-010	-6.700×10^{-3}	2.980×10^{5}
4.0	3.489	-0.10	-0.05	-3.859×10^{-3}	2.470×10^{5}
4.5	3.925	-0.05	0.00	-5.089×10^{-4}	3.660×10^{4}
5.0	4.362	-0.05	0.00	-5.089×10^{-4}	4.070×10^{4}
5.5	4.798	0.00	0.00	0.000	0.000
6.0	5.234	0.00	0.00	0.000	0.000

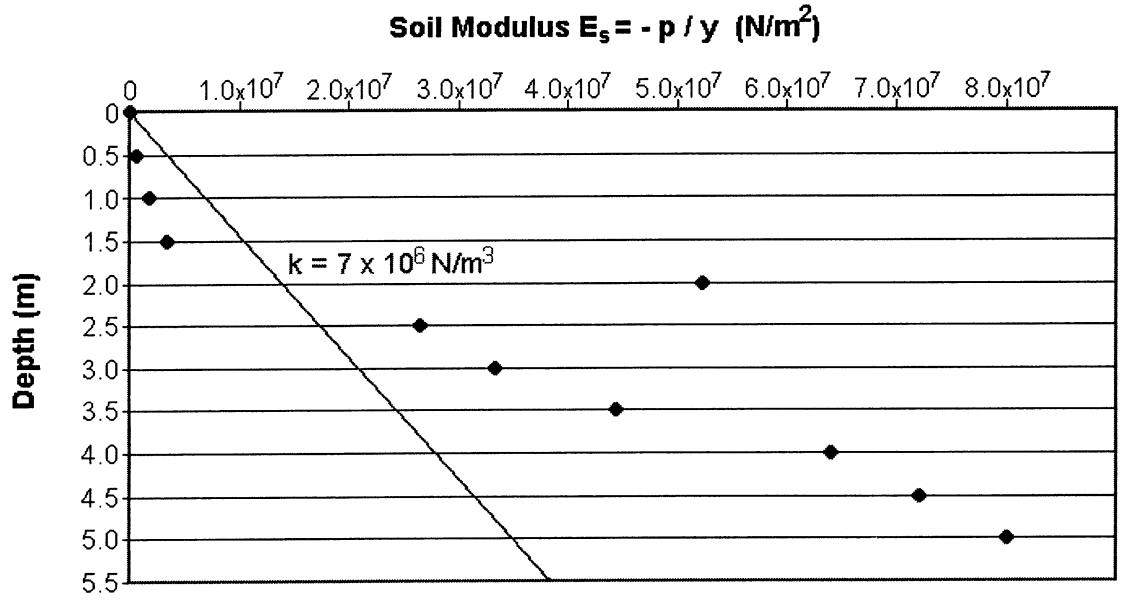

(a) First Iteration

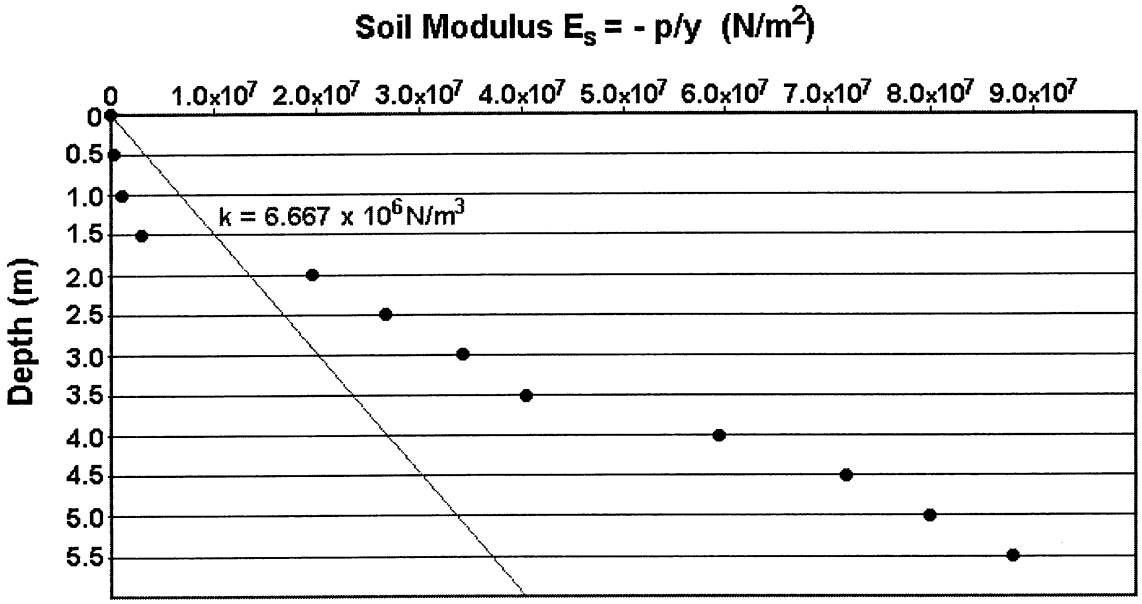

(b) Second Iteration

Figure E.5. Trial Plotting of Soil Modulus Against Depth

Table E.2. Plumb Pile Deflection Obtained by Elastic Analysis and Lateral Soil Response Obtained from the p-y Curves for the Second Iteration

Depth (m)	Z	A_y	B_y	y (m)	p (N/m)
0	0	2.30	1.60	0.165	0.000
0.5	0.370	1.85	1.00	0.110	3.620×10^{4}
1.0	0.739	1.20	0.60	0.068	6.730×10^{4}
1.5	1.109	0.90	0.25	0.035	1.029×10^{5}
2.0	1.479	0.45	-0.05	3.567×10^{-3}	7.030×10^{4}
2.5	1.848	0.20	-0.10	-4.566×10^{-3}	1.230×10^{5}
3.0	2.218	0.10	-0.10	-6.238×10^{-3}	2.140×10^{5}
3.5	2.588	-0.05	-010	-8.745×10^{-3}	3.540×10^{5}
4.0	2.957	-0.10	-0.05	-5.626×10^{-3}	3.340×10^{5}
4.5	3.327	-0.10	0.00	-1.671×10^{-3}	1.200×10^{5}
5.0	3.697	-0.10	0.00	-1.671×10^{-3}	1.340×10^{5}
5.5	4.067	-0.05	0.00	-8.357×10^{-4}	7.360×10^{4}
6.0	4.436	0.00	0.00	0.000	0.000

soil modulus is presented in Fig. E.5b. The straight line through the origin is drawn with weight given to points above 0.676 m, and the soil modulus is determined as 6.667 x 10^6 N/m^3. The new T value is therefore:

$$T = \sqrt[5]{\frac{EI}{k}} = \sqrt[5]{\frac{(24\times10^9\,N/m^2)(0.00132\,m^4)}{6.667\times10^6\,N/m^3}} = 1.366\,m$$

The final value of T is determined as 1.367 m, from the intersection of the equality line and the line through the points determined by the two iterations, shown in Fig. E.6.

The pile deflection and the soil reaction are calculated with the final T value according to Eqs. E.1 and E.5, and are presented in Table E.3. The soil reaction profile is shown in Fig. E.7.

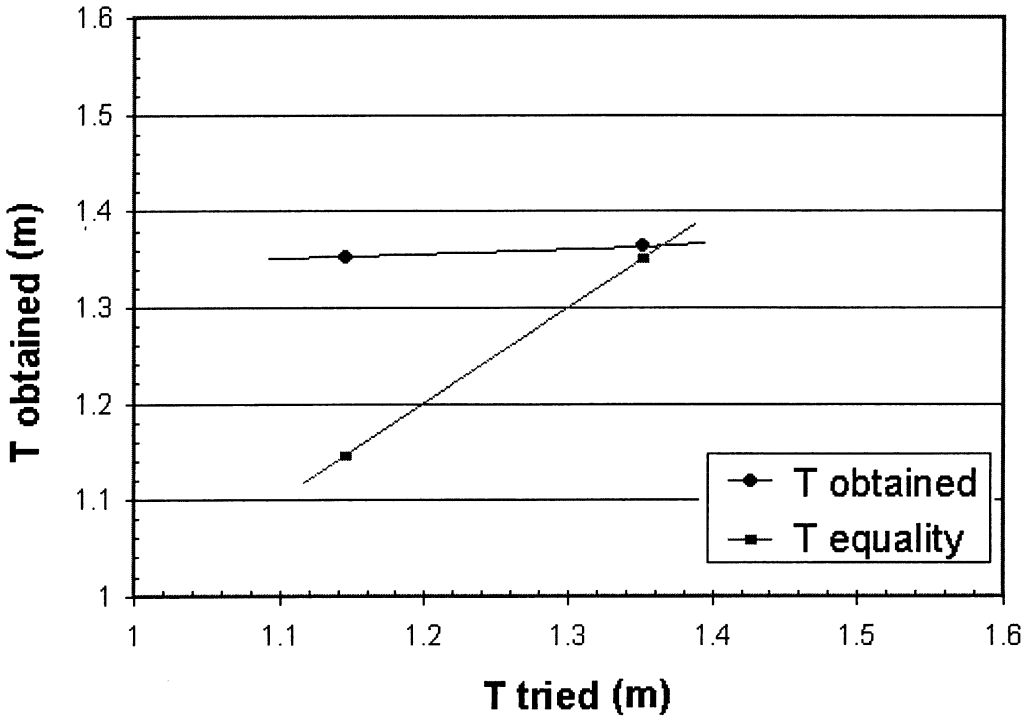

Figure E.6. Stiffness Factor

Table E.3. Plumb Pile Deflection and Soil Reaction with 33% Impact Load

Depth (m)	Z	A_y	B_y	A_p	B_p	y (m)	p (N/m)
0	0.000	2.30	1.60	0.00	0.00	0.1690	0.000
0.5	0.366	2.00	1.25	0.50	0.25	0.1360	2.615×10^5
1.0	0.732	1.60	0.85	0.85	0.40	0.0960	4.263×10^5
1.5	1.097	1.40	0.60	0.95	0.40	0.0730	4.419×10^5
2.0	1.463	1.00	0.45	0.95	0.40	0.0540	4.419×10^5
2.5	1.829	0.75	0.20	0.85	0.30	0.0290	3.530×10^5
3.0	2.195	0.50	0.10	0.75	0.10	0.0170	1.907×10^5
3.5	2.560	0.25	0.00	0.60	0.00	0.0043	9.394×10^4
4.0	2.926	0.10	-0.05	0.20	-0.15	-0.0023	-7.864×10^4
4.5	3.292	0.00	-0.10	0.20	-0.15	-0.0081	-7.864×10^4
5.0	3.658	0.00	-0.10	0.00	-0.20	-0.0081	-1.466×10^5
5.5	4.023	-0.05	-0.10	-0.20	-0.25	-0.0089	-2.146×10^5
6.0	4.389	-0.10	-0.05	-0.25	-0.25	-0.0058	-2.224×10^5

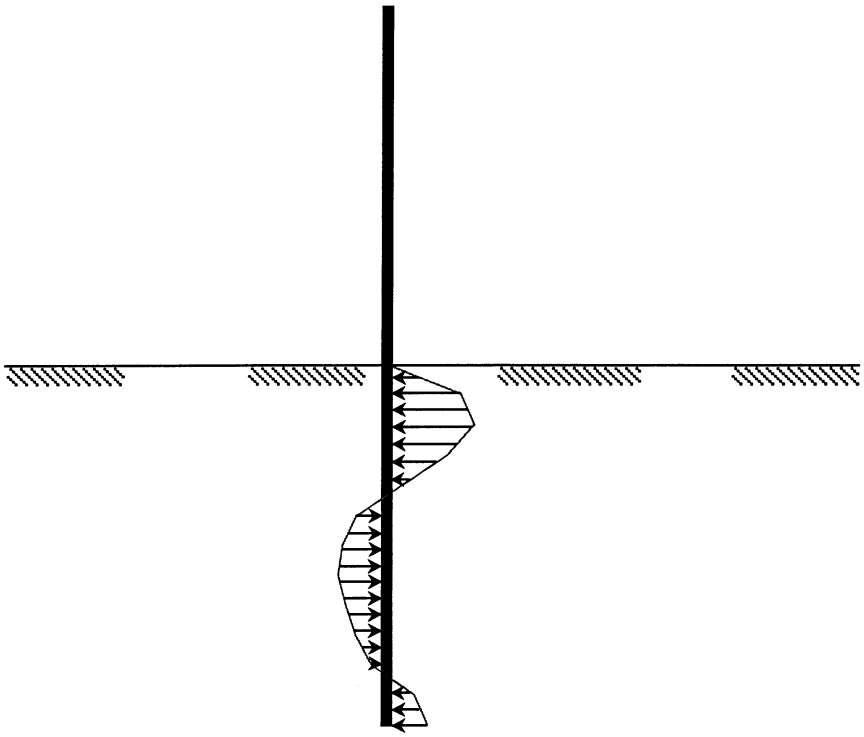

Figure E.7. Soil Reaction Profile for Plumb Pile with 33% Impact Load

Spring elements were placed on every pile node below the embedded depth. Spring stiffness coefficients for each element were calculated according to tributary areas, and are presented on Table E.4.

E.2.2. Soil Reaction Behind Batter Pile

Similar calculations were performed for the batter piles. The lateral load consisted of 40 % of the total load considered, or 142.7 kN (32 kips). Final values for pile deflection, soil reaction, and spring stiffness coefficients are presented on Table E.5.

E.3. Soil Reaction and Spring Coefficients for Total Impact Load

Soil reaction and spring coefficients were also calculated for the case of the total impact load. The lateral load applied to the plumb piles was 648.5 kN (145.8 kips), or 60% of the load, and that applied to the batter piles was 432.4 kN (97.2 kips). Results are presented in Tables E.6 and E.7.

Table E.4. Stiffness Coefficients for Spring Elements, Plumb Piles, 33% Impact Load

Depth (m)	Pile Deflection y (m)	Soil Reaction p (N/m)	Stiffness Coefficient K = p/y (N/m^2)	Coefficient for External Nodes (K/6) (N/m^2)	Coefficients for Internal Nodes (K/3) (N/m^2)
0.5	0.1360	2.615×10^5	1.923×10^6	3.205×10^5	6.409×10^5
1.0	0.0960	4.263×10^5	4.441×10^6	7.401×10^5	1.480×10^6
1.5	0.0730	4.419×10^5	6.053×10^6	1.009×10^6	2.018×10^6
2.0	0.0540	4.419×10^5	8.183×10^6	1.364×10^6	2.728×10^6
2.5	0.0290	3.530×10^5	1.217×10^7	2.029×10^6	4.057×10^6
3.0	0.0170	1.907×10^5	1.122×10^7	1.870×10^6	3.739×10^6
3.5	0.0043	9.394×10^4	2.178×10^7	3.629×10^6	7.259×10^6
4.0	-0.0023	-7.864×10^4	3.398×10^7	5.664×10^6	1.133×10^7
4.5	-0.0081	-7.864×10^4	9.734×10^6	1.622×10^6	3.245×10^6
5.0	-0.0081	-1.466×10^5	1.815×10^7	3.024×10^6	6.049×10^6
5.5	-0.0089	-2.146×10^5	2.400×10^7	4.000×10^6	8.000×10^6
6.0	-0.0058	-2.224×10^5	3.858×10^7	6.431×10^6	1.286×10^7

Table E.5. Stiffness Coefficients for Spring Elements, Batter Piles, 33% Impact Load

Depth (m)	Pile Deflection y (m)	Soil Reaction p (N/m)	Stiffness Coefficient K = p/y (N/m^2)	Coefficient for External Nodes (K/6) (N/m^2)	Coefficients for Internal Nodes (K/3) (N/m^2)
0.5	0.1260	1.475×10^5	1.171×10^6	1.952×10^5	3.905×10^5
1.0	0.0920	2.004×10^5	2.178×10^6	3.630×10^5	7.261×10^5
1.5	0.0580	2.087×10^5	3.598×10^6	5.997×10^5	1.199×10^6
2.0	0.0400	1.543×10^5	3.858×10^6	6.429×10^5	1.286×10^6
2.5	0.0092	7.248×10^4	7.897×10^6	1.316×10^6	2.632×10^6
3.0	0.0007	2.334×10^4	3.232×10^7	5.387×10^6	1.077×10^7
3.5	-0.0043	-5.329×10^4	1.2416×10^7	2.069×10^6	4.139×10^6
4.0	-0.0077	-5.590×10^4	7.228×10^6	1.205×10^6	2.409×10^6
4.5	-0.0089	-7.816×10^4	8.800×10^6	1.467×10^6	2.933×10^6
5.0	-0.0100	-9.060×10^4	9.060×10^6	1.510×10^6	3.020×10^6
5.5	-0.0100	-9.060×10^4	9.060×10^6	1.510×10^6	3.020×10^6
6.0	-0.0062	-7.663×10^4	1.244×10^7	2.073×10^6	4.145×10^6

Table E.6. Stiffness Coefficients for Spring Elements, Plumb Piles, Full Impact Load

Depth (m)	Pile Deflection y (m)	Soil Reaction p (N/m)	Stiffness Coefficient K = p/y (N/m^2)	Coefficient for External Nodes (K/6) (N/m^2)	Coefficients for Internal Nodes (K/3) (N/m^2)
0.5	0.411	7.925×10^5	1.928×10^6	3.214×10^5	6.423×10^5
1.0	0.292	1.292×10^6	4.425×10^6	7.374×10^5	1.475×10^6
1.5	0.220	1.339×10^6	6.086×10^6	1.014×10^6	2.029×10^6
2.0	0.162	1.339×10^6	8.265×10^6	1.378×10^6	2.755×10^6
2.5	0.088	1.070×10^6	1.216×10^7	2.027×10^6	4.053×10^6
3.0	0.051	5.779×10^5	1.133×10^7	1.889×10^6	3.777×10^6
3.5	0.013	2.847×10^5	2.190×10^7	3.650×10^6	7.300×10^6
4.0	-0.007	-2.383×10^5	3.398×10^7	5.664×10^6	1.133×10^7
4.5	-0.024	-2.383×10^5	9.929×10^6	1.655×10^6	3.310×10^6
5.0	-0.024	-4.442×10^5	1.851×10^7	3.085×10^6	6.169×10^6
5.5	-0.027	-6.502×10^5	2.408×10^7	4.014×10^6	8.027×10^6
6.0	-0.017	-6.739×10^5	3.964×10^7	6.607×10^6	1.321×10^7

Table E.7. Stiffness Coefficients for Spring Elements, Batter Piles, Full Impact Load

Depth (m)	Pile Deflection y (m)	Soil Reaction p (N/m)	Stiffness Coefficient K = p/y (N/m^2)	Coefficient for External Nodes (K/6) (N/m^2)	Coefficients for Internal Nodes (K/3) (N/m^2)
0.5	0.3830	4.472×10^5	1.168×10^6	1.946×10^5	3.892×10^5
1.0	0.2800	6.073×10^5	2.169×10^6	3.615×10^5	7.230×10^5
1.5	0.1750	6.324×10^5	3.614×10^6	6.023×10^5	1.205×10^6
2.0	0.1220	4.677×10^5	3.834×10^6	6.389×10^5	1.278×10^6
2.5	0.0280	2.196×10^5	7.843×10^6	1.307×10^6	2.614×10^6
3.0	0.0022	7.072×10^4	3.215×10^7	5.358×10^6	1.072×10^7
3.5	-0.013	-1.615×10^5	1.242×10^7	2.071×10^6	4.141×10^6
4.0	-0.023	-1.694×10^5	7.365×10^6	1.228×10^6	2.455×10^6
4.5	-0.027	-2.369×10^5	8.774×10^6	1.462×10^6	2.925×10^6
5.0	-0.030	-2.745×10^5	9.150×10^6	1.525×10^6	3.050×10^6
5.5	-0.030	-2.745×10^5	9.150×10^6	1.525×10^6	3.050×10^6
6.0	-0.0190	-2.322×10^5	1.222×10^7	2.037×10^6	4.074×10^6

REFERENCES

American Association of State Highway and Transportation Officials (AASHTO). (1991). "Guide Specification and Commentary for Vessel Collision Design of Highway Bridges. Volume I: Final Report." Washington, D.C.

American Association of State Highway and Transportation Officials (AASHTO). (1996). "Standard Specifications for Highway Bridges." Washington, D.C.

American Forest & Paper Association (AFPA) and American Wood Council (AWC). (1997). "Supplement National Design Specification for Wood Construction." Washington, D.C.

ANSYS Inc. (1996). *Introduction to ANSYS – Release 5.3.* SAS IP.

Balder, A.P. (1986). *Mariner's Atlas. Southeast Florida & the Florida Keys.* Chartcrafters, Baltimore.

Balder, A.P. (1988). *Mariner's Atlas. The Florida Gulf Coast & the Florida Keys.* Gulf Pub. Co., Houston.

Bas, B. M. (1998). *Principles of Geotechnical Engineering.* PWS Publishing Company, Boston.

Better Boating Association. (1979). *Chart-Kit, Region VIII, Florida West Coast.* Better Boating Association, Needham, Mass.

Bice, David A., *et. al.*(1989). *A Panorama of Florida.* Walsworth Publishing Company, Inc., Marceline, MO.

Bodig, J., and Jayne, B. A. (1993). *Mechanics of Wood and Wood Composites.* Kriefer Publishing Company, Malabar, FL.

Dietrich, D., and Levy, A. (1987). "Modeling in Structural Mechanics." *Finite Element Handbook.* Hayrettin Kardestuncer, editor in chief, McGraw-Hill Book Company, New York, 4.154-4.177.

Duncan, J.M., Byrne, P., Wong, K.S., and Mabry, P. (1980). "Strength, Stress-Strain, and Bulk Modulus Parameters for Finite Element Analyses of Stresses and Movements in Soil Masses" *University of California*, Report No. UCB/GT/80-01, Berkeley, CA.

Florida Department of Transportation (FDOT). (1996). *Standard Drawings*. Tallahassee, FL.

Florida Department of Transportation (FDOT). (1997). Project No. 79080-3544 - SR-600 Bridge and Approaches Bridges Nos. 790187 and 790188.

Florida Department of Transportation (FDOT). (1999). *Standard Specifications for Road and Bridge Construction.* Tallahassee, FL.

Gere, J.M., and Timoshenko, S.P. (1997). *Mechanics of Materials.* PWS Publishing Company, Boston.

Gilbert, C., Kreja, I., Wekezer, J.W. (1998). "Computer Impact Simulation in Retrofit Analysis of Concrete Bridge Barriers". *Proc., 12th ASCE Engineering Mechanics Division Conference.* LaJolla, CA, 150-153.

Habibagahi, K, Langner, J. A. (1984). "Horizontal Subgrade Modulus of Granular Soil." *Laterally Loaded Deep Foundations: Analysis and Performance.* Langner, Mosely and Thompson, eds., ASTM Publication code No. 04-835000-38, American Society for Testing Materials, 21-34.

Hoy, D., Warren, G., and Davis, D. (1996). "Environmentally Acceptable Piling for Use in Navy Pier Fender Systems." *Materials for the New Millenium Proceedings of the Materials Engineering Conference.* ASCE, New York, v.2, 1189-1198.

Hsu, R.K., and Trepper, R.J. (1995). "The Fenderless Fender System, Port of Texas City." *Proc., Ports 1995.* ASCE, New York, 862-868.

Kubo, M. (1967). "Lateral Resistance of Single Free-Head Batter Piles and Single Fixed-Head Vertical Piles." *Monthly Reports of Transportation.* Technical Research Institute, v. 12, n.2. (in Japanese).

Lambert, C.A. (1995). "Plastic Lumber's Pros and Cons." *Chilton's Hardware Age.* v.232, n.9, p.45.

Lampo, R., Nosher, T., Kerns, R., and Renfree, R. (1996). "Innovative Structural Design Concepts for Plastic Lumber Materials." *Annual Technical Conference and Exhibition.* v.3, n.54, p.3151.

LS-DYNA. (1999). "LS-DYNA Keyword User's Manual. Nonlinear Dynamic Analysis of Structures in Three Dimensions". Livermore Software Technology Corporation.

Malvar LJ, Crawford JE, Wesevich JW, Simons D.(1997). "A plasticity concrete material model for DYNA3D" *International Journal of Impact Engineering.* Vol. 19 No. 9-10, pp. 847-873

Matlock, H. and Reese, L.C. (1956). "Non-Dimensional Solutions for Laterally Loaded Piles with Modulus Assumed Proportional to Depth." *Proc. Eighth Texas Conference on Soil Mechanics and Foundation Engineering.* Austin, TX.

Matlock, H., and Reese, L.C. (1960). "Generalized Solutions for Laterally Loaded Piles." *Journal of the Soil Mechanics and Foundations Division.* ASCE, Oct. 1960: 63-91, Paper 2626.

Meyer, B.J., and Reese, L.C. (1979). "Analysis of Single Piles Under Lateral Loading." Research Report 244-1, University of Texas at Austin and Center for Highway Research.

Nawy, E.G. (1996). *Prestressed Concrete – A Fundamental Approach*. Prentice Hall, Upper Saddle River, NJ.

Plaxico, C.A, Patzner, G. S., Ray, M. H. (1998). "Response of Guardrail Posts Under Parametric Variation of Wood and Soil Strength." *Transportation Research Board 77th Annual Meeting.* Washington, DC.

Ray, M.H., Patzner, G.S. (1997). "A Finite Element Model Of The Modified Eccentric Loader Breakaway Cable Terminal (MELT)." *Proc., FHWA Vehicle Crash Analysis.* Publication No. FHWA-RD-96-212. Washington, D.C.

Ray, M.H. (1995). *The Use of Finite Element Analysis in Roadside Hardware Design.* Workshop on Important Issues for Improving Roadside Safety. FHWA, Irvine, CA.

Reese, L.C., Cox, W.R., and Koop, F.D. (1974). "Analysis of Laterally Loaded Piles in Sand." *Proc. Offshore Technology Conference.* Houston, TX. Paper no. OTC2080.

Reid, J.D., Sicking D.L. (1998). "Design and Simulation of a Sequential Kinking Guardrail Terminal." *International Journal of Impact Engineering*, v. 21, n. 9, p. 761-772.

Tomlinson, M.J. (1987). *Pile Design and Construction Practice.* Palladian Publications Limited, London.

Tsinker, G.P., Wozniak, Z.A., and Curtis, D.D. (1990). "New Concept for Protection Systems for Bridges Across Navigable Waterways." *Proc., Permanent International Association of Navigational Congress (PIANC).* Osaka, Japan, 35-41.

Tsinker, G.P. (1995). *Marine Structures Engineering: Specialized Applications.* Chapman & Hall, New York.

U.S. Department of Commerce, National Oceanic and Atmospheric Administration (NOAA), and National Ocean Service (NOS). (1992). *Atlantic Coast of North America Tidal Current Tables.*

Wekezer, J.W., Gilbert, C., and Kreja, I. (1996). "Conceptual Analysis of an Aesthetic Bridge Barrier." *Florida Department of Transportation Project No. WPI-0510750*, Tallahassee, FL.

Wekezer, J.W., Wuttrich, R., Ramaley, M., Ray, M. (1998). "Design Flaws and Structural Retrofit Analysis of Existing BCT Terminals". *IJCrash'98 International Journal of Crashworthiness Conference, Conference Proceedings.* Dearborn, MI, 531-542.

Whirley, R.G., Engelmann, B. E. (1993). "DYNA3D, A Nonlinear, Explicit, Three-Dimensional Finite Element Code For Solid and Structural Mechanics - User Manual." Lawrence Livermore National Laboratory, UCRL-MA-107254.

Wilson, C.M.D. (2000). "Investigation of Bridge Fender Systems for Barge Impact." Thesis. Florida State University.